CENTRO DE INVESTIGACIONES EN ÓPTICA, A.C.

Research and Prototyping of an Optical Fibre Refractometer with Customized Electronic Control

Como requisito para la obtención de grado en:

Maestría en Optomecatrónica

Asesor:

DR. Rodolfo Martínez Manuel

Estudiante:

Ronald N. Moorcroft

Febrero de 2018
Ags, Aguascalientes, México

Contents

Table of Figures

List of Tables

Abstract

Refractometers are sensory devices that measure the refractive index of liquids, gasses or solids. The refractive index of a medium indicates how fast an electromagnetic wave propagates through that medium. This measurement can be used to identify a chemical or measure certain characteristics of a substance. Using optical fibre as a sensory device provides many advantages, including, but not limited to, being chemically passive, corrosion resistant, electromagnetically immune, small in size, lightweight and highly sensitive.

The refractometer developed in this Masters project utilizes the coherent optical frequency domain reflectometry technique as interrogation method. This technique requires an optical (tunable) source that scans linearly through wavelength in time. A reference cavity with reflectors at the start and end of the cavity will cause a reflection of light. These reflections interfere and produce an interference pattern called a beat signal. The same applies for a sensing cavity – a reflection will occur at the starting interface of the cavity and the interface at the end, being the cleaved tip of the optical fibre. This beat signal produced from the sensing cavity contains data about whatever substance the cleaved tip of the optical fibre comes in contact with. Through various signal processing algorithms, an accurate measurement of the refractive index of the analyte can be obtained.

Custom electronics are designed and built to implement this method and to drive the distributed feedback laser diode that is used as the tunable source. An algorithm coded in a microcontroller controls a generated saw-tooth waveform. The produced voltage output from the microcontroller is then provided as input to a current source. This current source drives the laser diode with specific selected power characteristics to create a near linear saw-tooth wavelength emission, while keeping the laser diode within maximum power specifications. This stable spectrum generation results in stable frequencies of the beat signals, and consequently concentrated magnitudes in discrete linear frequency points when FFTs are performed by the coded microcontroller. These peaks in magnitude of frequency are key to the calculation of the refractive index.

Various signal processing steps are applied to the beat signals utilizing the microcontroller – the sensor is first calibrated employing the reference cavity. Systemic error is calculated and

considered with measurements. Irregularities in spectra are noticed and resolved. Different modulation frequencies are selected and compared.

The refractometer is compact and portable, not being confined to the laboratory, making it convenient to take measurements anywhere. Another important attribute is that the sensor of the refractometer is disposable – the tip of the optical fibre can simply be cleaved if the intensity of the reflections are reduced or if there is major damage to the sensor, it can be replaced by a FC/PC fibre patch cord. The resolution of the tested refractometer is 10^{-3} refractive index units, well in the range of existing commercial refractometers.

Chapter 1: Introduction

The Value of Refractometers Implementing Optical Fibre Sensing Methods

A refractometer is a sensory device that is able to measure the refractive index, or dimensionless number that indicates how light propagates through a specific medium of liquids, gases or solids. Refractometers are essential tools in many laboratories, ecological studies, agricultural industries, food and beverage industries, medical research and development as well as the manufacturing field due to the fact that several substances can be detected directly or indirectly through measuring their refractive indices [1].

Fibre optics have become increasingly popular as sensory devices, especially for the measurement of refractive indices for chemical and biological applications. Fibre optic technologies are rapidly being researched and developed. These types of sensors are more accurate and adaptable, with more advantages in different environments as compared to electronic sensors [2] [3].

Fibre optic sensors can be used in single, quasi-distributed and distributed architectures, measuring with high accuracy parameters, just to name a few: temperature, pressure, strain, angle, magnetic field and refractive index. Since fibre optic sensory systems can be used as remote sensing devices and also have the characteristics of being corrosion resistant and electromagnetically independent, they are also ideal for flammable, explosive, hazardous and/or highly secure environments as these systems remove personnel from secure or hazardous areas and enable them to do their required jobs in a safe environment. They are also favourable in applications such as explosive manufacturing, petroleum refineries and chemical production facilities as they alleviate the many risks that are accustom to electronic devices. Furthermore, fibre optical sensors have the advantages of being small in size, geometrically flexible, able to measure small sample volumes and are highly sensitive. Many techniques can be used for the analysis of data, some with greater benefits than others for specific applications, giving the advantage of having a much shorter response time which can greatly increase the performance and efficiency of the sensory system [1] [3] [4]. Chemical and thermal stability of quarts glass, which the optical fibre mainly consists of for the spectral ranges from ultraviolet to mid infrared, are comparable only with platinum [4].

There are many applications for refractometers, including the analysis of the brix or sugar concentrations in alcoholic beverages, such as wine and beer, during the brewing process. Other

uses include salinity monitoring by ecologists, hydrocarbon content of motor fuels, analysis of urea in urine by clinical laboratories and the testing of water for impurities at water purification plants. Some medical applications for refractometers include the measurement of red blood cell count in blood and the measurement of protein in a sample. Hence, there is the need for high precision, reliable, adaptable and portable devices that can be used by engineers and scientists alike in their respective fields.

Project Objectives

The main objective is to build a refractometer with custom electronics to control the optical source of the system which implements the coherent optical frequency domain reflectometry technique.

Thus, achieving the following objectives will conclude in a successful project:

- Creation of a fully operational refractometer as a prototype.
- Using an in-line interferometer. This requires implementation of simple reflectors that should be realized in the sensing probe to promote easy fabrication.
- A laser diode is required to sweep linearly through wavelength in time and the electronics that are needed for this should be custom built, as there are none that can be used commercially for this specific arrangement.
- Integration of the electronic and optical components and subsystems as a single unit.
- Characterization of the system for refractive index measurements.
- The system should be user friendly.
- The final prototype can then be tested in various applications, such as with laboratory chemicals.

Expected Results

The expected results of the project are to achieve all the objectives stated above. A custom prototype of a refractometer must be created that has a sensing probe that would not be difficult to fabricate, which would be ideal for commercial applications. The electronics must be able to control the light source of the refractometer so that a scan of the wavelength can be done, for the required coherent optical frequency domain reflectometry (COFDR) method. The refractive index of a liquid must be able to be measured through probing the sample and through the use of signal processing. The accuracy should be in the region of 10^{-3} RIU. The system should be usable outside the laboratory, be portable and compact.

Dissertation Layout

This dissertation starts with the introductory chapter, chapter 1, which explains the need for the project and the objectives for successful completion thereof. The dissertation continues to chapter 2, starting with a basic introduction of how the refractive index can be measured, to a more in-depth look at the theory behind the interrogation technique that would be used to enhance the results of the signal processing of the system. Detailed designs of the system, for both the optical and electronic aspects, are given in chapter 3, which also includes simulations of the different parts of the prototype to provide working concepts of the system and to provide expected results in a more ideal capacity. Chapter 4 provides the experiments that test the different parts of the system and the prototype as a whole. The performance of the system is thus tested in this chapter – the accuracy, repeatability, sensitivity and resolution form parts of the performance. Chapter 5 provides an elaborated look at the results of the created system and in the following chapter, chapter 6, a discussion will follow from these results. The conclusions will be given in chapter 7. Any further information that are not found in the chapters are placed in the appendices following the conclusion chapter.

Conclusion

In this chapter a brief introduction was given to show the importance of the creation of a portable prototype for the measurement of refractive index. The advantages of using optical fibre for the sensing probe of the refractometer was also discussed, highlighting that optical fibre is chemically passive, immune to electromagnetic interference and the probe can be designed in such a way that it could be used as a disposable sensor tip which will not be expensive to utilize.

Chapter 2: Literature Review

Introduction

Chapter 1 is the introductory chapter for the main concepts of the project and what is expected to be achieved on completion of this dissertation. Chapter 1 also provides what is expected from the fully functioning refractometer prototype. In this chapter, the literature review, explanations of the theoretical background are given. This is important because it is needed to design the prototype and the system necessary to achieve accurate results. This chapter contains information on all the different parts to the system, which can be called subsystems, such as the sensor, method of interrogation, the optical source and how to control it with the custom designed electronics.

Refractive Index Measurement using an Optical Fibre Tip

The physical principles of light interacting with mass are used in indirect and direct methods, where indirect detection uses suitable dyes or other chemical or biological material. Direct detection is measuring the change in refractive index with direct contact of the medium. The optical phenomena that are used in the optical fibre sensing systems are transmission $T(\lambda)$, attenuation $\alpha(\lambda)$, reflection $R(\lambda)$, fluorescence $I_F(\lambda)$, bioluminescence $I_B(\lambda)$ and phosphorescence $I_P(\lambda)$.

The prototype that is developed will use the tip of an optical fibre to measure refractive index. Refractive index measurement has been done with various different types of fibres, such as single mode fibre, multi-mode fibre, step index fibre and specialized fibre, such as photonic crystal fibre (PCF) – polymer clad microstructure fibre, hollow fibre, tapered fibres and fibres with an inverted gradient index profile [4]. Although there are many different fibres available to use as sensors, the wide commercially available single mode fibre (SMF) will be used. This is due to a few factors – primarily keeping the prototype at a minimal cost for the advancement of a commercial application for the prototype. The single mode fibre is not only the most cost effective, but provides all that is needed for an accurate and sensitive refractive index measurement. If the measurement of the evanescence field was used for the measurement of the refractive index, then other fibres could possibly have had an advantage over SMF. A reason for this could be the preparation for the fibre to use the evanescence field – SMF fibres have a bigger cladding surrounding the core, and

removing this cladding could be more difficult and time consuming than other with a thinner cladding surrounding the core of the optical fibre.

The refractive index can be measured from the tip of the fibre due to the Fresnel reflection that occurs between a change in the interface – in this case between the core of the optical fibre and the particles of whatever analyte is found by the tip of the optical fibre. Therefore, the electromagnetic wave is injected into the fibre core and propagates down the optical fibre waveguide. This wave will then continue to propagate until there is a reflection in the fibre, which will cause the light to change direction and, depending on the nature of the reflection, travel back up the fibre in the opposite direction with a percentage of the transmitted intensity. The magnitude of this reflected wave is dependent on the interface between media with different refractive indices – the reflectance R, given by [5]:

$$R = \left|\frac{n_c - n_A}{n_c + n_A}\right|^2 \tag{2.1}$$

where n_c is the refractive index of the core of the optical fibre and n_A is the refractive index of the analyte – whatever medium is touching the tip of the optical fibre. This is how the tip of the optical fibre can be used for the measurement of the refractive index of the sample that is probed.

The electromagnetic wave is guided through the optical fibre and propagates at a wavelength of 1550 nm – the same wavelength of standard telecommunications. This gives the advantage to the system that standard telecommunications grade equipment can be used for the design and fabrication of this prototype. There is no out of the ordinary optical equipment that needs to be bought or constructed, promoting the objective of keeping the cost of this system to a minimum.

Detection Configurations

Some refractometers that have been designed will now be shown and compared. A parameter that is used in the systems that result in differences in signal processing is the type of detector that is used – either an optical spectrum analyser (OSA) or a photodetector. Systems using an OSA generally work with the frequency and amplitude of the wave and the systems using a photodetector with the power that is measured, each having a specific advantage to the system, dependant on how the system is desired to function and what the system should accomplish.

Generally, the photodetector is used for faster analyses or processing of the system, since the OSA can be slow and could provide information not needed for the accomplishment of the objective, such as the wavelength of propagation and exact optical power of the detected electromagnetic wave.

Optical Frequency Domain Reflectometry

The optical technique that will be used in this application is the optical frequency domain reflectometry (OFDR) technique and more specifically, coherent optical domain reflectometry (C-OFDR). When compared to the optical time domain reflectometry (OTDR), the OFDR method avoids the dead zone problem that is inherent to OTDR (the limited distance between two sensing points) and provides high resolution and high sensitivity [6]. In this section a summary of the operational principle of this technique is made.

OFDR is a high resolution reflectometry tool that can be used for component metrology and locating faults in optical networks. This method is not only limited to measuring single or discrete reflections, but it also can be utilized to measure the distributed backscattered light in optical fibres and therefore also measure the spatial distribution of optical parameters in the fibre, e.g. the birefringence, differential group delay [6] and other non-linear properties.

There are two main methods for the OFDR technique – one is incoherent OFDR and the other is coherent OFDR. The different trends of this technique is shown in Figure 1 [6] [7]:

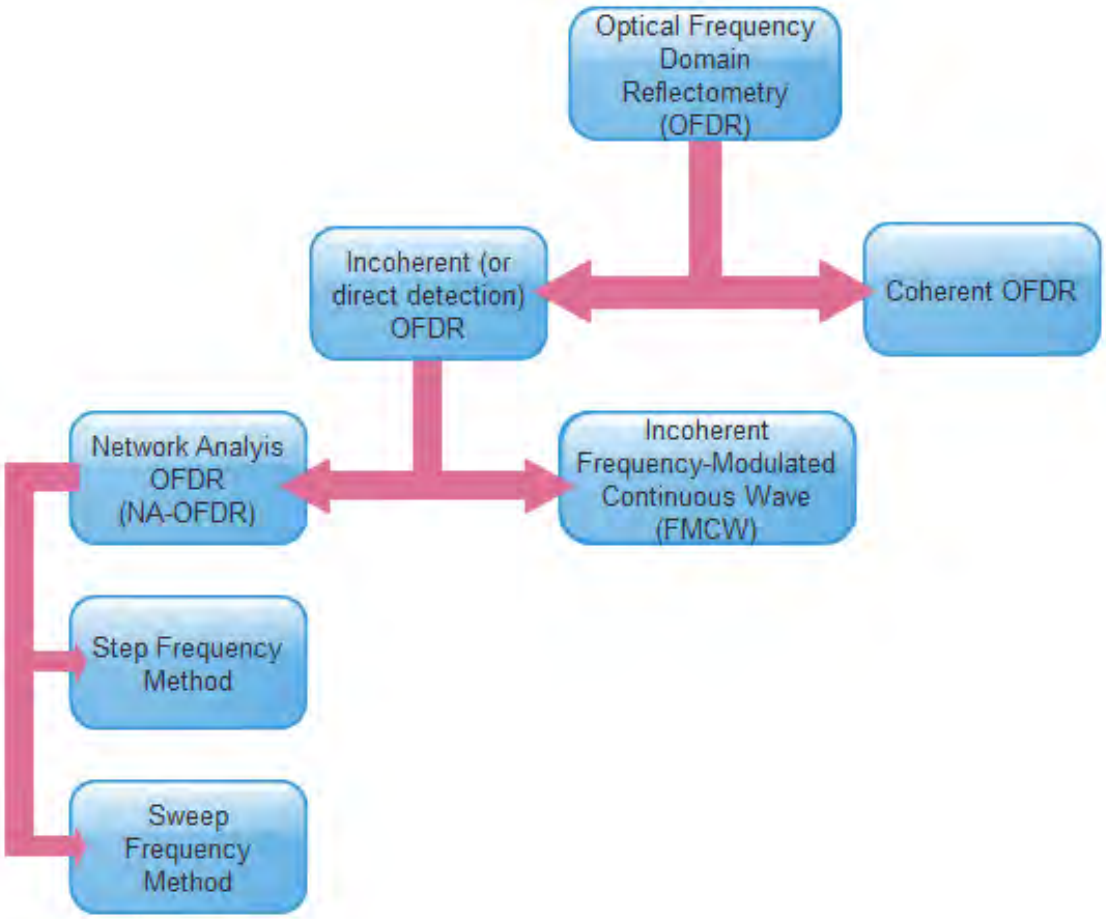

Figure 1: The different classifications of the OFDR technique

For the sake of being complete, a short discussion will be given on IOFDR, but the main focus will be on COFDR, since this is the method that will be implemented for this application.

Incoherent Optical Frequency Domain Reflectometry

For the IOFDR method, a continuous wave is used as the optical carrier or for the probe signal. This signal is intensity modulated by a constant amplitude radio frequency signal whose frequency is changed in a certain manner. This may be done in a stepwise way or it may be done continuously. After the probe signal is pre-processed in this manner, it is ready to be used for the system.

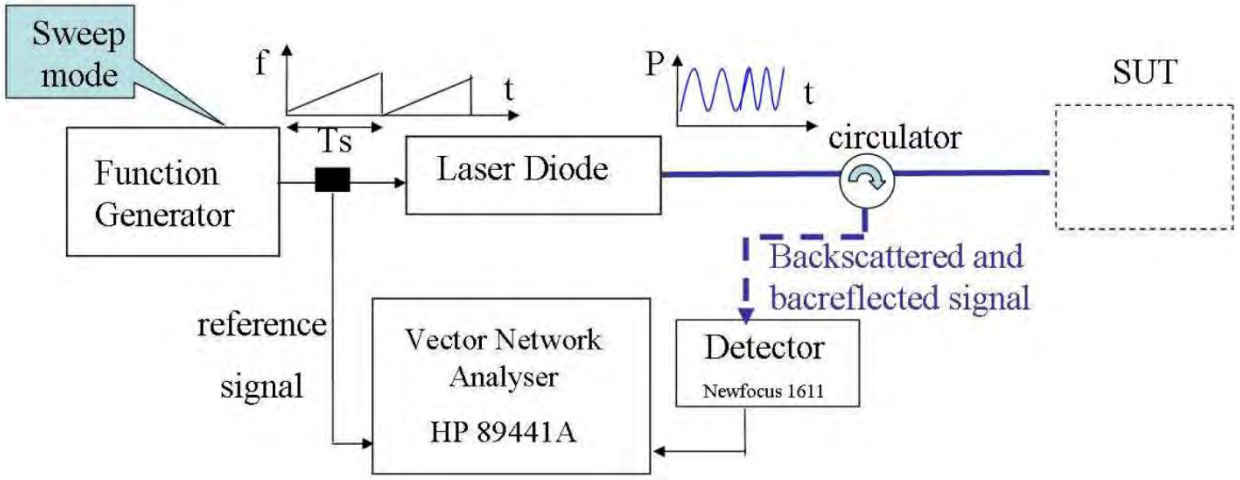

Figure 2: Example of an IOFDR setup [6]

In a distributed sensing point of view, the Rayleigh backscattered light is detected as a function of that modulation frequency that was used to pre-process the probing signal. The spectrum that is then measured is the frequency response in the time domain – applying the Fourier transform of the signal which then gives the time domain impulse response of the signal, provided that the condition is met that the scanned frequency range is large enough. Analysis can be done on the Fourier transformed spectrum or the inverse Fourier transformed spectrum, depending on the application.

In another subgroup of this method, the Incoherent Frequency Modulated Continuous Wave (IFMCW) method is also found. The modulated signal of this method is also swept in frequency, but the detecting probe signal is mixed with the modulated RF signal in the electrical domain and then viewed on an electrical spectrum analyser. The delay times that are experienced in the probe signal can then be viewed in the frequency axis. With the knowledge of the speed of light, this axis can be turned into the spatial resolution of the system.

Coherent Optical Frequency Domain Reflectometry

In the COFDR method, which is also sometimes referred to as coherent frequency modulated continuous wave (CFMCW), a tunable laser source is needed that is swept through wavelength in time. The ideal case of this tunable laser source would be that it is a very narrow line width and a linear sweeping of the wavelength in time, but as no ideal source exist, there needs to be some compensation done for this non-linear sweep. This sweeping is done without any mode hops.

This signal from the source is then divided into two parts (shown in Figure 3) – the reference signal, also referred to as the local oscillator, and the sensing signal, which is guided down the sensing arm where the perturbation of some nature will be measured. When the sensing signal travels down the sensing arm, the signal is then reflected in some manner, either by a mirror, metallic deposit of a thin film, FBGs or some interface that causes a reflection of the light, which simply could be the end of the fibre tip or with the intrinsic properties of the fibre itself using Rayleigh backscattering.

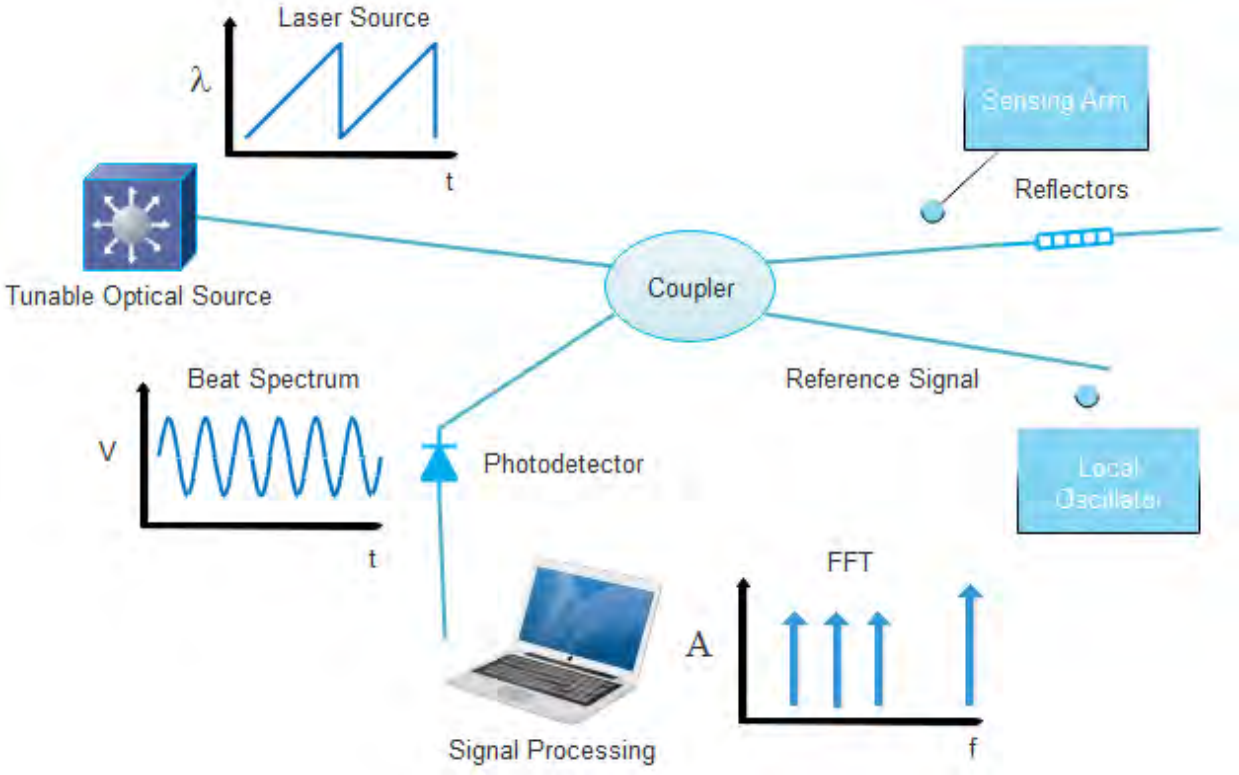

Figure 3: Example of a COFDR system

The reference signal and sensing signal then combines by some means and coherently interferes with each other, whether it be at a coupler that combines the reference signal and sensing signal or at some other interface where the signals interfere. This interference of the reference signal and sensing signal causes a beat frequency to occur. This beat frequency that occurs is dependent on how fast the tunable laser source is scanning, the range of the scan of the optical source and on the length of the cavities or distances between the reflections. This beat frequency and also the phase contain information about the sensing signal.

When a FFT is performed on the signal, the beat frequencies of the combined reference and sensing signal appear as peaks in the frequency spectrum. Each reflection in the sensing arm will interfere with the local oscillator and will cause a specific frequency in the Fourier domain. Figure 3 shows an ideal case using COFDR. There is a linear scan through wavelength from the tunable laser source and this light splits and passes to the sensing arm and reference arm. The laser source graph shows the ideals case of this linear scan. The sensing and reference signal interferes at the coupler and the beat spectrum graph shows the detected signal. When a FFT is done, the discrete frequency points can be seen in the FFT graph. When a linear optical frequency sweep is applied to the tunable laser source, the beat frequencies can be mapped into distance scale, therefore the sweeping rate of the tunable laser source is proportional to the beat frequency as well as the spatial resolution of the system. The reflectivity of each reflection site can be determined by taking the squared magnitude of the signal at each beat frequency [7].

Some advantages of using this method include that the photocurrent measured is not proportional to the reflected optical power, but is proportional to the square root of it, which means that with this method, signals with large amplitude differences can be measured. Another advantage is that the detector's bandwidth does not need to be very high, due to a low laser bandwidth that could be used, opposed to high bandwidth requirements in the OTDR technique. This reduces the noise produced and increases the dynamic range. When the measurement of active devices requires to be done, the COFDR method holds another advantage, as the measurement can be done without saturation as only low power continuous wave signals are used. Another advantage is the dead zone avoidance, since the detector does not saturate as with OTDR methods. The dead zone of the OTDR method can be described as the time it takes for the avalanche photodetector (APD) to recover from the bright reflection received from the OTDR test port [8], causing that closely spaced reflectors cannot be detected that follows another reflector [9].

The disadvantage of using the COFDR technique is that measurement cannot be done with long distances, as the measuring distance is limited by the source's coherence length. The coherence length of a laser is described as the average length of the light beam from the laser along which the phase of the wave remains unchanged [10]. The coherence time of the laser is a measure of the average time interval over which the correct phase can be predicted at any given point in space. The coherence length, L_C is related to the coherence time, t_C, by:

$$L_C = ct_C \tag{2.2}$$

An example of the coherence length of light sources is that it can be thousands of kilometres for a Helium-Neon (He-Ne) laser and only a few fractions of a centimetre for a sodium lamp light source. Considering that the prototype will not contain a long measuring distance, there is almost no disadvantage of using this method as a solution for the proposed system.

Optical Source Options

The spatial resolution and measurement range is directly dependent on the optical source of the COFDR method. A laser source with a large coherence length, large frequency tuning range and narrow line width provides optimal results for the system. With the knowledge that the tunable laser source is of high importance to the COFDR technique, there are some proposed optical sources that can be used [7]:

- Tuned Nd:YAG ring laser
- Piezoelectric tuned Nd:YAG ring laser
- Current-directly-modulated distributed feedback laser diode
- Fibre grating external cavity laser
- Three section distributed feedback laser
- Externally phase modulated Er-Yb laser
- Piezoelectric tuned narrow line width fibre laser
- Mode-locked fibre laser
- Frequency shifted feedback laser

Tuned Nd:YAG ring laser

For the tuned Nd:YAG ring laser, a very high coherence length is realized that gives the advantage of being able to make measurements at very long/large distances for this type of technique. These distances could range up to 50 km when the laser is operated at 1320 nm with a line width of 2 kHz [11], with the change of frequency being achieved by changing the temperature of the laser crystal. The disadvantage of using this laser source is that the spatial resolution is not less than 380 m [7].

Piezoelectric tuned Nd:YAG ring laser

A different way of achieving the change in the optical frequency with the same laser crystal is to use a piezoelectric laser cavity that varies in length. When the length of the laser resonating cavity

is changed, it affects the frequency. A measurement range of 20 m was achieved with the resonating cavity length of 5 cm [12].

Current-directly-modulated distributed feedback laser diode

Using the distributed feedback laser (DFB) gives the advantage of a less expensive laser that can be used. Modulating the current directly changes the peak of where the line width of the main emission wavelength is located, therefore varying the frequency of the laser. These lasers have a short coherence length compared to the Nd:YAG lasers. An example of the resolution obtained for a measurement range of 500 m was 50 cm by using a multi quantum-well distributed feedback laser [13].

This is the chosen optical source for the project. This optical source meets the objectives of the project – being compact in size and a less expensive source than the others. Even using the COFDR as the high resolution reflectometry technique, this DFB laser, with its shorter coherence length, should be implemented to use that method of interrogation.

Fibre grating external cavity laser

A GaAs quantum-well laser diode was used for the fabrication of the fibre grating external cavity laser. It was spliced to a grating which was wrapped around a piezoelectric transducer cylinder. Any change in the length of the cavity then changes the wavelength that is emitted. Some results that were obtained for this laser was a resolution of 2 m over 115 m [14].

Three section distributed feedback laser

For an option that has a better resolution for the application that needs to be implemented, a three section (three electrodes or three legged) distributed feedback laser can be used. The optical frequency is swept by changing the current that is used as the source for the laser. A resolution of 400 μm for a measurement range of 10 cm was achieved [15].

Externally phase modulated Er-Yb laser

When using the externally phase modulated Er-Yb laser an external electro-optic phase modulator is employed. A resolution of 5 m over a range of 30 km was obtained [16].

Piezoelectric tuned narrow line width fibre laser

For achieving the piezoelectric tuned narrow line width fibre laser, the laser cavity that was used was an Yb-doped or Er/Yb co-doped laser cavity that had FBGs for the use of the mirrors to form

the laser cavity. A piezoelectric transducer can then be used to modulate the frequency of the laser, by expanding and contracting the laser resonator which then affects the wavelength that is generated. A small line width can be achieved with this type of laser. A resolution of 16 cm over 150 m have been demonstrated [17] with measured Rayleigh backscattered light at over 95 km [18].

Mode-locked fibre laser

There are a few components that the mode-locked fibre laser consists of. These include isolators, couplers, a polarization controller, a scanning Fabry-Perot filter and an erbium doped fibre that is pumped by a laser diode, all arranged in a unidirectional ring configuration. An example of the spatial resolution that can be achieved is 100 μm over a few centimetres [19] with a wavelength sweep of 20 nm.

Frequency shifted feedback laser

A resolution of 50 μm over 1 m was obtained by [20] using the frequency shifted feedback laser.

COFDR Challenges

There are some challenges that exists with this method and can lead to difficult interpretation of the results and also lessen the accuracy and resolution of the system. These include some of the following phenomena:

Intermixing signals (ghost reflection)

When there are multiple reflections in the test arm, there exists some additional mixing terms that are produced by the different reflectors. These intermixing signals produce extra peaks on the beat spectrum and do not correspond to real reflections, making the interpretation of the results more difficult. There are ways to overcome this challenge. The measurement can be repeated with a lower frequency local oscillator signal. The result of this will be that the real reflections change in amplitude, but the intermixing terms do not change. Frequency shifters can be used as well to place the useful frequencies elsewhere. Intermixing terms that stay at baseband and therefore, as another solution, a low pass filter can be applied to filter out these frequencies. A practical way to remove the intermixing terms is to add an extra fibre delay into the test arm [7].

Polarization dependence

Due to the COFDR method being a coherent technique, the intensity of the measured signal is highly dependent on the polarization state of the light that returns from the reference arm and the sensing arm. Therefore, if the light at the detector is orthogonal towards each other, no light will be detected by the detector. There is a method that could be applied to resolve this. This is through the incorporation of a polarization diversity receiver [17]. This is done by splitting the sum of the reference and test signal into two polarization states orthogonal towards each other and then these states are detected by two photodetectors. These detected signal's intensities are summed making the measurement independent of the polarization state. Another method is that the measurements are repeated many times while changing the polarization state and then keeping the measurement with the maximum intensity.

Laser intensity noise

The power of the reference signal is much higher than the power of the test signal [7]. When a single photodetector is used, the reference signal produces a DC offset which then superimpose all intensity fluctuations of the light source [15]. The laser intensity noise can be eliminated by using a balanced photodetector that consists of two matched photodiodes and a low noise impedance amplifier that generates an output voltage, or also called a RF signal, that is proportional of the difference of both photodiodes. This means that the common noise of both reference and sensing signal is cancelled out.

Non-linearity in the frequency sweep of the source

The ideal case for when the optical source sweeps through the different wavelengths in time is that this sweeping is done in a linear fashion. This is, however, not the case and non-linear sweeps are done. These non-linear sweeps include not sweeping at the some scanning rate all the time, as well as not starting or stopping at the same points in wavelength with each scan. These fluctuations in the scanning causes the result of non-uniform sampling in optical frequency which then, as a result, makes the analysis of the signal measured by the photodetector more difficult to analyse, broadens the energy that should be spaced at one frequency throughout a range of different frequencies in the area of the main frequency and therefore degrades the spatial resolution of the system. There are a few ways to overcome this:

Improvement of hardware: The non-linearity in the tunable laser source exists because of the physical parameters of that source. More expensive equipment can be bought to compensate for the fluctuations that occur when the signal is being swept through wavelength. As this will directly influence the cost of the system and because one of the objectives of this system is to produce a prototype, this might not be the best option to improve the linearity of the scanning of the optical light source.

Signal processing: Another method that can be implemented to improve the signal obtained from the system is to apply signal processing techniques to the signal. Post signal processing techniques can greatly improve the resolution of the system. Before the FFT is applied to the beat spectrum, the signal can be smoothed that will already provide better results. After the FFT is applied (to view the magnitude and frequency of where these beats occur), filters can be applied to single out the principle frequency of the system and to narrow the energy spread that occurs. Various different ways can be implemented to provide a better signal for analysis in different stages of the signal. This provides a method that does not cost more to implement an accurate system.

Sampling at frequency points: When the interference signal is sampled at equidistant instantaneous optical frequency points rather than equally spaced time intervals, this non-linearity challenge can also be avoided. There are a few different ways to do this:

Auxiliary interferometer: When measuring the instantaneous optical frequency using an auxiliary interferometer, some feedback mechanisms are used to correct the non-linearity of the source. This feedback mechanism is adapting the modulated waveform according to the measured instantaneous optical frequency.

Signal processing: After the signal is recorded, the auxiliary interferometer's information is used to resample the interference signal with an accurate equidistant optical frequency grid after data acquisition.

Frequency sampling: The time optical frequency is simultaneously monitored by the auxiliary interferometer. The zero crossing point of the signal at the detector output of the auxiliary interferometer are used to generate trigger pulses which are then used as an external sampling clock. This method of frequency sampling is limited by the path difference of the auxiliary interferometer in order to satisfy the Nyquist theorem.

Interrogation Principle using OFDR [21]

A description of the mathematical principles of how the technique can be used will now be explained. When the paths are split from the frequency modulated signal form the source, the light propagates down the reference and the sensing arm at the same time. The time for the reference signal to travel from the source to the point of the local oscillator and then to the detector is given by τ_{ref}. In a similar fashion, the time that it takes from the source of the system to the discrete reflection point in the sensing arm is τ_{s1}. The number in the subscript can then be substituted for the number of the discrete sensor that is being investigated in the sensing arm.

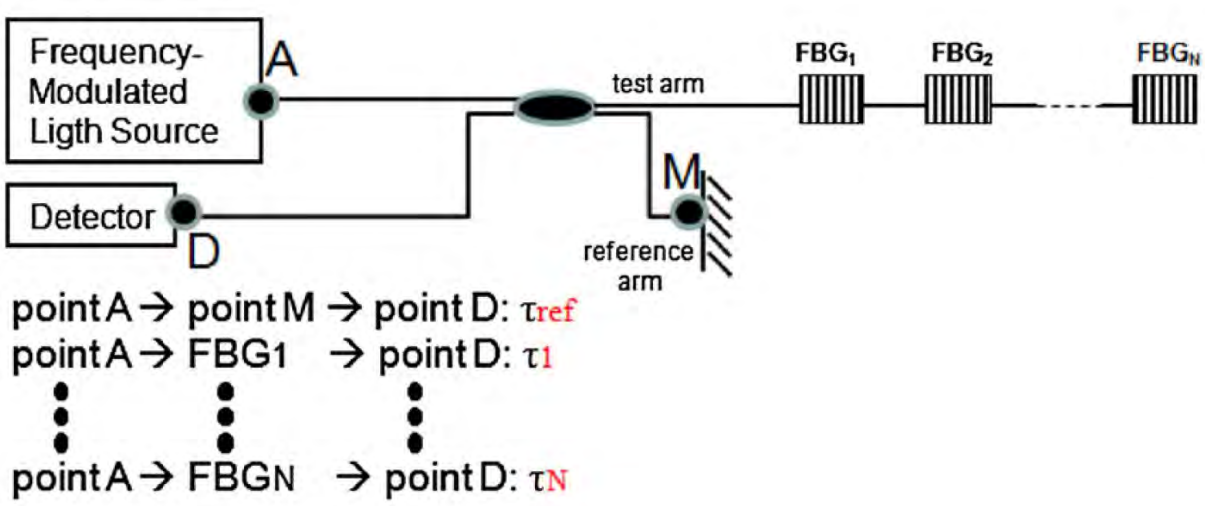

Figure 4: Simple COFDR experimental setup [21]

When using a setup such as shown in Figure 4, the electric field E(t) from the sensing arm is:

$$E(t) = E_0 \exp[i\varphi(t)] \tag{2.3}$$

where E_0 is the amplitude of the electric field, i is the complex number and φ(t) is the phase component. The angular frequency ω(t) is the first derivative of the phase with respect to time. Therefore:

$$\omega(t) = \frac{d\varphi(t)}{dt} \tag{2.4}$$

Then taking the integral of the angular frequency gives the phase, adding the initial phase component. Doing this yields:

$$\varphi(t) = \int_0^t \omega(u)du + \varphi_0 \tag{2.5}$$

When a saw tooth waveform is taken with no mode hops and the wavelength is linearly swept, then the angular frequency can be expressed as:

$$\omega(t) = 2\pi\gamma_f t + \omega_0 \tag{2.6}$$

where γ_f is the tuning rate of the saw-tooth wave optical frequency modulation, t is the elapsed time in the system and ω_0 is the initial angular frequency. Therefore, the phase signal at the tuneable laser source output can be expressed as:

$$\varphi(t) = \pi\gamma_f t^2 + \omega_0 t + \varphi_0 \tag{2.7}$$

When substituted into (2.3), the electrical field of the tuneable laser source, E(t), is:

$$E(t) = E_0 \exp\left[i\left(\pi\gamma_f t^2 + \omega_0 t + \varphi_0\right)\right] \tag{2.8}$$

The electrical fields from the sensors and the reference arm are needed to acquire the value of the superimposed wave with interference from the reflectors and the reference arm. Starting with the electric field produced by a sensing reflector, j, in the *j*th position, $E_{Rj}(t)$

$$E_{Rj}(t) = \eta_{IL} E\left(t - \tau_j\right) r_j\left[\omega\left(t - \tau_j\right)\right] \exp\left(\frac{-\alpha l_j}{2}\right) \tag{2.9}$$

where η_{IL} is the insertion loss constant of the optical coupler in use, τ_j is the total round trip time from the tuneable laser source to the *j*th reflector and back to the detector. $r_j[\omega(t)]$ is the complex reflection factor of the *j*th reflector, α is the attenuation coefficient and l_j is the path length to the *j*th reflector. The electric field for the reference arm, E_{ref}, is then described by

$$E_{ref}(t) = \eta_{IL} E\left(t - \tau_{ref}\right) \exp\left(\frac{-\alpha l_{ref}}{2}\right) \tag{2.10}$$

where τ_{ref} is the total round trip time from the tuneable laser source, via the reference arm to the detector and l_{ref} is the path length of the local oscillator. The reflection is taken as a 100% reflection

from the reference reflector in this case. The signal from the different sensing reflector in the system interferes with the reference signal and the detector measures the signal, u(t), given by

$$u(t) = \sigma \left[\sum_{i=1}^{N} E_{Rj}(t) + E_{ref}(t) \right]^2 \tag{2.11}$$

where σ is the photodetector sensitivity constant and N is the total number of sensing reflectors used in the sensing arm of the interferometer. A beat signal is obtained by sampling the detector output and taking its FFT. The square of the magnitude of the beat signal provides the reflectivity of a specific reflector. The rate of change of the optical frequency provides a factor that is proportional to the beat signal and the distance, therefore the frequency domain can be transformed into distance. The beat frequency, f_{beatj}, for the *j*th sensing reflector, is thus given by [22]:

$$f_{beat} = \frac{\gamma_f OPDm}{\lambda_0^2} \tag{2.12}$$

where OPDm is the optical path difference in the Michelson interferometer architecture (shown in Figure 4) and λ_0 is the starting wavelength of the tunable laser source. If there is a change in the angular frequency, it causes a change in the time shift of the specific reflector, τ_{shift}, producing the equation:

$$\tau_{shift} = \frac{c\Delta\lambda_B}{\lambda_B^2 \gamma_f} \tag{2.13}$$

A data acquisition card is the component in the system that is used to sample measurements from the detector. The higher the sampling rate or frequency resolution, Δf, the better the quality of the signal that is recorder and the more accurately the signal can be processed due to having more sample points. The best spatial resolution is obtained when the optical source has a perfectly linear sweep with a zero line width and also when the data acquisition card has a very good frequency resolution. In fact, the best spatial resolution is determined by the optical frequency of the data acquisition card that is swept [21]. The more samples that are taken in the time domain to be used in the FFT process, the better, because the FFT will be more accurate since there are more samples to work with. The spatial resolution, Δz can then be determined of where the sensor is located by using the following equation:

$$\Delta z = \frac{c}{2n_g\gamma_f}\,\Delta f \tag{2.14}$$

where c is the speed of light in a vacuum and n_g is the group refractive index of the sensing arm of where the sensor is located. It is again important to note that this applies to a frequency that is linearly swept in time with a constant tuning or sweeping rate, γ_f.

To get a value for the perturbation in the system or in the case of the refractometer, the analyte, amplitude modulation is used for the determination of the RI of the substance. Two ways using the amplitude of the reflection will now be discussed.

Amplitude Modulation for Refractive Index Determination

Visibility or Contrast

Visibility quantitatively describes the quality of the fringes produces in an interferometer, normally measured with an optical spectrum analyser (OSA). A very useful parameter that can be applied to evaluate the performance in different optical system is the contrast or visibility, V (it is also called the modulation in some texts) [5] [22]. This provides the equation of:

$$V = \frac{I_{max} - I_{min}}{I_{max} + I_{min}} \tag{2.15}$$

where I_{max} and I_{min} are the irradiances corresponding to the maximum and minimum of the fringes, respectively.

When working with multiple beams in a system, the two beam interference result, I_{result}, can be written as:

$$I_{result} = I_1 + I_2 + 2\sqrt{I_1 I_2}\cos(\Delta\varphi) \tag{2.16}$$

where I_1 and I_2 are the two intensities from the different waves and $\Delta\varphi$ is the phase difference between these waves and can either be: $\Delta\varphi_{FP}$ for the phase difference of a Fabry Perot interferometer and $\Delta\varphi_M$ for the phase difference of a Michelson interferometer and can be described by:

$$\Delta\varphi_{FP} = \frac{2\pi}{\lambda}(n_c 2\Delta l) \tag{2.17}$$

$$\Delta\varphi_{M} = \frac{2\pi}{\lambda}(n_c \Delta l) \tag{2.18}$$

where n_c is the refractive index of the core of the fibre, λ is the wavelength and Δl is the path difference between the two interfering waves, e.g. the difference of the arm lengths. The terms in the brackets are the optical path differences (OPDs) of first the Fabry Perot interferometer and second the Michelson interferometer. The visibility can also be written in a different way when working with two waves, thus:

$$V = \frac{2E_1E_2}{(E_1^2 + E_2^2)} \tag{2.19}$$

where E_1 and E_2 are the two waves that interfere, where the one can be used as a reference, or when working with the irradiance, the equation can be written as:

$$V = \frac{2\sqrt{I_1 I_2}}{I_1 + I_2} \tag{2.20}$$

where I_1 and I_2 are the two irradiances from the different waves. This is derived from the Schwartz inequality [5] and is applicable when the two beams of interfering light have the same coherence. I_1 and I_2 in (2.20) can be replaced with I_2 and I_3 from the setup in Figure 5, making it more specific.

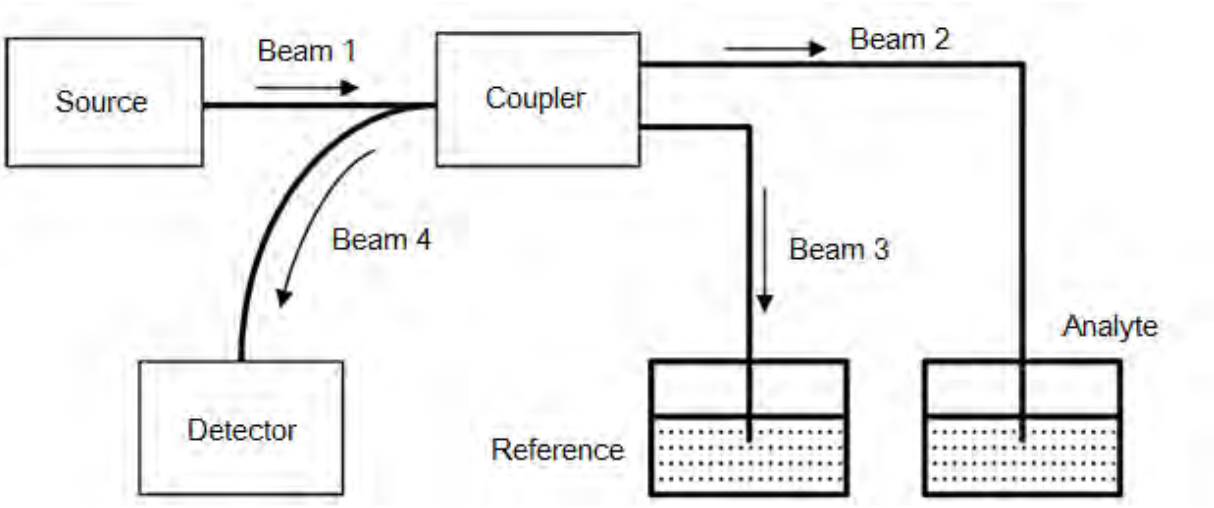

Figure 5: Example of interference happening at the coupler

In the setup of Figure 5, interference will occur at the coupler. Beam 1 from the source will be divided by the coupler into beam 2 and beam 3. There will be a reflectance from the tip of each fibre that will interfere at the coupler. The intensity of beam 3 is a function of the Fresnel reflection and is determined by:

$$I_3 = \left(\frac{n_c - n_{ref}}{n_c + n_{ref}}\right)^2 I_1 \tag{2.21}$$

where n_{ref} is the refractive index of the reference solutions (what the fibre tip of beam 3 is dipped into) and I_1 is the percentage of intensity that comes from the source through the coupler. Similarly beam 2 is given by:

$$I_2 = \left(\frac{n_c - n_A}{n_c + n_A}\right)^2 I_1 \tag{2.22}$$

where n_A is the refractive index of the analyte. Therefore, taking the reference and analyte signals and substituting them into the visibility equation and manipulating algebraically, it is found that the visibility is:

$$V = \frac{2(n_c - n_{ref})(n_c - n_A)}{(n_c + n_{ref})(n_c + n_A)\left[\left(\frac{n_c - n_{ref}}{n_c + n_{ref}}\right)^2 + \left(\frac{n_c - n_A}{n_c + n_A}\right)^2\right]}. \tag{2.23}$$

Taking a reference visibility measurement with both the tips of beam 2 and beam 3 being in the same substance and then comparing the magnitude of visibility of when one of the tips is placed in the analyte to the reference can be used to determine the refractive index of the analyte. Therefore, the visibility of the reference measurement can be written as:

$$V_{ref} = \frac{(n_c - n_{ref})^2}{(n_c + n_{ref})^2\left(\frac{n_c - n_{ref}}{n_c + n_{ref}}\right)^2}. \tag{2.24}$$

More signal processing can be performed to improve the signal and to get a more accurate result, but in essence the measurement with the analyte can be compared to the reference measurement and the refractive index of the analyte can be determined.

Amplitude Reflection Coefficient or Reflectance

For the systems that utilized the frequency component to get the amplitude reflection coefficient, r, or the reflectance, R, an OSA can be used, although many systems use a photodetector. For the analysis of a perturbation of the sensor system, a FFT is taken from the beat signal in the time domain, where an OFDR trace is obtained in the frequency or Fourier domain. From here, a bandpass filter can be applied to single out the specific sensor that is affected if many sensors are present. With the Fourier analysis, the shift in the time domain can be determined as this is equivalent to a shift in the phase slope in the frequency domain. For all of the spectra that a bandpass filter have been applied to, an inverse FFT (IFFT) can be applied to recover the spectrum of each individual sensor in the system, when there are more than one sensor used in the system.

It is therefore seen that the method that is used for the interrogation of the system is more versatile and can be used for other applications and not only for the current application. When the FFT is done to the beat spectrum, there are peaks found from the different frequency characteristics that are generated from the cavities in the system. These frequencies have specific magnitudes and can be seen from doing the FFT.

For the characterization of the sensory system, it is necessary to contain a reference measurement and/or cavity. To get the result, the reference measurement can then be used with the variable measurement, as follows:

$$\frac{|A_{VAR}|}{|A_{REF}|} = Kr \tag{2.25}$$

where A_{VAR} is the magnitude of a specific frequency component in the FFT measurement taken from the variable element or analyte in the system. This specific frequency component is generated by the resonant cavity that comes in contact with the analyte. Similarly, A_{REF} is the magnitude of a specific frequency component in the FFT reference measurement. This specific frequency component is generated by the resonant frequency of the reference cavity. K is a constant which depends from the setup and different elements of the system, which remains a constant throughout the measurements of that specific system and r is the amplitude reflection from the measured variable or analyte. Therefore, it is needed to firstly determine the value of K in the system, where a value of a known amplitude reflection coefficient needs to be used. For this, we use air. By using

the Fresnel equations we can describe how to get the refractive index of the analyte, because the Fresnel equations describe the behaviour of light moving between media with different refractive indices. This behaviour is described at uniform planar interfaces. The law of reflection indicates that the incident angle is equal to the reflected light angle, therefore [5]:

$$\theta_i = \theta_r \tag{2.26}$$

where θ_i is the angle of the incident light and θ_r is the angle of the reflected light. From Snell's law we know:

$$n_i \sin\theta_i = n_t \sin\theta_t \tag{2.27}$$

where n_i is the refractive index of the incident light and n_t and θ_t is the refractive index and the angle of the refracted light, respectively. From here, the power of the reflected light can be described by the reflectance, R, and for s-polarized light (incident light that is polarized with its electric field perpendicular to the plane containing the incident, reflected and refracted rays) this is:

$$R_S = \left|\frac{n_i \cos\theta_i - n_t \cos\theta_t}{n_i \cos\theta_i + n_t \cos\theta_t}\right|^2 \tag{2.28}$$

and for p-polarized light (incident light that is polarized with its electric field parallel to the plane of incidence):

$$R_P = \left|\frac{n_i \cos\theta_t - n_t \cos\theta_i}{n_i \cos\theta_t + n_t \cos\theta_i}\right|^2. \tag{2.29}$$

For the case of normal incidence, where $\theta_i = \theta_t = 0$, this is simplified to

$$R = \left|\frac{n_i - n_t}{n_i + n_t}\right|^2 \tag{2.30}$$

Thus not having a distinction between the s and p polarization. From here, the amplitude reflection coefficient is related to the reflectance by $R = r^2$ and therefore the analyte's refractive index can be determined by:

$$r = \frac{n_i - n_t}{n_i + n_t} \tag{2.31}$$

Therefore, by using the tip of an optical fibre, the refractive index of the substance that is probed can be determined.

Solutions for Refractometers

In this section a summary is made of similar systems that have measured the refractive index of liquids and chemicals with different techniques and equipment. All of the systems use optical fibre as the sensor and measure the change in the refractive index, which was the base of choosing these systems as similar work.

The systems are shown with their experimental setups, which is then further discussed and analysed as to what are the pros and cons of the system (the sensor and the interrogator) and how the systems will differ from this system being developed in order to complete all the desired objectives.

Sugar Sensor [23]

A fibre optic system that was used for the measurement of sugar concentrations in solutions is presented in [23]. An intensity-modulated intrinsic fibre optic sensor is used and the reason for the use of intensity-modulation is that it is the easiest to realize. These type of sensors employ amplitude modulation of transmission in the sensing region of the fibre. With the simplicity of the modulated technique, there are some limitations, namely the intensity sensitivity of the detector is limited by thermal noise and shot noise due to the statistical nature of the arrival of photons at the detector.

An interesting aspect of this system, specifically of the optical fibre that is used for sensing is that a plastic fibre is used (made of polymethylmethacrylate), which is not common for sensing applications. No specific reason in [23] was given for the use of the plastic optical fibre. This aspect is not advantageous for the system that wants to be developed in this dissertation, because the system, which needs to be a working prototype for the final solution, needs to be designed in such a manner that could be used commercially, meaning that the parts must not be difficult to acquire or fabricate and should not be expensive. The normal communication grade SMF28 optical fibre is thus more appropriate for use, since it is durable, widely available and inexpensive.

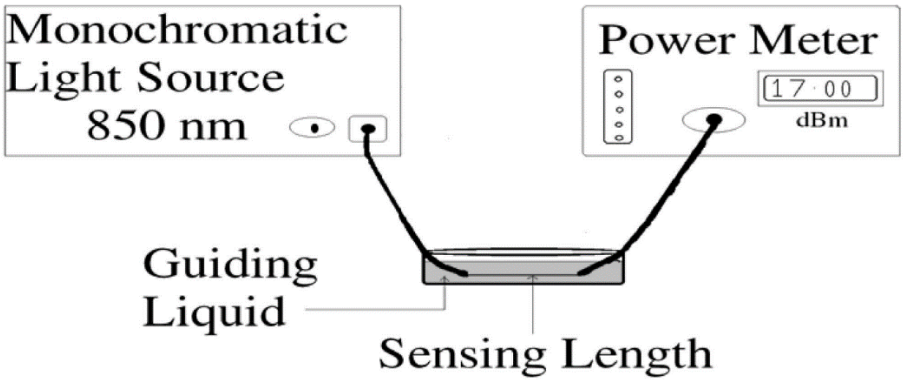

Figure 6: The experimental setup for the sugar sensor [23]

The experimental setup is shown in Figure 6 where the plastic optical fibre's outer jacket and cladding was stripped with 1 cm, 2 cm and 3 cm portions and placed in various sugar concentration solutions. Therefore this system uses the evanescent wave properties of the optical fibre for power loss measurement. The results of the system suggests that the power decreases as the sugar concentration increases, with a bigger loss in power for the bigger stripped area. No specific refractive index results where shown.

In the approach for this prototype being designed, a dip sensor will rather be used for the sake of easily dipping the tip of the optical fibre sensor into the analyte or substance that want to be measured. The evanescent field is not in use, but rather the reflected intensity.

Fabry-Perot Suspended Core [2]

A Fabry-Perot refractometer using a suspended core photonic crystal fibre is presented in [2]. The Fabry-Perot cavities are formed using a suspended core fibre that is spliced to a single mode fibre and then again another single mode fibre spliced to the other end of the suspended core fibre, as viewed in Figure 7. There is also a small insert of what the suspended fibre core looks like in Figure 7. The end of the last piece of single mode fibre is cleaved. The first cavity is then used as the reference cavity, because it is isolated from the liquids that are measured with the cleaved tip of the single mode fibre. The second cavity is one that is formed by the end of the suspended core fibre and the cleaved end of the SMF. A third cavity is formed by the conjunction of the other two and is the one used to measure the refractive index by comparison to the reference.

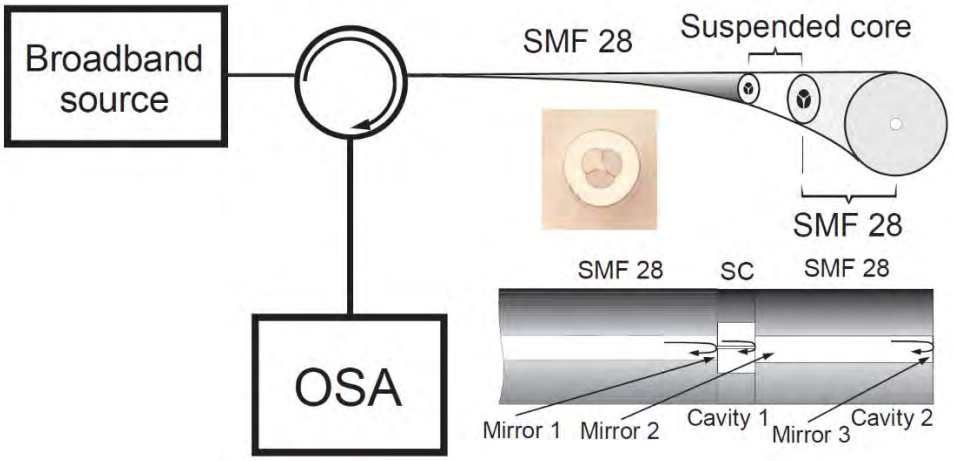

Figure 7: Experimental setup with the suspended core fibre [2]

In the experimental setup of the system, a broadband source is used with a bandwidth range of 100 nm. A circulator is then used for the interrogation of the Fabry-Perot cavities' reflection, which is then viewed on an optical spectrum analyser.

The change of the analytes'/samples' refractive index changes the intensity of the response, but there is no change in the phase. By applying a FFT to the spectral response of the system, the amplitudes, frequencies and also lengths of the different cavities can be seen. The signal of the tip of the fibre decreases in intensity and the ratio of the reference and the sensing peaks are taken to determine the refractive index of the samples. For the refractive index measurement, using the FFT method, a sensitivity of -11.27 ± 0.34 RIU with a resolution of 2 x 10^{-4} was determined. When the visibility method for the system was used, the results concluded to have a sensitivity of -2.03 ± 0.09 RIU with a resolution of 7 x 10^{-4}. This makes the FFT method superior due to the better results. This is due to the translation of the spectral response to the spatial frequency which allows the decomposition of the spectral response into different spatial frequencies and therefore enables the measurement of a single spatial frequency with higher sensitivity.

It was stated that this system was also tested with solutions at different temperatures and the temperature did not affect the measurement of the refractive index of the samples, but this is so due to the range and resolution of the system that was implemented. The refractive index does, however, change with temperature, although it is very small, which is the same occurrence that happens not only to the analyte, but to the core of the optical fibre as well [24].

Therefore, analysing this system gives the advantage of the temperature not having an effect on the refractive index measurements. Also, with the reference being in the same arm as the sensor makes the sensor more compact, which is one of the characteristics that needs to be kept in mind when designing a prototype of this sort. Using the photonic crystal fibre, however, is a con for the application in the prototype, because the components that are used should be kept relative inexpensive and at the moment the photonic crystal fibres are extremely expensive when compared to SMF28 telecommunication fibres.

Michelson Interferometer [25]

For this implementation of a refractive index sensor, a Michelson interferometer was implemented for the main purpose of avoiding complex or expensive fabrication methods for the sensor [25]. The two ends of the Michelson interferometer arms were cleaved at the end. The experimental setup is shown in Figure 8.

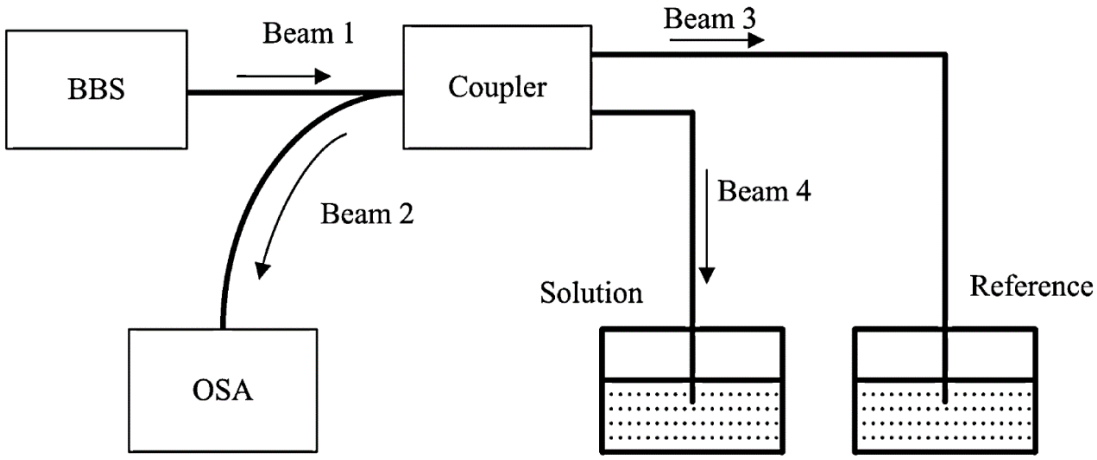

Figure 8: Experimental setup for the Michelson interferometer [25]

The working principle is to measure the fringe contrast from the reflected spectrum and by doing that, deriving the refractive index. The Fresnel reflection that is obtained from the ends of the cleaved fibre tips will change according to the refractive index of the liquids that are measured. The reflected light from the reference and sensing arm interfere at the coupler that can be seen by the optical spectrum analyser.

For this setup, the reference arm is placed in water (that has a known refractive index). The average sensitivity was found to be 103 dB/RI. The resolution of the system is 9.6 x 10^{-6} for the measured range.

By analysing this system it is seen that the advantage of the system is the simplicity and the sensitivity that is achieved from such a relatively simple system. One of the necessary objectives of the interferometer prototype is to keep it small and compact, thus using the Michelson interferometer could take up some more space due to the reference and sensing arm being two fibres. And for the price and compactness it is necessary to have a different component for result analysis, as an optical spectrum analyser is way too expensive and bulky for this process. In order to accomplish that objective, a photodetector and different sampling controller need to be implemented.

Fibre Bragg grating refractometer [26]

In this system a side-polished FBG refractometer is used for the measurement of the refractive index of liquids and the compensation for temperature and polarization is given [26]. When looking at the sensor in Figure 9, there is one FBG found as the refractometer sensor and the other as the temperature sensor. The refractometer sensor is side polished so that the core can be exposed to the analyte and can react with the evanescent field. The FBG being used as the temperature sensor is not affected by the analyte and only measures the temperature of the glass block that the two FBGs are adhered to.

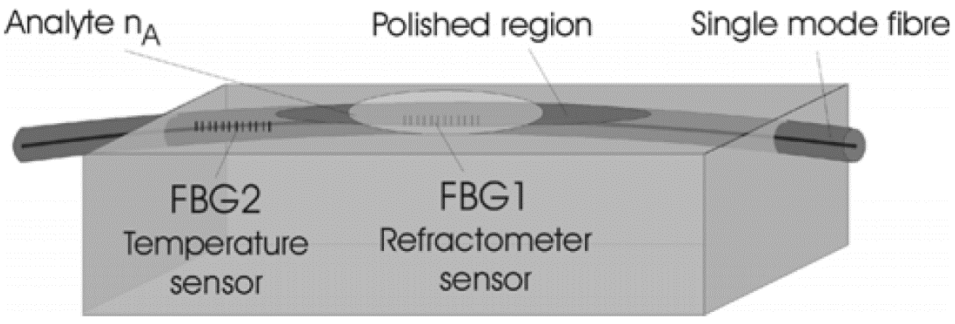

Figure 9: The sensor head of the FBG refractometer [26]

The measuring unit of the FBG refractometer is seen in Figure 10. A broadband light source is used with a polychromator and CCD as the detector. For the dependence of the polarized state of

light on the Bragg wavelength and how this effects the measurements of the refractive index, the emitted light is polarized and the state of polarization is controlled manually.

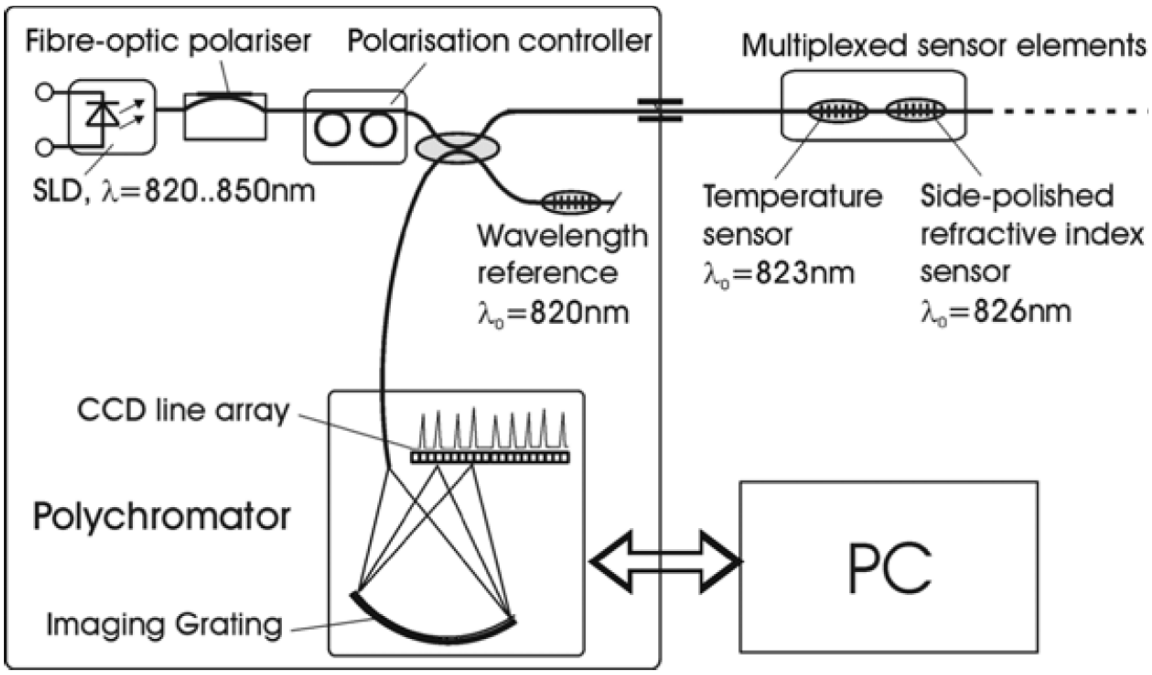

Figure 10: Measuring unit of the FBG interferometer [26]

This refractometer's working principle is as follows: the properties of the sensor is determined by the Bragg wavelength and more specifically the change in the Bragg wavelength as a function of the refractive index of the analyte. It is assumed that there is a linear change between the change of the Bragg wavelength and the change of the effective refractive index of the guided fibre mode.

The sensitivity of the system is influenced by the film thickness (anything above 5 μm provides maximum sensitivity) and the sensitivity is also influenced by the wavelength – increasing wavelength makes the evanescent field penetrate more deeply which increases the sensitivity. The sensitivity that was obtained is 300 nm per RIU at a used 980 nm wavelength. The resolution that was obtained for the refractive index for the analyte was 2×10^{-5} around 1.45 refractive index and 10^{-3} in the region of 1.33 refractive index.

The disadvantages of this system is that the sensor requires fabrication that is not simple enough for a prototype of the nature that wants to be constructed for this dissertation. There is a lot of attention that the stripping of the outer jacket and cladding requires for the refractive index sensing

and, for higher sensitivity at lower refractive indices, more intricate methods follow for example: depositing thin-film layers on the stripped part of the fibre. This causes that the field distribution of the guided fibre mode shifts more towards the substrate and the relative part of the field inside the substrate increases. Also, for the temperature compensation, a second FBG is used and the temperature coefficient of the analyte needs to be known in this system, or various measurements need to be taken to firstly determine the temperature coefficient of the analyte, making it less useful for the purpose of producing a prototype of a refractometer. Also, more time and expenses need to be yielded if the fabrication of a FBG is needed, making the intended commercial application of the refractometer more expensive and difficult to manufacture.

There are also easier methods to obtain the same amount, or better sensitivity.

Detection of adulterant traces in coconut oil [27]

An application that was done for measuring trace amounts of paraffin oil and palm oil in coconut oil is presented in [27].

The sensing head that is used is a plastic multimode side-polished fibre. The reason given here for the use of a plastic optical fibre is because of the low cost, high degree of mechanical flexibility, tensile strength and breaking strength. For the system being developed in this dissertation, it will not be appropriate to make use of plastic fibre. Even with these stated advantages, the cost, flexibility, durability and strength is more than enough that is present for the use of normal SMF28 communication fibre in the project. The core of the plastic fibre is 980 μm with a numerical aperture of 0.5. The core and the cladding refractive indices are 1.49 and 1.41 respectively.

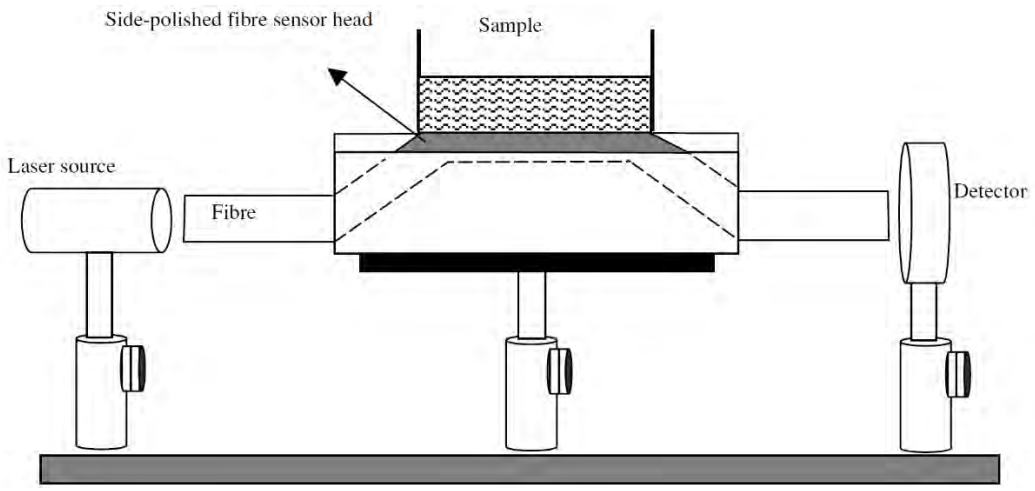

Figure 11: Experimental setup for the adulterant coconut oil detection [27]

The fibre is polished for the reason of coupling a large number of core modes to the analyte and therefore increases the sensitivity of the sensor.

The experimental setup of the system is shown in Figure 11 with the laser source being a 4 mW diode laser emitting at 670 nm. The fibre bent in some portions for the reason stated that it increases the sensitivity of the fibre. The increase in sensitivity is due to more modes being coupled to the sample placed on it. The detector that was used was a power meter. The refractive indices were measured with an Abbe refractometer with a resolution of the order of 10^{-3}. As the adulterants increase, the refractive index increase with a minimum detection limit of 2% paraffin/palm oil in coconut oil. The response time of the system is 7 seconds.

For the refractometer prototype that is designed, the use of a tip sensor is more appropriate, as it makes it easier to just dip the tip of the sensor in a substrate and can be easily wiped and cleaned for further use or even easily replaced if there is damage or stained parts to the sensor tip. If this type of sensor was used, the fibre could not just be inserted and cleaved, but had to be carefully polished which would make the fabrication of the commercial intended prototype more difficult.

Temperature Insensitive Michelson Interferometer [3]

In this system, intensity-modulation is used for the refractive index sensor, because of the direct comparison to wavelength-modulation and that wavelength-modulation has the inherent characteristic of the cross-sensitivity problem that makes it sensitive to temperature [3].

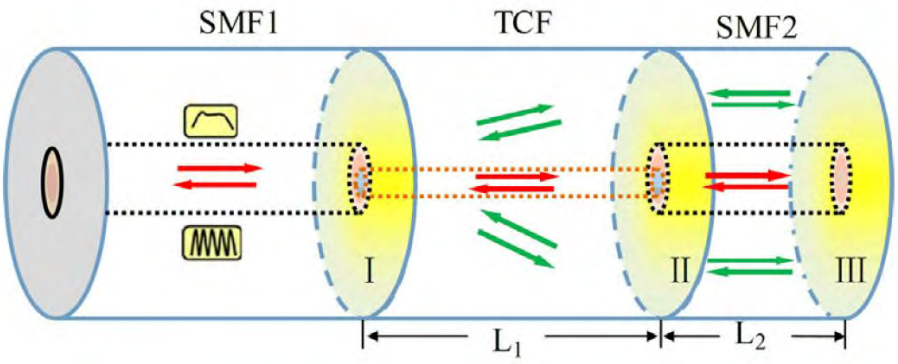

Figure 12: Schematic diagram of the Michelson interferometer [3]

The system uses an in-fibre Michelson interferometer that is constructed by splicing a thin core fibre in between two standard single mode fibres. The experimental setup is as follows: the first SMF was connected to a broadband light source with wavelength range of 1250 to 1650 nm and to an optical spectrum analyser via a 3dB coupler and the end of the second SMF was cleaved. The SMFs have a core diameter of 8.2 μm and the thin core fibre has a core diameter of 4 μm.

This type of setup can also be viewed as a Fabry-Perot interferometer, but this system does not use it in that way. Instead, the working principle is that the core of the SMF is larger than the core of the TCF, and therefore the core modes will be coupled to cladding modes when the light propagates from the first SMF to the TCF. To view this graphically, an example of the splice is shown in Figure 12. The light is then reflected off the surface at the end of the TCF and returns to the interface between the first SMF and the TCF, but the energy found in the core mode is much higher than that of the cladding modes and therefore the second SMF is utilized to couple more of the core mode in the cladding modes when the light is reflected off of the cleaved end of the second SMF and is coupled at the interface between the second SMF and the TCF. This gives the interfering spectra better fringe visibility and can be better analysed. Furthermore, the fringe visibility and free spectral range can be improved by altering the lengths of the thin core fibre and the second SMF.

The results of the refractive index sensor provides a sensitivity of -208.24 and 125.44 dB/RIU at the refractive indices of 1.44 and 1.5 respectively. The resolution of the system was not given.

A major disadvantage of the proposed system as is, is that the absolute refractive index cannot be determined, but only the refractive index relative to the effective refractive index of the core of the

fibre. This means that for example when the refractive index is 1.36 or 1.56, it cannot be determined which is which, but it can only be determined that it is one RIU away from the effective refractive index of the core of the fibre (the refractive index of silica was taken here as 1.46).

Also, the splice of the TCF is done in a specific way and could require an expensive splice machine to successfully splice the fibres together, making the fabrication for a commercially intended device more expensive, difficult and time-consuming.

Self-referred Refractometer [28]

In this work, the refractometer that was created uses Fresnel reflection from the cleaved end of a SMF standard telecommunications fibre. One of the important objectives stated that needed to be accomplished with this system is to either completely be immune to the temperature cross sensitivity or to compensate for it in some way. This was achieved by using an in-line twin-grating (FBG) setup. The reflectivity of the FBGs is low, about 0.02%. An example of the system used is shown in Figure 13.

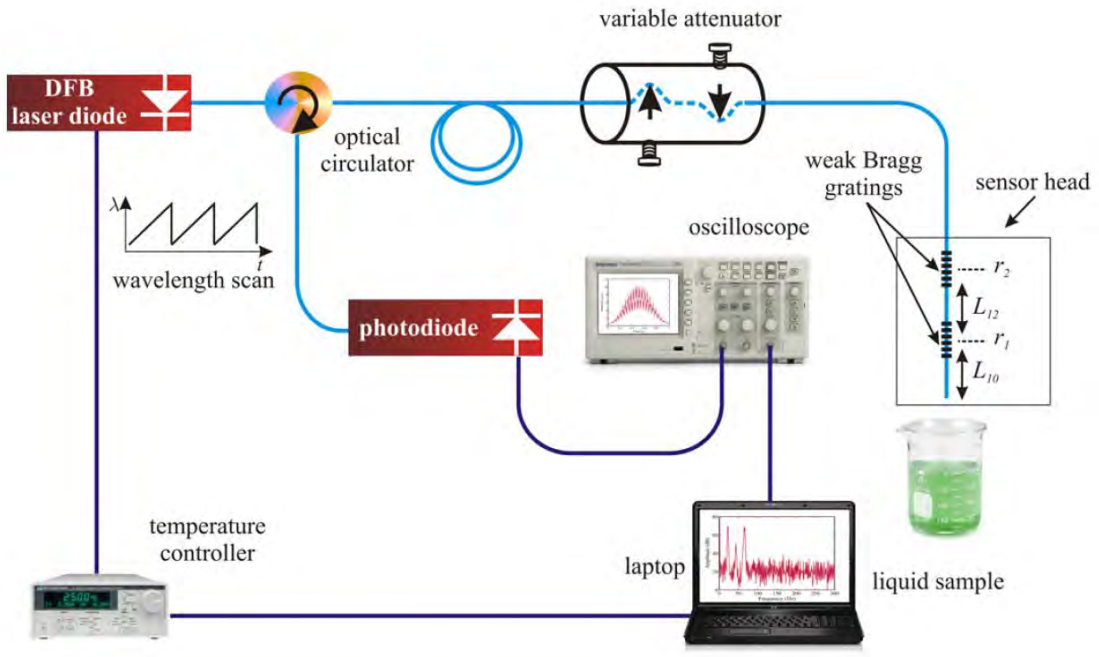

Figure 13: Setup for the self-referred refractometer [28]

In this presented system, to make the sensor intensity self-referred, there must be interference (therefore a reflection) that is not effected by the refractive index change from the analyte that

measured at the cleaved end of the fibre tip. This is done by using the cavity that formed between the two FBGs as reference, since the reflection from these cavities are independent from whatever substance the tip of the fibre is placed in. The method that was used for interrogation is the COFDR technique with a tunable laser source in the telecommunications wavelength range, therefore the length of the cavities will determine the frequency of the beat signal that is generated and all will have different frequency components that can be easily seen in the frequency domain. When the ratio of the magnitude of frequency is taken from the cavity that is formed from the end of the cleaved tip of the fibre to the first grating found from the tip and the reference cavity, it will provide the information that is needed to get the refractive index of the analyte.

The experimental results show an accuracy of measurement to the value of 5×10^{-5} RIU with a standard deviation of 4.3×10^{-5} RIU while measuring sunflower oil for 20 measurements and a standard deviation of 6.5×10^{-5} RIU when measuring a silica index matching liquid Cargille 06350 at a wavelength of 1534.5 nm.

With the use of the FBGs in this system makes the manufacturing of this system's sensor not simple enough to use in this dissertation. One of the objectives of implementing this prototype is that the sensor of the system must be easy to fabricate, making it less expensive and even easily replaceable if the sensor gets damaged or can't be used anymore.

Current Source

A tunable optical source is needed for the implementation of the COFDR interrogation technique. This requires that the current through the laser source is tuned to provide the scanning effect through wavelength in time by the laser. Hence, the requirement of a custom current source arises that can control the current that is fed to the optical source. This current must be provided in a certain way – as the COFDR method required a saw-tooth scan with wavelength, so does the current source require a saw-tooth scan through current to be fed to the laser.

There would be two parts to the electronics that provide the optical source with this saw-tooth scanning ability – a microcontroller and a current source. The microcontroller can be controlled by logic (code) that is able to scan through voltage in time and would be the device that controls the modulation frequency of the system. The current source should have a linear change from input to output, accepting this scan of voltage and in turn producing the current necessary for the laser.

This current should be sufficient to pass the threshold current of the laser, so that the laser can produce stimulated emission for a stable central wavelength emission.

Architecture

The simplest current source is a circuit with a voltage source and a resistor in series with the voltage source, shown in Figure 14. If the load voltage or load resistance is much smaller compared to the source voltage or the source resistance, respectively, then the current will change very little in the load. If the load voltage is several volts big and the accuracy of the current that needs to be provided within a few percent, then a circuit like this can be used, but this means that the source voltage needs to be several hundreds of volts big – making this circuits impractical.

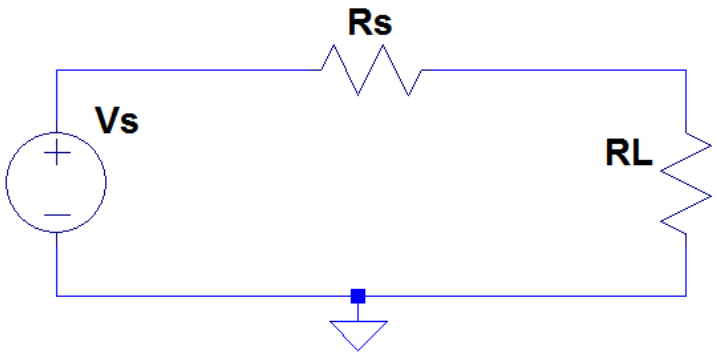

Figure 14: Basic Constant Current Circuit

With a transistor and current limiting diode

When a transistor is introduced in the circuit, then the need for a high voltage source is eliminated. The current through the collector determines the current output of the circuit. The shortcoming of the circuit in Figure 15 is the low output current [29] that is provided by the transistor. The circuit can provide a constant current, as long as the transistor is not saturated. An example of a circuit with a transistor that can be used for a current source is shown in the Figure 15.

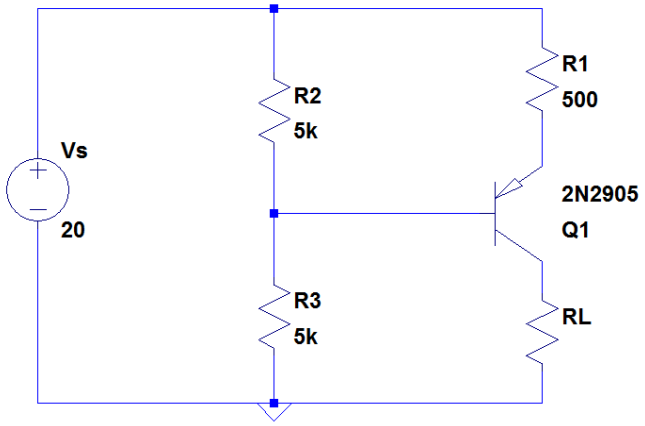

Figure 15: Transistor Constant Current Source

A voltage divider is used for the base of the transistor, while a resistor is placed in the path of the collector and emitter. The load current, I_L, can be calculated as:

$$I_L = \frac{V_S R_2}{R_1(R_2 + R_3)}$$

where Vs is the voltage of the source, R2 is the resistance in the top of the voltage divider and R3 is the resistance in the bottom of the voltage divider, with R1 is the resistor in the path of the collector. The constant current of the circuit is provided by the current through R1, as long as the transistor is not saturated. For the transistor not to be saturated, the following condition needs to be met:

$$V_L < \frac{V_S R_3}{(R_2 + R_3)}$$

where VL is voltage across the load. This circuit can, however, be improved and stabilized through introducing a zener diode in the place of R2 [30], such as shown in Figure 16. The zener equivalent is a battery in series with a low resistance of usually 20 Ω. With a variation in the supply voltage, this circuit can provide great stability. Without the zener, 50% of the change in Vs would affect the transistor bias. With the zener, 0.04% of change in Vs can affect the bias. The main problem that is encountered here is the current output of the circuit, which is in the range of 10 mA, which just falls short of the total operating range for the DFB laser diode. There is also a leakage current in the transistor.

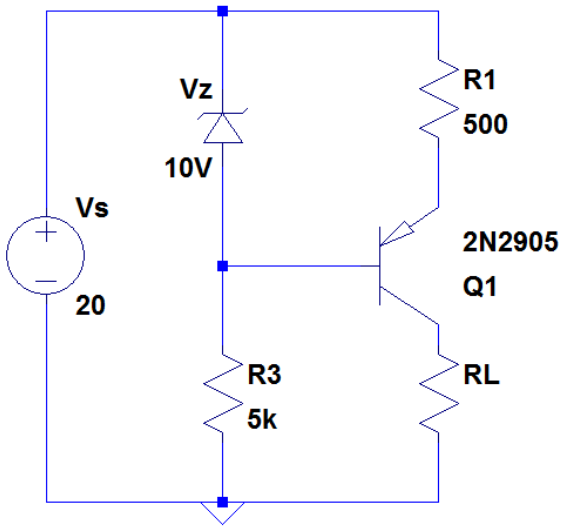

Figure 16: Stabilized current source

There are other commercial terminal adjustable current sources available, such as the LM134, LM234 and the LM334, but these only provide a programmable current between 1 µA and 10 mA [31], thus the output of using these current sources will not be sufficient with providing the laser diode with enough current.

Conclusion

In this chapter, the interrogation technique has been described as well as the advantages, disadvantage and ways to overcome the challenges of the COFDR method. The main points that need to be kept in mind is that a tunable laser source that sweeps linearly through wavelength in time, in a saw tooth fashion, needs to be used with some type of reflector in the sensor for interference to occur. This interference pattern gives the characteristics of the system and perturbation to the system can be measured and analysed though signal processing technique, such as applying a FFT to the interference signal.

Different applications from various authors have been discussed and the advantages and disadvantages have been made to this application of the prototype that needs to be developed.

In the following chapter, the evolution of the design of the system is shown and discussed.

Chapter 3: Design and Simulations

Introduction

In this chapter the design of the system will be discussed, keeping in mind the theoretical background and project objectives that need to be accomplished. For the design of the system, research was done with existing systems and designs, some initial experiments to steer the start of the design in the correct direction and the help of some people that have existing knowledge in the field. Preliminary designs were conducted and tested, seen where improvements can be made and then they were made.

The different parts of the prototype all needed to be designed, tested and improved. The research and development of the project is continuous, from when the first ideas of the project sprouted to the final wording in the conclusion. Constrained by time, the final design is given for complying with regulations and with the fulfilment of all the project objectives.

For the different systems – the electronic current source, optical components and fibre optic setup is designed and discussed. Starting with the architecture, why it was chosen with its advantages for the system to what components where chosen and why will be given.

This evolution will now be discussed.

Electronic System

The electronic system consists out of different parts – the microcontroller, the display and the current source. The microcontroller and the current source is vital to the operation of the refractometer prototype and the screen gives the prototype a complete look as a compact package.

The specifications of the microcontroller and display are given, with the design and simulation of the current source following after.

Microcontroller

The microcontroller used was a Nucleo-144 board from ST Microelectronics. The STM32F767ZIT6 is the larger board in the range with a bit more processing power and random

access memory. A lower range microcontroller can be used for the signal processing, but using the display with the signal processing requires the extra processor power and RAM capacity. The key specifications of the microcontroller are:

- ARM Cortex M7 216 MHz processor,
- 2 MB Flash, 512 kB SRAM,
- ST Zio extension connectors for the Arduino interface breakouts and ST morpho headers (for the compatibility of the display),
- Mbed enabled (for support),
- 5 V and 3.3 V output with 100 mA, sufficient for the input to the current source and
- 144 pins, sufficient for the input and output of the display, current source and detector.

With the abovementioned specifications, the selected microcontroller will be sufficient to perform the needs of control and display of the prototype and being an Arduino clone, a more cost effective solution as well.

Display

The display used was a gen4 4.3 inch display by 4D Systems. The reason for selecting this display is due to some elements: it gives the user a crisp interface, is compatible with the microcontroller, it has an on board processing to assist in the display needs and has supporting software for the coding.

This display provides a clean interface for the user, not being expensive and good compatibility.

Current Source

The bandwidth of the laser is dependent on the current that is fed to the laser as well as the temperature under which the laser operates, therefore laser diode must be provided with a current that remains stable and temperature that can also be kept at a constant value. The laser module that is used is a 1550 nm DFB diode - coaxial pigtail, 2mW (PN: LDM-1550-DC-1-FA).

Practicality is a very big part of the design of this circuit, since the prototype should be kept as compact as possible, while using the current available power sources that are widely available. Another big factor is the current that the circuit needs to supply and the other power factors discussed below.

Power Aspects

The following performance aspects must be considered:

Power supply

The power supply of the circuit must be defined. Since this prototype must be able to be mobile, it must be able to be plugged in a wall outlet, therefore full wave rectification must be done with an output of preferably between 0 V and 2.5 V of the rectifier, since this is what the circuit as the final solution requires as a voltage input. This can be done with the use of a microcontroller to control the saw-tooth waveform as input to the current source. The current output to the load of the current source should be between 0 mA and 250 mA. This would enable the laser diode to be driven properly, since this provides sufficient current output. When a split rail power supply is used, it can protect the laser, particularly during supply sequencing.

Output current

The output current of the current source must be able to be tunable and provide sufficient current to the DFB laser diode. The tunable current source will provide the laser diode to have a tunable wavelength, which is needed for the modulation technique that is required for the system. The laser diode requires a threshold current around 5 mA and the current that the laser diode requires for over temperature conditions, is around 30 mA and the maximum current supplied to the laser diode should not exceed 100 mA.

Output voltage

The output voltage of the current source must be sufficient to power the laser diode. The required voltage is between 1.1 V and 1.5 V.

Efficiency

The heat build-up in the circuit due to the power dissipation and the compact space can be a concern. Therefore, this can negatively impact the efficiency of the current source. For low current diodes, linear regulation can be adequate. For higher current solutions, switching regulator based solutions might be needed.

Laser connection

Dependent on how the laser needs to be connected also needs consideration. Perhaps the laser may float off ground or other applications require that the anode and the cathode be grounded for operation.

Stability

Line, load and temperature changes should minimally affect the laser. There the current source should be well regulated against these changes. Typical temperature drifts are in the range of 0.01% and line and load induced variations should be kept within 0.05% [30].

Output current programming

A programmable port voltage is used to set the output current. This can be done from a potentiometer, filtered PWM or DAC. Typically, with a range in between 0 V and 2.5V corresponds to an output current range of between 0 mA and 250 mA. The accuracy of these programmable ports must be considered.

Noise

The noise produced by the current source can modulate laser output and this must be minimized. Noise bandwidth to 100 MHz is of interest. When a current source is linearly regulated it has inherently low noise and usually gives no problems. When the current source needs to contain a switching regulator technique then a special method needs to be applied to maintain low noise.

Overshoot

When there is overshoot, it can be destructive to the DFB laser diode. Any improper control of input or power supply turn on/off characteristics must be considered. Any spurious laser current must be avoided and is impermissible under any condition. This is important since some of the circuitry may have undesirable or unpredictable responses during powering the laser.

Acquiring sufficient output current

With the task of producing a sufficient output current, the concerns that arise for the laser current sources and the main ones include the performance and the protection of the device. The magnitude and the stability of the current source as well as the output connection restrictions, efficiency, voltage compliance and power requirements form part of the performance aspects of the current sources. The protection aspects of the current sources must also be highly considered, because not doing so might cause that the laser and optical components might get damaged. This must be avoided, since the laser is an important item, and considering the other optical components to be quite durable (such as the circulator), the laser could be the most expensive component in the circuit, with regard to it just being fed a bit too much current and then it will be destroyed.

Therefore, proper design must include to protect against inputs and other factors like hot plugging, although some might not be the case in the exact setup that will be used in this project.

The Solution

The circuit [30] presented in Figure 17 provides the current source with the necessary characteristics that is needed for powering the laser:

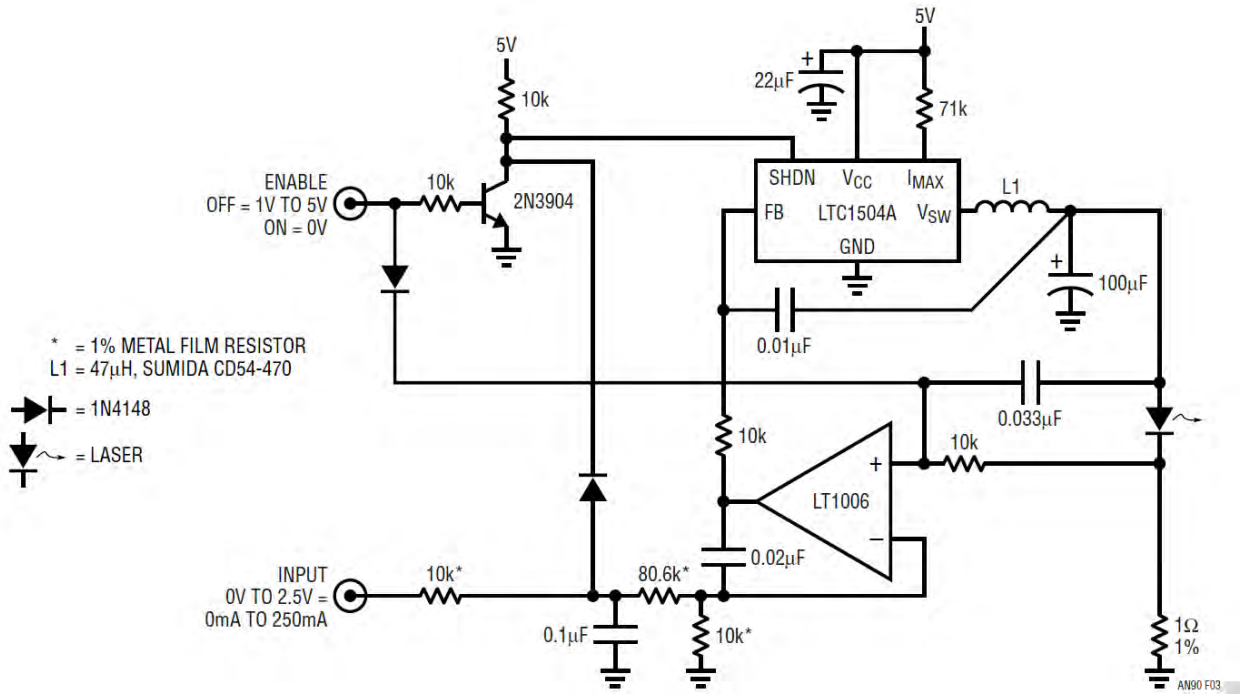

Figure 17: Circuit providing sufficient current for the laser diode.

The amplifier and the step-down switching regulator in the circuit is able to supply a load current of up to 250 mA. This will be sufficient to provide the DFB laser diode with all the current it requires, but also provides too much and could cause damage or complete failure to the laser diode, so safety measures needs to be taken so that the current source does not damage the expensive laser diode.

The amplifier in the circuit controls the laser current by exhibiting the 1 Ω shunt voltage at a potential that is given by the programming input. Therefore, by just limiting the input to the circuit, it is possible to control the amplification of the current. There are other methods that could be used, such as using a current limiting diode [29] that does not exceed the maximum current of the laser diode. The LTC1504's output causes that there must be attention given to the loop compensation,

as the LC filter introduces a phase shift. For loop damping, the capacitors are introduced in the circuit.

There is, however, an improvement to the circuit relating to the cost. Using a step-down switching regulator provides an advantage of eliminating a transistor's heat if one is used, but does increase the cost of the system. Figure 17 implements a switching regulator for higher efficiency, but Figure 18 provides a lower cost current source with sufficient efficiency for this application, maintaining the other power characteristics of the first presented circuit.

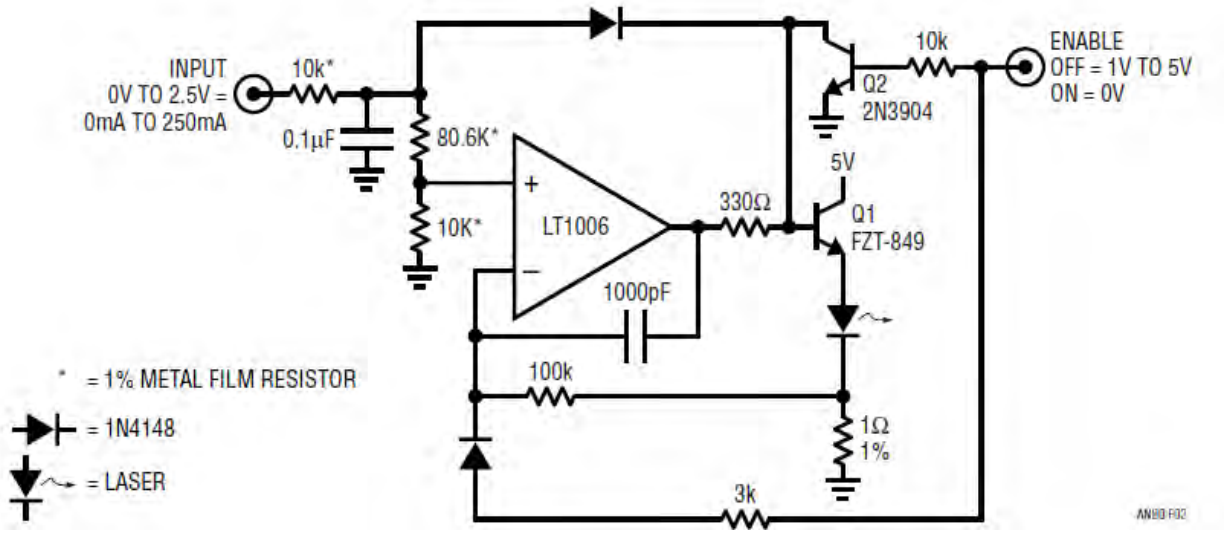

Figure 18: The amplifier in the circuit controls the current by comparing the 0.1 Ohm resistor to the input. The transistor (Q1) replaces the switching regulator

In Figure 18 it is seen that the step-down switching regulator is replaced by the transistor, Q1. Although the initial circuit provides somewhat higher efficiency, this approach provides sufficient efficiency for this application, with all the power characteristics of the first circuit, but being lower in cost and simpler to construct, which meets the project objectives.

There are many similarities between these circuits. The linear approach is still kept as in the previous circuit. The loop is stabilized with local compensation at the amplifier and the 0.1 µF capacitor filters out the input commands. This is a way that the circuit prevents overshoot that could damage the laser diode. The enable option to the circuit does two things – firstly it turns off the current source by grounding Q1's base and also, at the same time, starving the amplifier's

positive input while biasing the negative input high. This measure also ensures that the amplifier is able to smoothly ramp to the desired output current when the enable is switched low.

With this presented circuit, the current source is possible to provide the DFB diode laser with all the power characteristics that it needs to perform the COFDR interrogation method, while being efficient, low in cost and easy to construct.

Current Source Simulation

The circuit to drive the laser diode was designed to be adequate in the current and voltage to drive the 1550 nm DFB LD module (LDM-1550-DC-1-FA) and also to keep the maximum specifications of the diode into consideration, by not supplying the laser module with too much of either voltage or current. For the input of the current source, which is between 0 V and 5 V, the maximum voltage output across the laser diode should not be more than 1.5 V, as this is the maximum voltage that can be supplied to the laser diode [32].

The simulation was done in LTSpice, with the values of the different components used like in the real circuit. Figure 19 shows the current source circuit that was simulated. A saw-tooth wave was the input to the circuit. The LOAD_DFB_LD is the indicated spot where the laser diode was placed and the where the output values were measured. The laser diode or any diode that had similar specifications as the laser diode was not available in the software. The simulation was run for four cycles (the number of cycles are arbitrary at this point, it is only to see that the characteristic output of the circuit does not change at different cycles, showing there is no saturation of components).

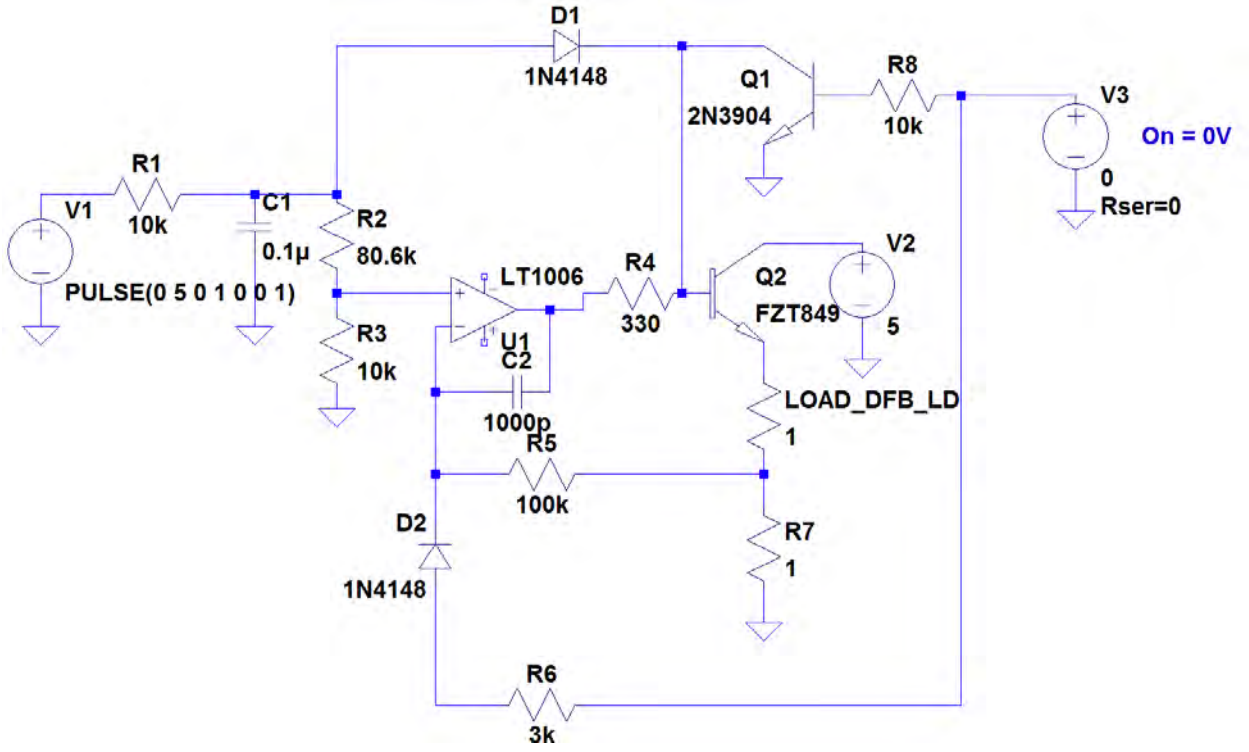

Figure 19: The simulated current source circuit

The input to the system is a saw-tooth wave that was generated from 0 V to 5 V with a frequency of 1 Hz. The wave in green in Figure 20 shows the input to the circuit.

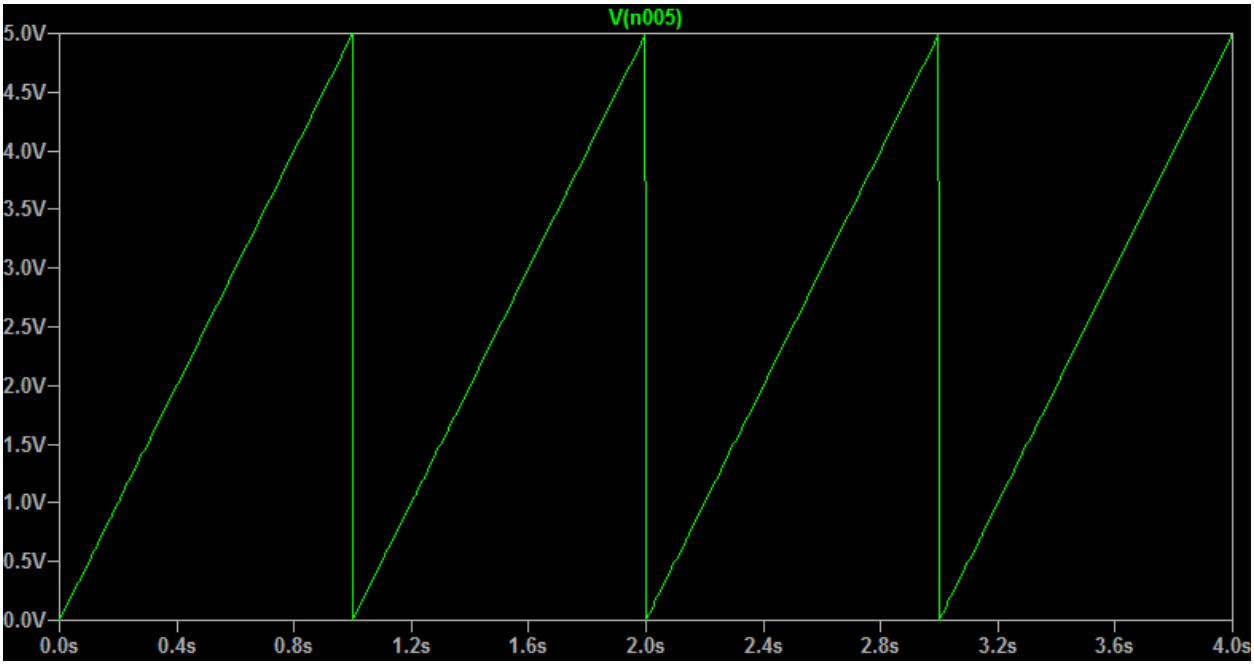

Figure 20: The saw-tooth wave that was the input to the simulated current source

With the simulation of the input starting from 0 V a delay in the switch of the transistors causes a delay in the current provided to the laser diode, as can be seen in Figure 21. For the linear sweeping of the current to be as ideal as possible, it is crucial to make adjustments for this to happen. With the input voltage changed to start at 1 V, this problem is avoided, as seen in Figure 22. Now the linear sweep of the current can be achieved to provide the laser diode to achieve a linear sweep through wavelength.

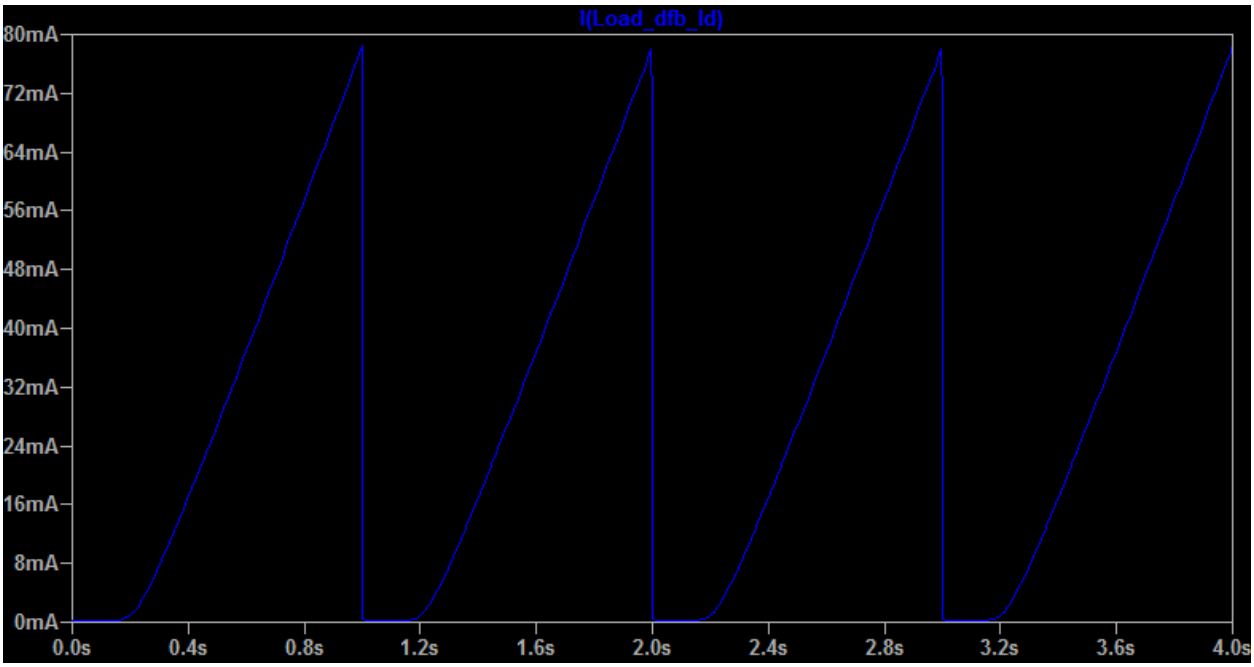

Figure 21: The current through the laser diode with an initial delay

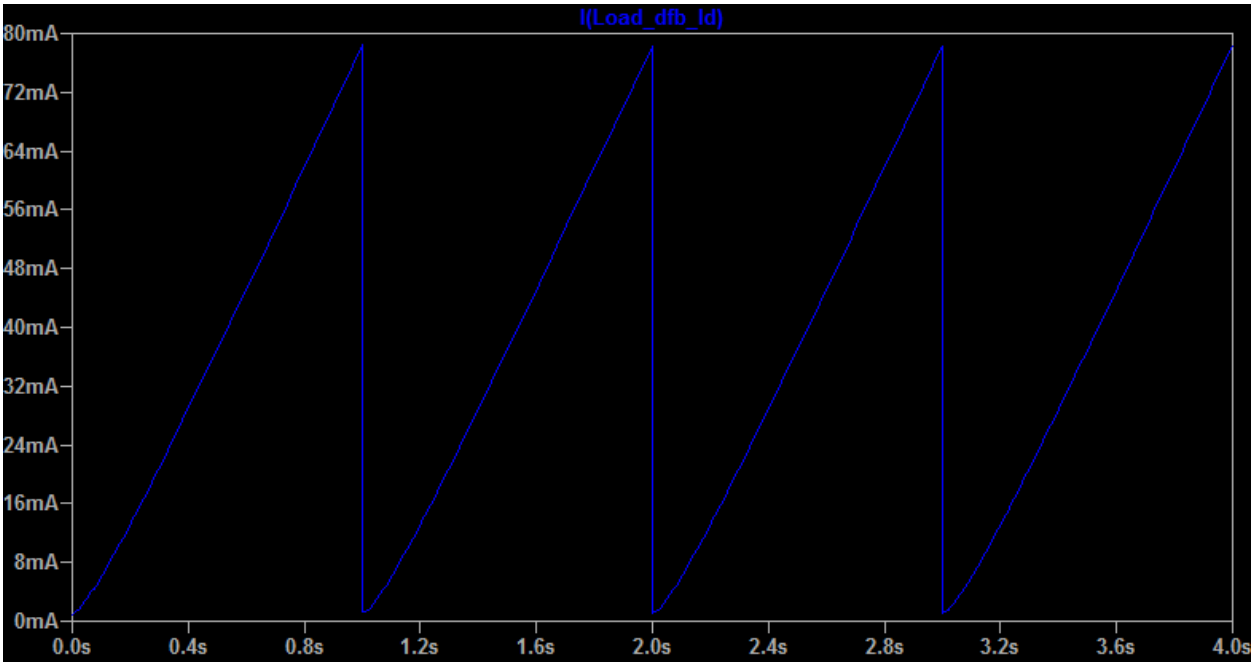

Figure 22: The current through the load resistance (laser diode) with starting input voltage adjusted

The simulated voltage across the laser diode is also measured (the reference is changed to the node below the LOAD_DFB_LD resistor). The resultant voltage can be seen in Figure 23.

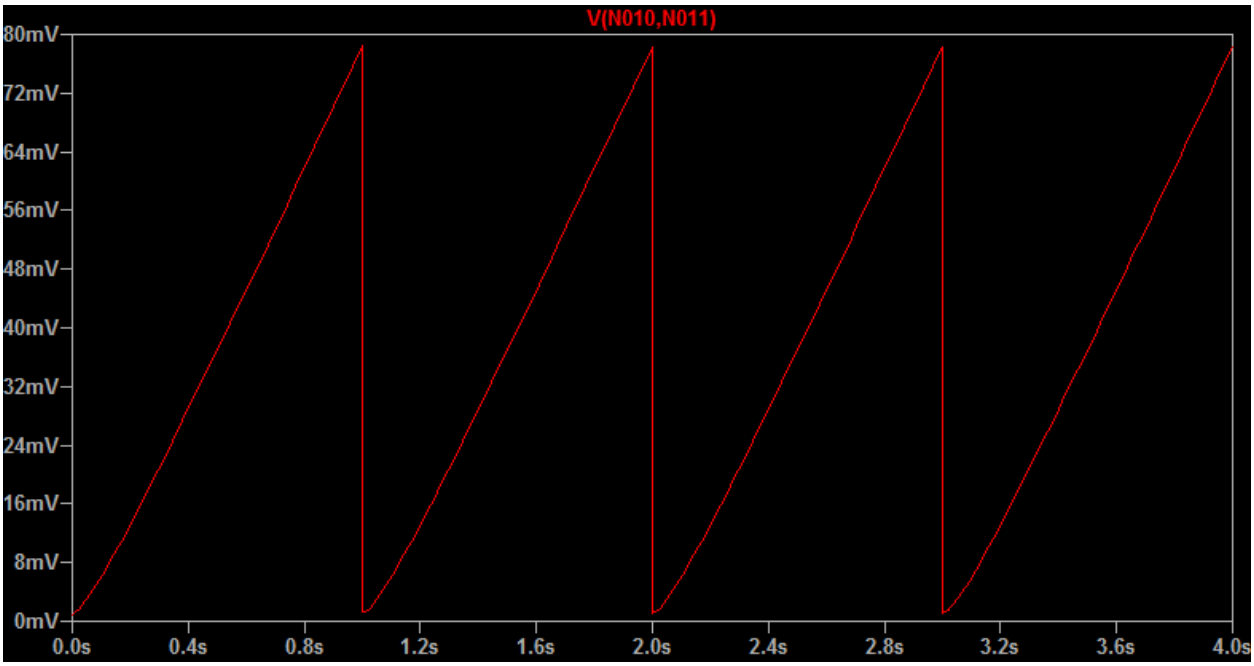

Figure 23: The voltage measured across the load (laser diode)

The simulated output current and voltage characteristics are successful for the operation of the laser diode. Although these are very good results and simulations are great to predict the working of the current source, further experiments were done before the laser diode was introduced to the current source and are further discussed in chapter 6.

Optical System

The first implementation as the optical source of the system, an Erbium doped fibre ring laser is used to test the optical system.

Tunable Laser Source

For the preliminary system, the tunable laser source was created with an Erbium fibre laser, consisting of a laser diode as the light source at 980 nm. From here, a wavelength division modulator (WDM) coupler is used where the light continues to a wound piece of Er^{+3} doped fibre. This Er^{+3} doped fibre is used as the gain medium where the light passes an optical isolator for unidirectional light movement after the Er^{+3} doped fibre. The path of the light then continues to a Fabry-Perot filter where the voltage to the filter is controlled by an external power source that linearly changes the applied voltage to the filter in time. This causes the effect if the piezoelectric mirrors in the filter to change the distance between them, making the filter vary the wavelength in time. Therefore, the source of the system contains the characteristic of tuning the wavelength linearly in time. After the filter, the path continues to a 1x2 coupler – one of the exits is the output of the source and the other continues back to the WDM to the Er^{+3} doped fibre cavity once again, to enhance the stimulated emission of the Erbium doped fibre ring laser.

The Erbium doped fibre ring laser was used for initial design to get familiar with a scanning wavelength source and what characteristics it contained and challenges need to be overcome for the effective use of it.

Air Capillary forming a Fabry-Perot Cavity

To make a good design that is in line with the project objectives, the interferometer needs to be compact. This is done by making the size of the interferometer small by having the reference signal and the sensing signal in one arm.

After the tunable laser source has been implemented through the setup described above, the output of the source continues to the sensor that consists of single mode fibre (SMF) and a capillary of air with another SMF spliced to the end of the capillary. The end of the second piece of SMF is cleaved. This, in essence, forms a Fabry-Perot interferometer. There are three cavities that are formed in this interferometer – the first is the cavity of the capillary, second is from the end of the capillary to the cleaved end of the second piece of SMF. The third is then the combined cavity that is formed by the first and the second. The diameter of the capillary matches that of the cladding of the SMF, which is 125 µm and is 1 mm in length. The length of the SMF piece that is spliced to the end of the capillary varied in the experiments, but was longer than that of the capillary.

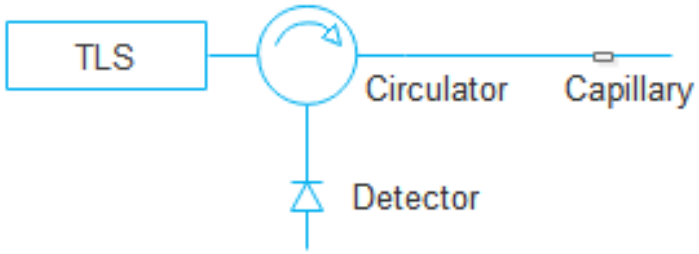

Figure 24: An example of a Fabry Perot interferometer using an air capillary

The expected results from this preliminary design is described as follows: there will be a beat signal generated between the different cavities. This beat signal will contain three different frequency components that can be seen when a Fourier analysis is performed on the beat signal. Although the ideal case of the Fabry-Perot filter will perform a linear scan of the voltage in time and therefore a linear scan in wavelength in time, but due to the real case, there will not be a linear scan of wavelength in time, so the frequency components will not by perfect components, instead it will consist of an energy spread over a few different frequency components, which will cause the results of the system to not be so easily interpreted and also not as accurate as what it can be when only single frequency components are generated.

In this case, the first frequency component (the component with the smallest frequency) will be the component of the capillary, since the length of this cavity is the smallest compared to the others. The cavity of this capillary is also independent of the analyte that will be measured at the end of the cleaved tip, as the interface is always the same – from glass to air and vice versa. This means that this cavity can be used as a reference cavity for the light intensity and with an initial calibration process, becomes intensity independent due to the ratio taken of the magnitude of the reflection of

the capillary that is in no way affected by the analyte and the magnitude taken of one of the other cavities that are influenced by the analyte. When the magnitudes are taken and are used in the interrogation process, the system becomes wavelength independent, since only the amplitude or the intensity is used. Through this, the parameters that could affect the accuracy of the measurements by influencing the wavelength of the system are now excluded from the system. This gives a distinct advantage to the system, as perturbations, such as temperature, will not affect the accuracy of the system.

The reference signal, namely the capillary cavity, has a frequency component, ω_{ref}, which can be written as [28]:

$$\omega_{ref} = \frac{4\pi\gamma n_c L_{ref}}{\lambda_{in}^2} \tag{3.1}$$

and a phase component, ψ_{ref}, which can be written as:

$$\psi_{ref} = \frac{4\pi\gamma n_c L_{ref}}{\lambda_{in}} \tag{3.2}$$

where γ is the scanning rate of the tunable laser source, n_c is the effective refractive index of the fibre, L_{ref} is the length of the cavity and λ_{in} is the initial wavelength. This is similar for all the cavities that are found in the sensor, therefore the frequency, $\omega_{cav\#i}$, of any cavity formed in the sensing arm of the optical fibre and it's phase component, $\psi_{cav\#x}$, can be written as:

$$\omega_{cav\#i} = \frac{4\pi\gamma n_c L_{cav\#i}}{\lambda_{in}^2} \tag{3.3}$$

$$\psi_{cav\#i} = \frac{4\pi\gamma n_c L_{cav\#i}}{\lambda_{in}} \tag{3.4}$$

where $L_{cav\#i}$ is the length of the i^{th} cavity of the system. It can be seen that the length of the cavities determine the frequency and the phase components that are generated and clearly distinguishes the different cavities.

When the capillary is used as reference, being independent of the analyte, the ratio of the magnitude of the resonant reference frequency and either one of the other cavities' resonant frequency magnitudes can be used, therefore:

$$\frac{|A_{cav}|}{|A_{ref}|} = Kr \tag{3.5}$$

where A_{ref} is the reference cavity that is not affected by the analyte, A_{cav} is any other cavity affected by the analyte, K is a parameter of the setup and envelopes specific characteristics of the system. The K value remains a constant for the same system for each measurement and r is the amplitude reflection coefficient dependent of the effective refractive index of the core of the fibre, n_c, and the refractive index of the analyte, n_A, as follows [5]:

$$r = \frac{n_c - n_A}{n_c + n_A} \tag{3.6}$$

which is related to the reflectance, R, by $R = r^2$ and thus gives:

$$R = \left|\frac{n_c - n_A}{n_c + n_A}\right|^2 \tag{3.7}.$$

When the system is being calibrated, to find the value of K, air will be used for the calibration process, substituting r with r_0, since the value of air is known and can be used as a reference, making:

$$r_0 = \frac{n_c - n_{ref}}{n_c + n_{ref}} \tag{3.8}$$

where n_{ref} being the known reference refractive index or in the case of calibration, the refractive index or air, is used.

FC/PC Connected Fibre Piece forming a Fabry-Perot Cavity

There is a major limitation that is present in the discussed systems thus far, namely the refractive index cannot be measured absolutely, meaning that the exact value of the refractive index of the analyte cannot be measured. The refractive index can only be measured relatively to the effective refractive index of the core of the optical fibre. Therefore, if this value is one RIU above the refractive index of the core or if it is one RIU below this refractive index, it cannot be determined which is higher or lower.

To overcome the concern of the absolute refractive index of the substance being measured, further processing of the signal needs to be done. This forms part of the signal processing after the measurements have been taken. When the FFT is done for the beat signal of the different cavities in the system using the COFDR technique, the phase is determined from this measurement. It is found that when the analyte possesses a refractive index that is greater than the refractive index of the core of the optical fibre, then there will be a phase change in the system of π or 180°. Therefore, this forms the solution of determining the absolute refractive index of the analyte.

The final optical design includes using a cavity that is formed by physical contact (PC) connectors in the system. These connectors allow a small portion of the light to be reflected, but it is large enough to have a measurable effect that can easily be used to form a cavity. Angled physical contact (APC) connectors reduce the amount of light that is reflected and will not be used. This provides a method that does not involve a difficult splicing operation to fabricate an air cavity in the sensor, thus allowing an easier fabrication method for the prototype. This provides the system with a low cost Fabry-Perot interferometer. The same method of interrogation and signal processing can be followed as when the air capillary was used to form the Fabry-Perot interference cavity.

Tunable Laser Source

The tunable laser source that was used in the latter part of the experiment was a distributed feedback (DFB) laser diode This source can be adjusted to scan through different ranges and rates and needed to be used to verify that a relatively small scanning range and rate can be used for the COFDR technique that will be used for the interrogation of the system as well as using a different sensor.

Optoelectronics

DFB Laser Diode as Tunable Laser Source

The tunable laser source that will be used is a DFB laser diode that will, with the use of the microcontroller and current source, be swept through current in time. This will cause the output wavelength of the laser to change proportionally to the current that the laser diode is driven with. This is the reason for the custom current source that is built – to properly provide power aspects that will tune the laser.

The light source that will be used is a 1550 nm DFB laser diode - coaxial pigtail, 2mW (PN: LDM-1550-DC-1-FA). Following are a few of the specifications of the laser diode [32]:

Table I: Absolute ratings of the laser diode

Parameter	Symbol	Unit	Minimum	Maximum
Case Operating Temperature Range	T_C	°C	-20	85
Storage Temperature Range	T_S	°C	-40	100
Relative Humidity	RH	%	-	95
Laser Diode Reverse Voltage	V_{RL}	V	-	2
Laser Diode Forward Current	I_{FL}	mA	-	100
Monitor Diode Reverse Voltage	V_{RD}	V	-	15
Monitor Diode Forward Current	I_{FD}	mA	-	2
Lead Solder Temperature	-	°C	-	260
Lead Soldering Time	-	s	-	10

The physical pin layout for the laser is seen in Figure 25 as follows: the first and second pins are for the anode and cathode of the laser diode respectively and the third and fourth pin is for the detector and is for the cathode and anode respectively. The total length of the DFB laser diode 46 mm.

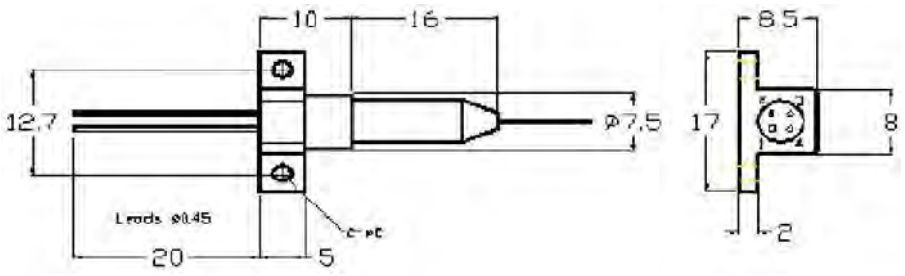

Figure 25: Pin layout and physical measurements of the DFB laser diode [32]

The typical threshold current of the laser is rated at 10 mA and the maximum current of the laser is 15 mA for the laser not to go over temperature, but it is possible for the laser to go to 30 mA. The central wavelength of the laser diode will be around 1550 nm at the maximum current. The operating voltage of the laser is between 1.1 V and 1.5 V. In the following table there are different specifications of the laser diode from the vendor's website:

Table II: Electrical specifications of the laser diode

Parameter	Symbol	Unit	Min	Typ	Max	Test Condition
Electrical Characteristics						
Operating Voltage	V_{op}	V	-	1.1	1.5	
Threshold Current	I_{th}	mA	-	10	15	
				-	30	Over Temperature
Analogue Bandwidth	BW	MHz	1800	-	-	-3 dB
3rd Order Distortion	CTB	dBc	-	-	-60	f1 = 872 MHz f2 = 874 MHz, Over Temperature
Monitor Current	I_m	µA	100	700	-	CW, V_{RD} = 5 V at rated p_0
Monitor Dark Current	I_d	nA	-	-	10	CW, V_{RD} = 5 V
						CW, V_{RD} = 5 V, Over Temperature

Table III: Optical specifications of the laser diode

Parameter	Symbol	Unit	Min	Typ	Max	Test Condition
Optical Characteristics						
Optical Output Power	P_O	mW		2.0		CW, I_{OP} = 35 mA
Slope Efficiency	SE	W/A	0.08	0.1	-	-
Central Wavelength	λ_c	Nm	1290 1530	1310 1550	1330 1570	CW
Spectral Width	$\Delta\lambda$	Nm	-	0.1	1	CW, -20 dB
Side Mode Suppression Ratio	SMSR	dB	30	40	-	
Rise/Fall Time	Tr/Tf	Ns	0.3	-	0.7	
Monitor PD Capacitance	C	pF	-	-	10	V_{RD} = 5 V, f = 1 MHz
Optical Isolation	Iso	dB	30	-	-	

Photodetector

The photodetector of the system have a high bandwidth capability, which makes the photodetector not have to be so specific for the system that needs to be implemented. A note on the signal to noise ratio (SNR) of the detector is the following:

$$SNR = \frac{\eta_{eff} P}{h\nu\Delta} \tag{3.9}$$

Where η_{eff} is the quantum efficiency of the detector, P is the optical power incident on the detector, h is Plank's constant, ν is the frequency of the light, (hν together providing the photon energy) and Δ is the bandwidth of the photodetector. Therefore, for intensity based modulation schemes there

could be some limitations due to the shot noise of the detector [23], because of the statistical nature of the rate of arrival of photons. The minimum observable increment is therefore proportional to the square root of the arrival of photons at the detector in the time interval ($1/\Delta$). If the modulation signal from the sensor is small, the SNR is then reduced.

There could also be some calibration needed for intensity modulation based sensors, due to them not being absolute devices [23].

Optical System Simulation

The simulation of the Fabry-Perot interferometer was performed by using the necessary design elements as described in chapter 3. The simulation was done for the COFDR method using Corning SMF28 telecommunications grade fibre with a tunable laser source operating with a saw tooth tuning rate of 200 $nm.s^{-1}$ between 1505 nm and 1630 nm. A sampling rate of 10 MHz was used.

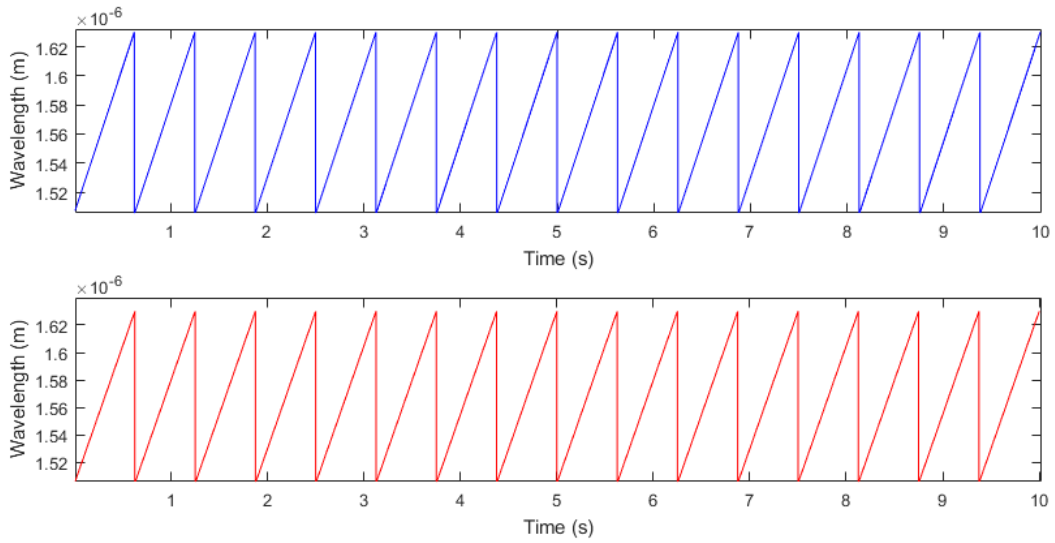

Figure 26: Graphs of the ideal (top in blue) and real (bottom in red) sources

Figure 26 shows the graphs of the generated signals of the ideal linear (top in blue) and nonlinear (bottom in red) sources. For a clearer comparison, Figure 27 superimposes these different generated sources on top of each other and zoomed one cycle. The thicker (red) line shows that the generated wavelengths vary from the nonlinear source, while the thinner (blue) line does not contain this generated error in the wavelengths. The error of the produced wavelength is 1%.

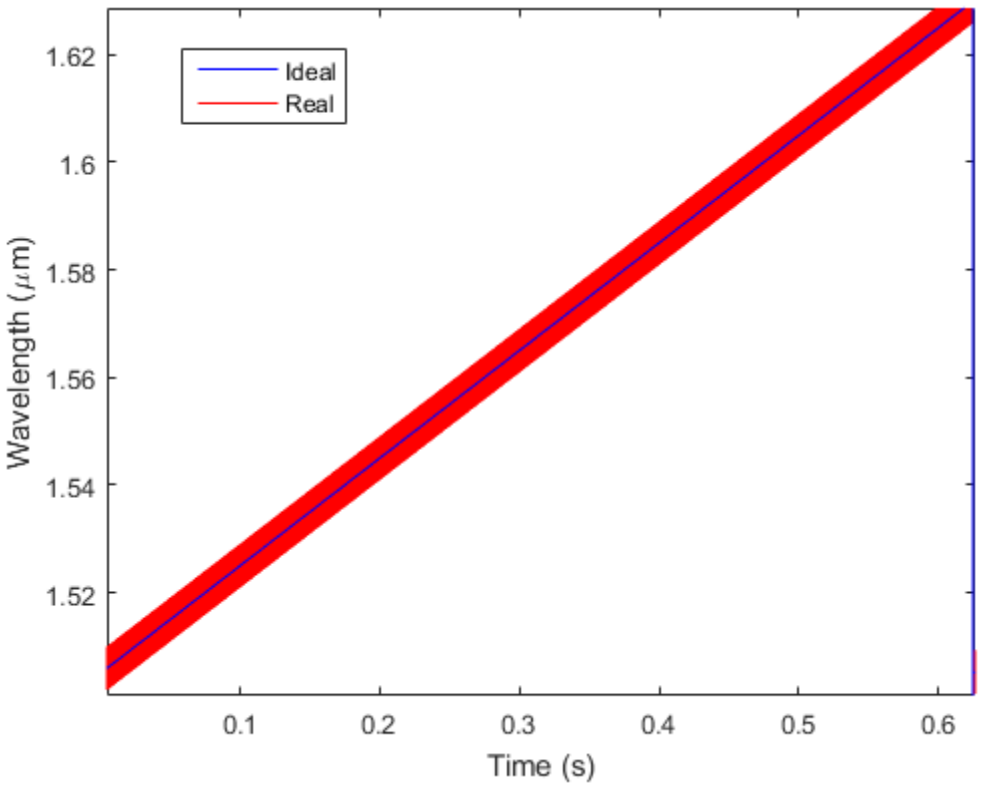

Figure 27: Superimposed and zoomed graph of ideal linear (blue) and nonlinear (red) tunable sources with 1% error

The simulated results from the sources are then used for the generation of the beat signal. Figure 28 shows the different interference patters for the different cases – a) when an ideal linear tunable source is used and the beat signal is sampled with an adequate sampling rate, b) when an ideal linear tunable source is used and the beat signal is sampled with an inadequate sampling rate and c) when a nonlinear (real) tunable source is used and the beat signal is sampled with an adequate sampling rate.

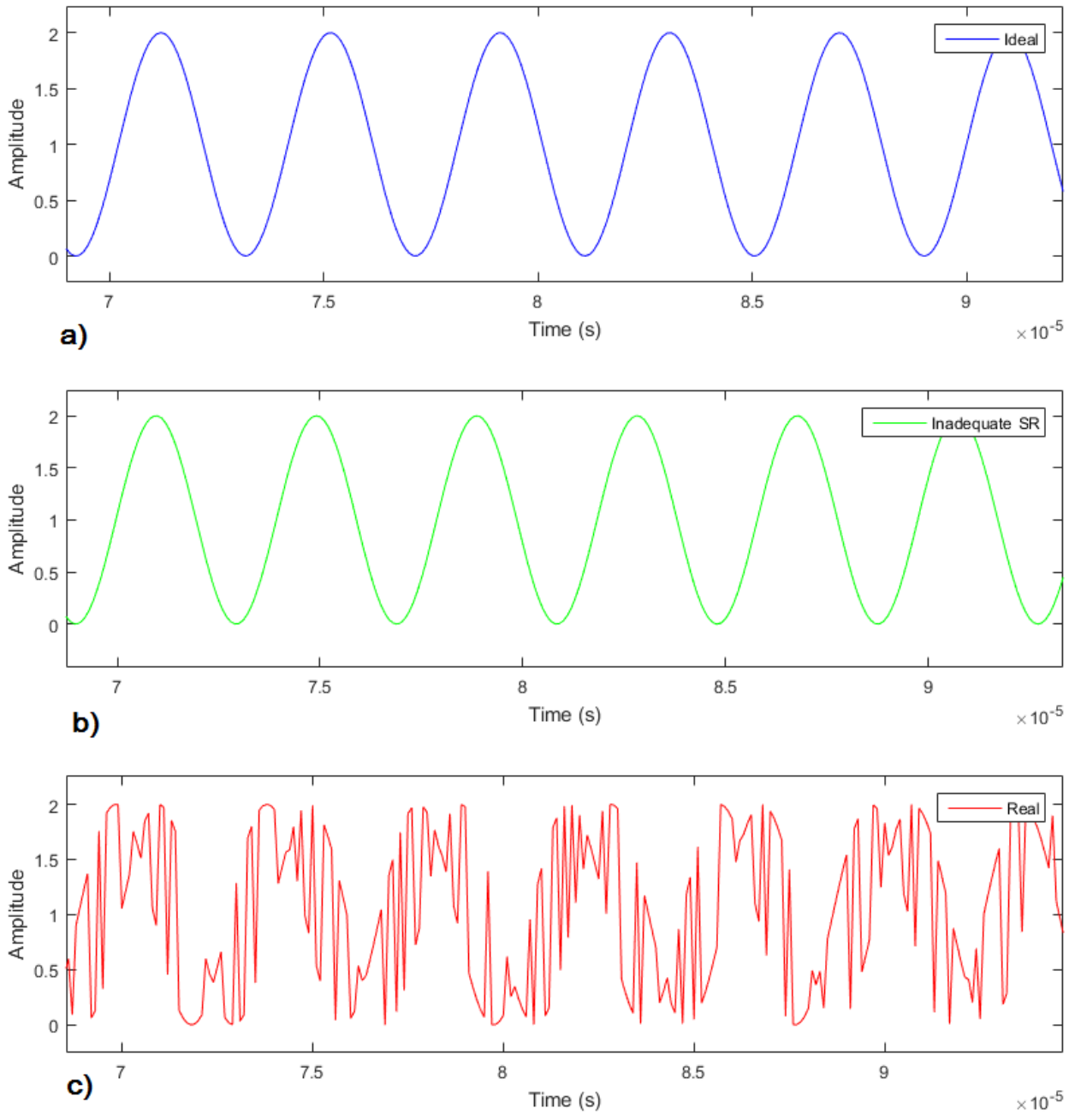

Figure 28: The difference between the interference beat patterns of a) a linear ideal with adequate sampling rate, b) linear ideal with inadequate sampling rate and c) nonlinear with adequate sampling rate cases

For case a) the interference pattern has an ideal shape – such as a sinusoidal signal with a constant frequency. For case b) the pattern seems similar to a sinusoidal signal, but the curves of this signal is sharper than the adequate sampling case. The third is c) when a nonlinear (real) source is used, therefore having a wavelength generation error and causing the beat signal to not have an ideal sinusoidal pattern. The error of 0.005% in wavelength generation is encountered.

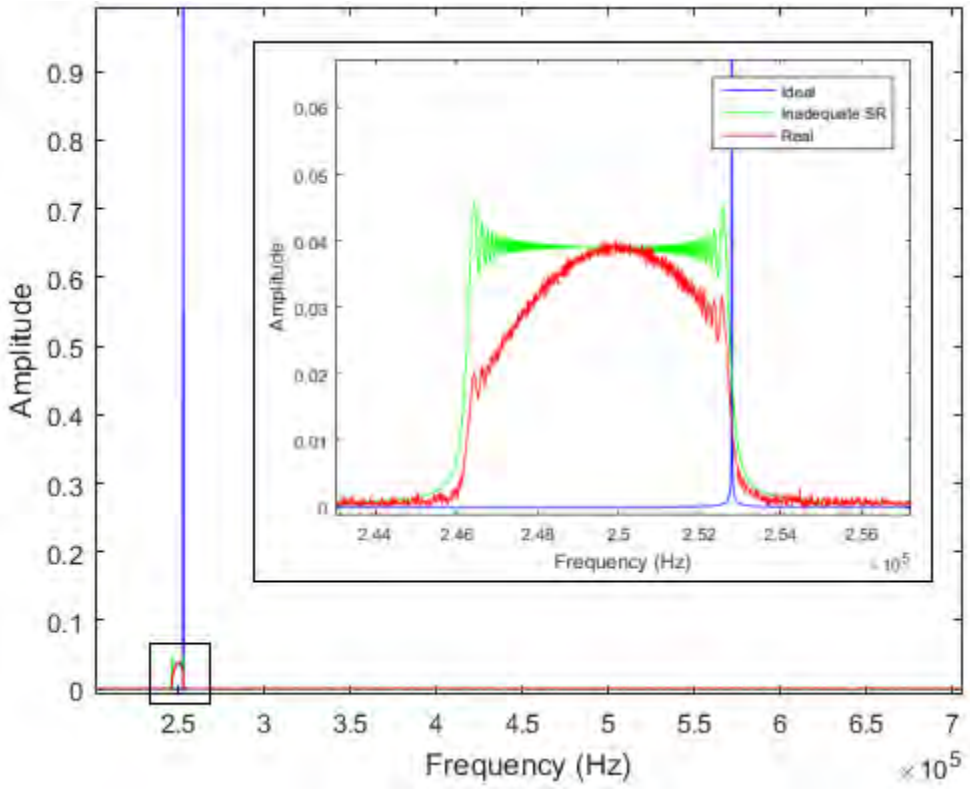

Figure 29: The FFT of the beat signals for an ideal linear source with adequate sampling rate (blue), an ideal linear source with an inadequate sampling rate (green) and a nonlinear (real) source with an adequate sampling rate and error of 0.005% (red)

After the beat signals were generated, a FFT was performed on the different beat signal and the result can be seen in Figure 29. When the ideal linear source is used with adequate sampling of the beat signal, the blue trace is generated. For the ideal linear source with an inadequate sampling rate of the beat signal, the green trace is the result and when the nonlinear source is used with an adequate sampling rate of the beat signal, the resultant trace can be seen in red. The nonlinear source has a wavelength generation error of 0.005%.

The magnitude of the ideal trace is much larger than those of the inadequate SR and real traces, with the magnitude located at a single frequency. The magnitudes of the inadequate SR and real traces are smaller and are spread out through difference frequencies. The simulated results in Figure 29 of the inadequate sampling rate using an ideal linear source and adequate sampling rate using a real (nonlinear) source with a sweep error rate of 0.005% show the importance of the recovery of energy. The ideal source with an adequate sampling rate has a magnitude of 0.9978 situated at 25281 Hz. The spread of the inadequate sampling rate spans a frequency range from

24644 Hz to 25259 Hz with a 615 Hz step interval and with a maximum amplitude of 0.0458 and the nonlinear source ranges in frequency from 24658 Hz to 25263 Hz with a frequency step interval of 610 Hz with a maximum amplitude of 0.0113.

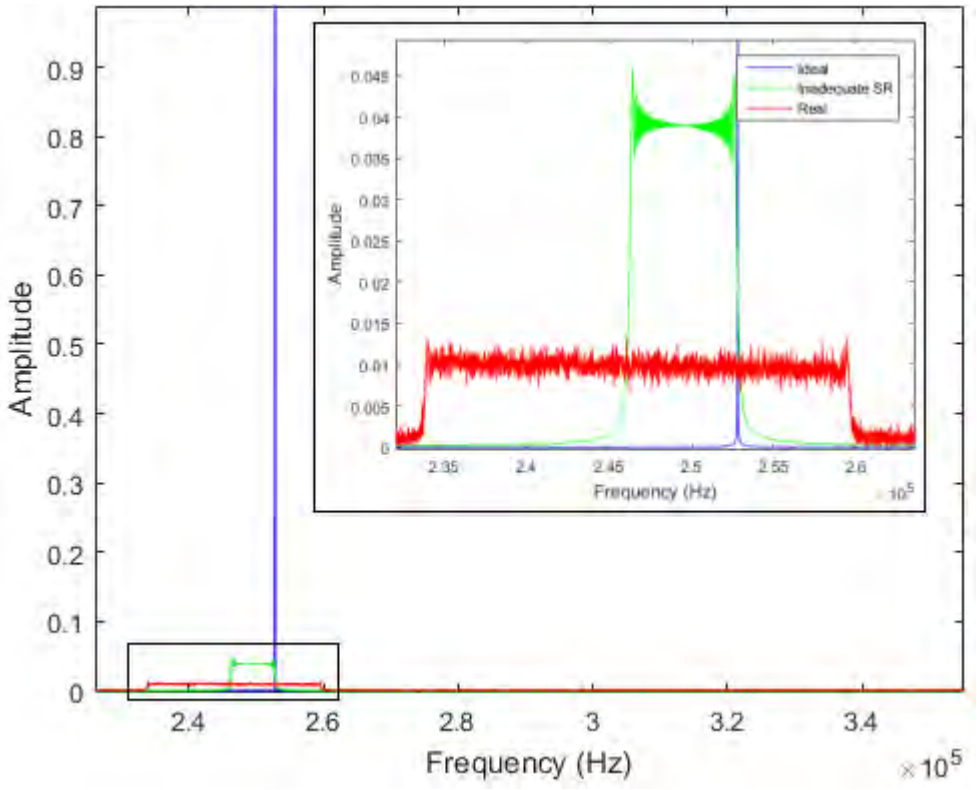

Figure 30: The FFT of the beat signals for an ideal linear source with adequate sampling rate (blue), an ideal linear source with an inadequate sampling rate (green) and a nonlinear (real) source with an adequate sampling rate and error of 1% (red)

Figure 30 is an example of how the energy spread changes when a wavelength error of 1% is used for the tunable source. The spread of the inadequate sampling rate has the same frequency range from 24644 Hz to 25259 Hz with a frequency step interval of 615 Hz and a maximum amplitude of 0.0458 and the nonlinear source now ranges from 23401 Hz to 26658 Hz with a frequency step interval of 3257 Hz and a maximum amplitude of 0.0113. The spread of the energy though different frequencies have increased dramatically with the wavelength generation increase of the source.

The main area of the spread in frequencies in the simulated signals are first analysed. The Gaussian distribution model is taken and applied to the energy spread over the range of frequencies. The reason for the use of the Gaussian probability distribution function is because all the frequencies in the area of spread have the same amount of probability of occurrence. Although the model of

the Gaussian distribution is used, the curve has to be fitted to the data, not making it a real Gaussian probability distribution model, since the total energy spread over the frequencies will not necessarily always be equal to one [33]. The curve is then fitted to the data by adjusting the height of the Gaussian distribution model to a factor that is in relation to the mean of the sampled data. Figure 31 shows the filtered data and Gaussian distribution. Although it seems that the mean is a bit low, there are zero elements that are not displayed, thus lowering the mean to the top of the shown distribution.

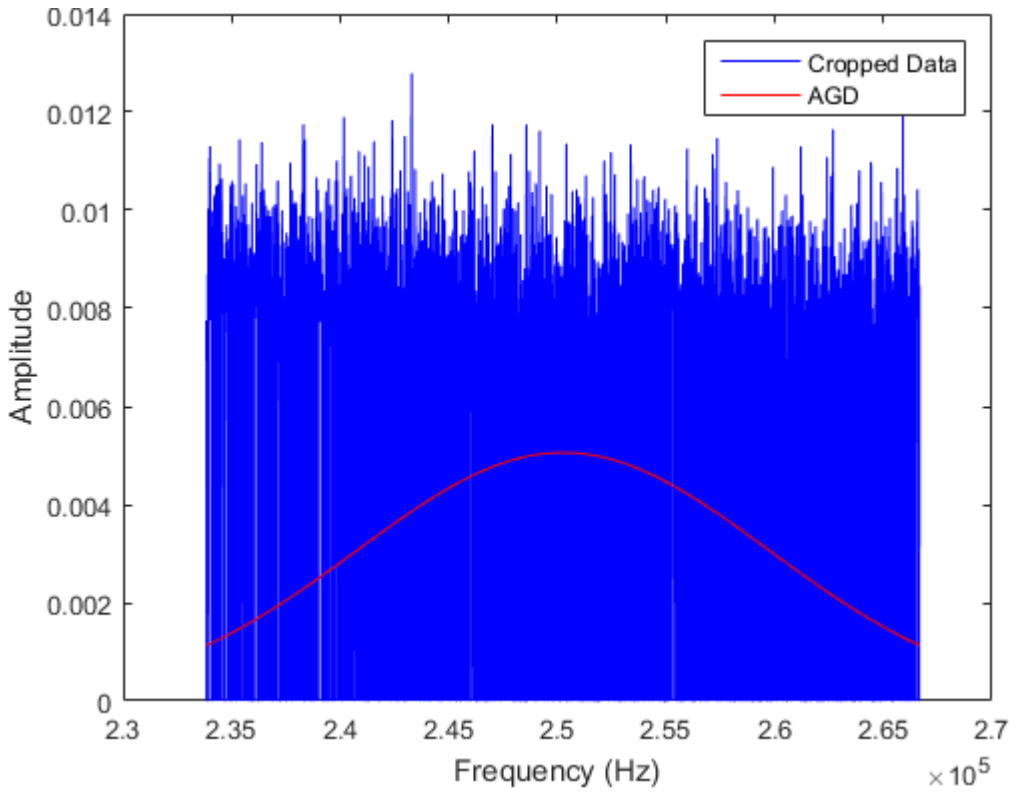

Figure 31: Filtered data (blue) with adjusted Gaussian distribution (AGD - red)

For the calculation of the energy that is contained under the curve, the integral is taken of the values under the curve from the point of –σ and σ, where σ is the standard deviation of the spread frequencies. The total energy is now kept constant as the variance of the distribution model is made smaller, to simulate the decrease in the frequency spread.

As a result of the variance being reduced, the energy spread is reduced and the energy is recovered at a specific frequency. Figure 32 shows when the variance is adjusted to a values of 25 x 10^6 smaller than the original variance.

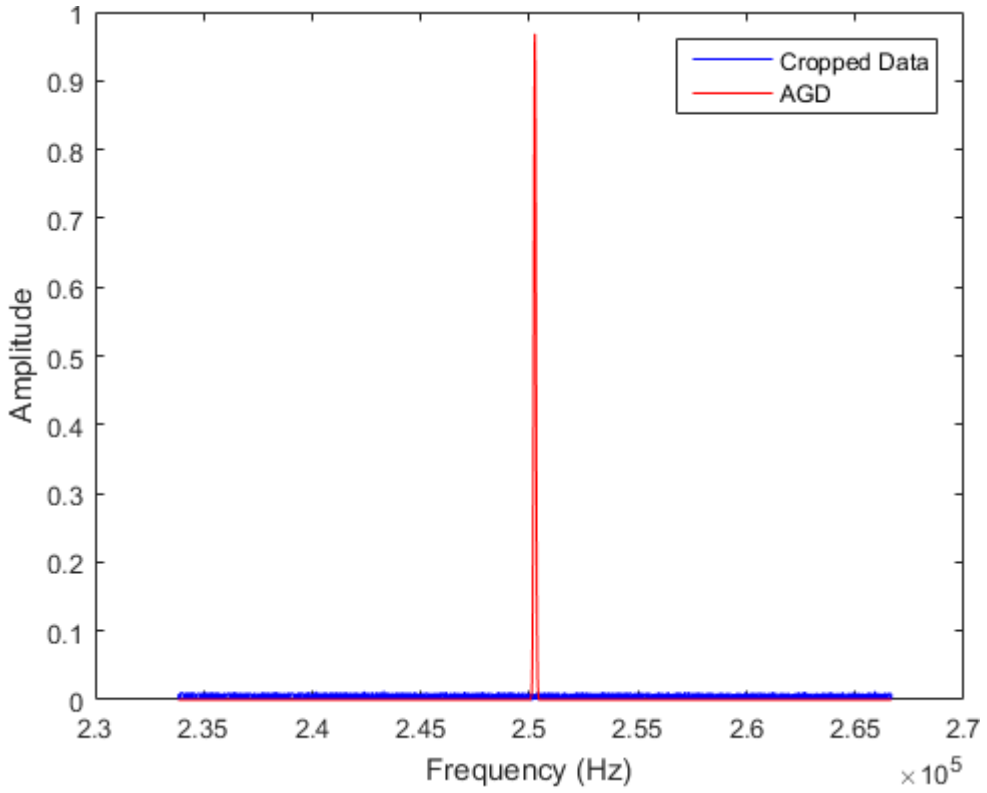

Figure 32: Energy recovered from frequency spread by reducing the variance of the energy spread. The blue is the spread energy that was filtered and the red indicated the adjusted Gaussian distribution (AGD)

This result shows that the magnitude that is recovered is not exactly equal to the ideal signal when there is no error in the tunable wavelength source. Figure 33 shows where the maximum magnitudes of the ideal (blue) and recovered (black) signal is marked. This is due to the some of the energy lost due to the limited frequency band that was considered. The frequency that is recovered differs from the ideal frequency due to the Gaussian distribution model used that centres the sample and to the randomness of the errors generated from the tunable laser source.

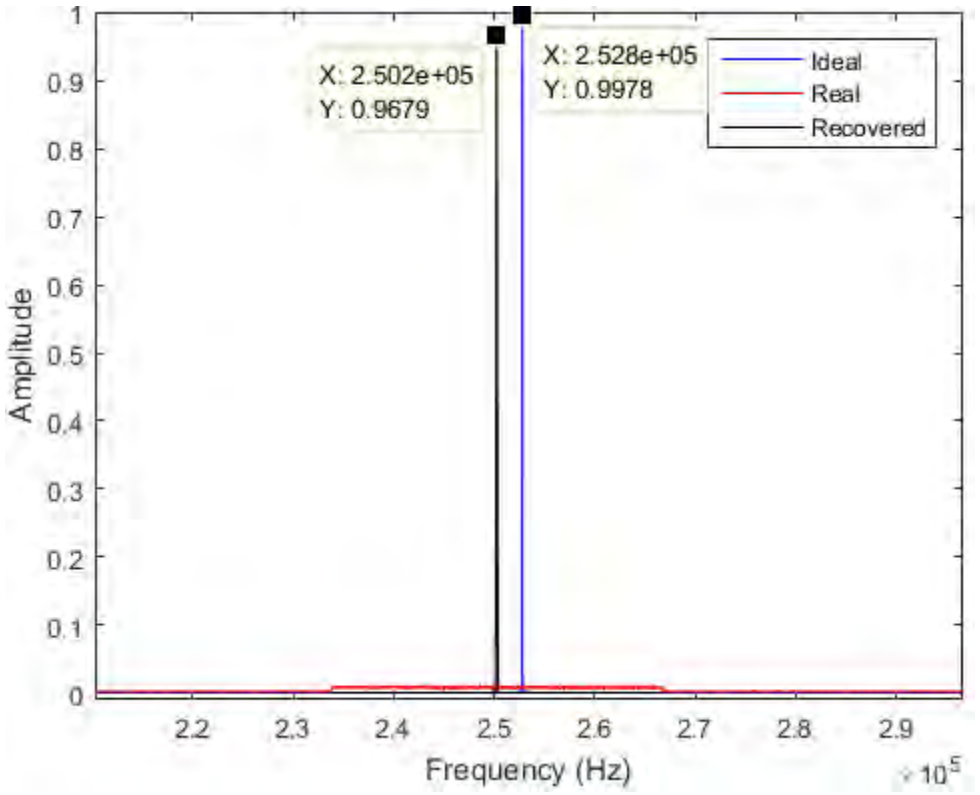

Figure 33: Comparison of the ideal (blue), nonlinear (real in red) and recovered (black) signal

The energy that has been recovered is now located at a single frequency of 25028 Hz with a magnitude component of 0.9679, whereas before it was located between23401 Hz and 26658 Hz that spanned a frequency interval of 3257 Hz with a maximum amplitude of 0.0113.

This linearization algorithm can be used for systems that have a larger scanning range, where the frequency spread would occur as in the presented simulation. The system that is desired to be implemented with a DFB laser diode and the electronics to drive the optical source accurately, should have an expected scanning range of approximately 1 nm. The desired system is now simulated with a scanning rate of 1 $nm.s^{-1}$ (the modulation frequency that will be implemented by the electronics), with a scanning range between 1550 nm and 1551 nm (the expected scanning range of the DFB laser diode). The sampling frequency of 10 MHz is kept the same. Figure 34 below is the simulated ideal and real life case results of the system implemented with the DFB laser diode.

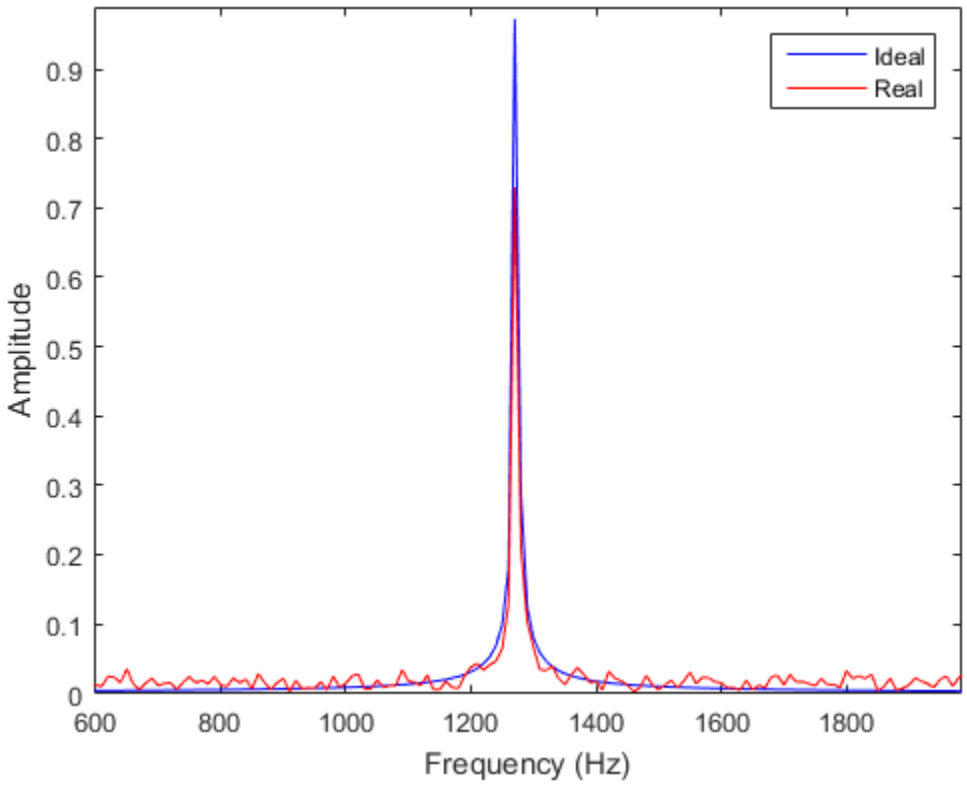

Figure 34: The simulated FFT results of the desired system to be implemented

It can be seen that the peak of the real results (blue) have a higher magnitude at the specific beat frequency as the real case (red). This is expected due to the energy spread that occurs over a range of frequencies for the real case, because of the non-linear scanning of the optical source. The energy is spread to the sides of the peak and the frequencies to the left and right of the peak seem noisier for the real case. Although there is a loss of energy, there might not be a need for linearization if the outcome of the results are as the simulated results above for the desired system. If there is a major loss in energy and a big variance in the frequencies when the FFTs are performed with the real implemented system, a linearization algorithm can be performed like the suggested algorithm above, but otherwise, considering the small frequency scanning range of the DFB laser diode, the results can be processed as the simulated results in Figure 34 suggests.

Conclusion

In this chapter the designs of the different parts of the system are given. This progressed to a smaller sensing system, a Fabry-Perot interferometer, which contains the sensing and reference cavity in the same arm, making the system more compact. First the reference cavity of the Fabry

Perot interferometer was formed by an air capillary that was spliced between two pieces of single mode standard telecommunication fibre. This provided a high power reflection for the reference cavity that can be used for the calculation of the refractive index of the analyte, but the fabrication of this sensor is more difficult to perform. Finally, the Fabry-Perot cavity was formed by a piece of single mode telecommunication fibre that was connected with a PC connector tip. This provided an easier fabrication method for the sensor.

The tunable laser source that was first used was the Erbium doped fibre ring laser. This tunable laser source contained many different components to achieve the scanning of wavelength and also added challenges to the signal processing. As the scanning was not done completely linear, linearization had to be done for better results. The final design of the tunable laser source was the DFB laser driven by a custom made current source and microcontroller.

The simulation for the current source was done using LTSpice and yielded the desired results to drive the laser with stability and keep the laser within the maximum boundaries of the power specifications to avoid damage. With these results the operation of the DFB laser diode will not only be successful, but also prevent any damage that could occur to the laser diode which will result in extra cost to the project. This is a very important implemented property, as the laser diode is an important and expensive component in the circuit and the safety of it is vital to the project and the prototype being created.

The simulation of the optical system, with the real case included, gives an idea of what to expect when the experiment is conducted. There will be a spread in frequency in the beat signal due to the non-linear properties of the laser source. This might be a big factor on the accuracy of the results on the system, but as the latter part of the simulation suggests, the DFB laser diode, with its small scanning range, might not contribute to a big spread in frequency. The proposed method supplies a solution to deal with this spread in frequency if the need arises to apply the linearization algorithm.

Chapter 4: Experiments

Introduction

In this section, the experiments will be described that were undertaken by the different systems and the experimental results will also be discussed in the next chapter. There are various experiments that have to be conducted in order for all the different parts of the prototype to fit and function together.

The experiments include the optical experiments that need to be conducted to investigate and improve the refractometer's performance through the use of the signal processing methods, but before the optics can be use, the electronics must be setup to control the optical subsystems. It is the electronic aspect that is used for the control of the laser diode that is used for the linear sweeping of the wavelength in time.

A microcontroller will be implemented for the control of the current source. The microcontroller needs to control voltage input to the current source. The current source drives the laser, providing sufficient power characteristics for the laser to sweep the wavelength to perform the COFDR method that is implemented for interrogation.

The prototype uses all the subsystems to successfully measure a refractive index. All the subsystems functioning together, with accuracy, as well as a compact package, will result in a good prototype.

Preliminary Experiments

The preliminary experiments were conducted to test each piece of the prototype and to see if the different ideas and subsystems would work. The optical parts are focused on such as the sensor – as it should be an inline sensor, with a fabrication method that would not be expensive or require an extensive procedure to produce.

For the electronics of the system, the microcontroller should be tested for the stable control of the current source. The stability and linear sweeping of the voltage, in this case done by the microcontroller, is crucial, since this will ultimately mean that the laser sweeps as ideal as possible

linearly in wavelength. The linear sweep of wavelength will cause a beat signal to be generated from the reflection of the cavities in the sensor. These beat signals will generate an interferogram – a combined interference pattern from all the reflections in the sensor. These interference patterns that are generated look like sinusoidal waves in an ideal case, having a single frequency component for each cavity. Since the frequency of the beat signal is dependent on the range of wavelength that is scanned by the laser, the scanning rate of the wavelength and also the length of the cavity, each cavity will generate a unique frequency that can identify that cavity. If the sweeping of wavelength by the laser varies too far from linear, the phase of the wave will change, meaning that these ideally sinusoidal patterns will contain different frequency characteristics, where it should only have a single frequency element. Therefore, the magnitude of the frequency components will decrease and broaden in the frequency domain, causing a loss of accuracy.

The current source should be tested to turn on the laser correctly, control the laser with good stability and to not destroy the laser by feeding it more than the maximum power specifications. Also, the current source should be tested with the laser to analyse the characteristics of the laser so that the laser can be used optimally with the COFDR method.

Air Capillary forming a Tip Sensor

The experimental setup included a scanning wavelength optical source which consisted of a 980 nm optical source that is connected to a 2x1 wavelength division multiplexer (WDM) that then continues to a wound piece of Erbium doped fibre (EDF), as seen in Figure 35. The 980 nm light source is used as a pump for the EDF laser. This light source excites the Erbium ions in the fibre to the state where, firstly spontaneous emission occurs, and then with a greater pump, stimulated emission occurs, in the 1550 nm wavelength region. The light then passes the optical isolator and continues to the filter, now being in the 1550 nm wavelength region.

The filter that was used was a Fabry-Perot filter controlled by a voltage source that sweeps linearly through voltage in time. The Fabry-Perot filter then causes the light to vary in wavelength in time as the voltage is swept in time. This effect is done in a linear fashion, but in essence it is not a purely linear sweep in time and causes the non-linear effects that is discussed in the COFDR method of interrogation. This swept light then continues to a 1x2 coupler, where one of the arms travels back to one of the inputs of the WDM, where it contributes to the enhancement of the

stimulated emission. The arm that is labelled as the output continues as the light source for the sensor. The experimental setup up and till the description of the coupler acts as the scanning wavelength optical light source.

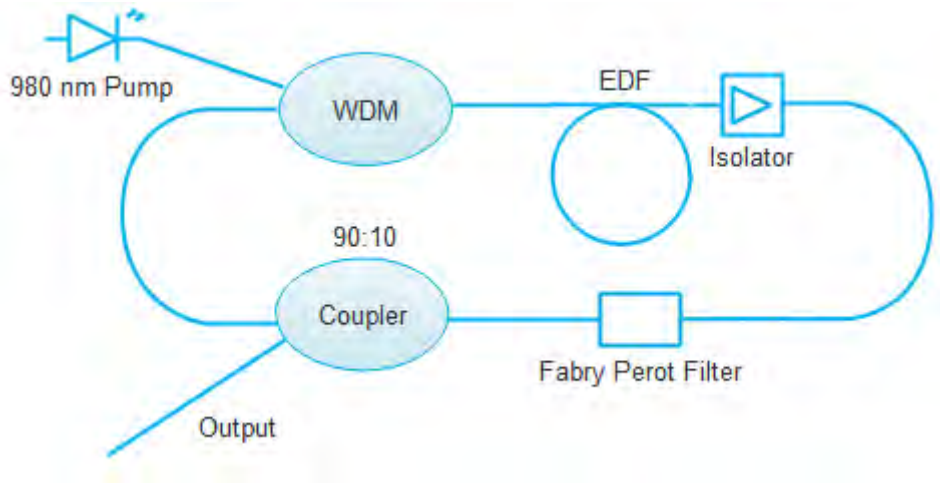

Figure 35: Experimental setup of the tunable laser source

Figure 35 shows the experimental setup of the tunable laser source. In it there is a coupler with a 90:10 ratio, meaning that one of the exit arms contains 90 % of the output power, the other exit arm contains 10 % of the output power. The 10 % output of the coupler that doesn't return back to the WDM continues to the piece of optical fibre containing the sensor, in other words, only 10 % of the power is used by the sensor, the other 90 % returns to the WDM to contribute to the pumping and enhancing the stimulated emission of the EDF laser.

This preliminary experiment was conducted with a sensing tip utilizing an air capillary. Fabry-Perot cavity. The cavity consisted of an air capillary that was spliced to two ends of a SMF and being 1 mm in length. An example of the probe is seen in Figure 36. The end of the SMF was cleaved.

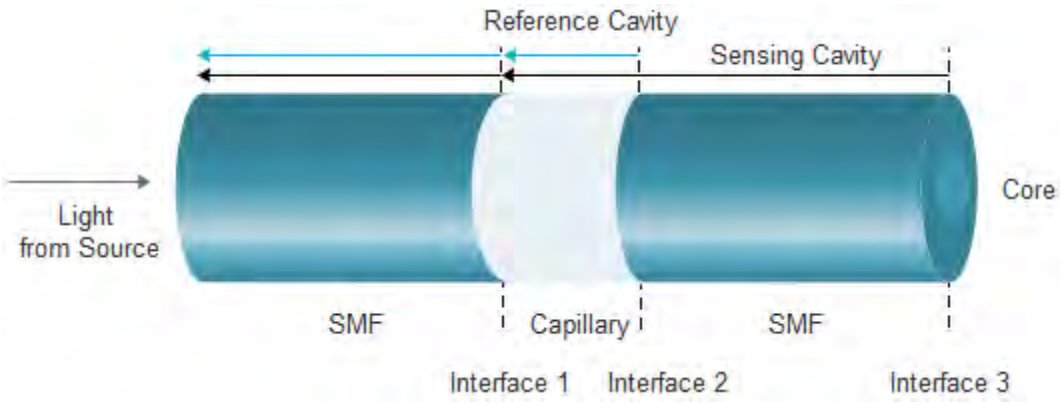

Figure 36: The sensing probe

Fabry Perot cavities are formed by the Fresnel reflections from the different interface changes. A reference cavity is formed from the air capillary. The reflection from the first and the second interface interfere and this produces a reference beat signal. Two sensing cavities are formed and both utilize the end of the fibre probe (interface 3) – one sensing cavity is then formed with the first and third interface and the other sensing cavity is formed with the second and third interface. Both the sensing cavities produce a beat signal that will superimpose with each other and the reference beat signal. Either one of the sensing cavities can be used for the calculation of the refractive index of the analyte.

The cavities that are seen in Figure 36 work with the COFDR method as follows: with each interface change in the sensor there will be Fresnel reflection that takes place due to the refractive index change between the two interfaces. There are three interfaces in the sensing probe – the first interface is encountered at the splice between the first SMF and the capillary. The medium changes from silica to air. The second interface is where the second piece of SMF is spliced to the capillary. The medium changes from air to silica. The third interface change is at the cleaved end of the optical fibre probe. The medium thus changes from silica to whatever substance is at the end of the tip of the sensor, giving the reflection needed for the measurement of refractive index.

The fibre containing the capillary was then used as a probe and dipped into different liquids. The first measurements were taken in air, alcohol and water. Figure 37 shows the experimental setup of the Fabry Perot interferometer.

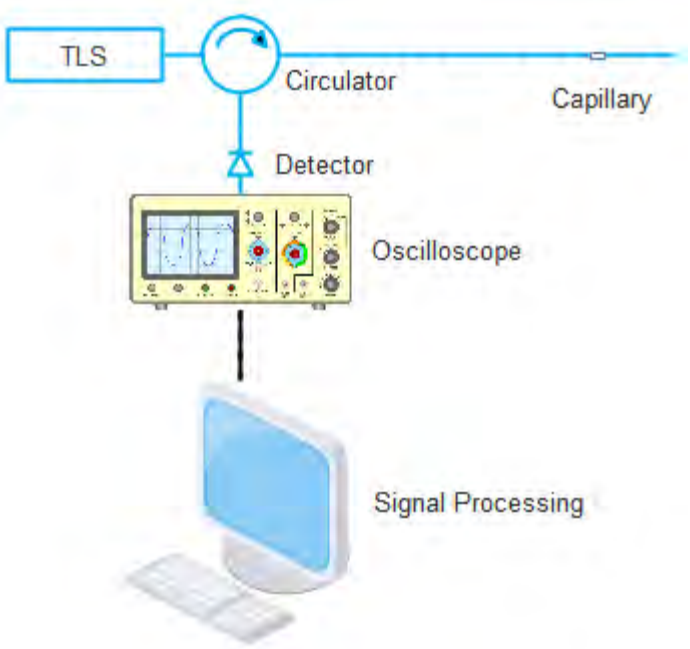

Figure 37: Experimental setup of the sensor system

The expected results of the system is that there will be a global interference pattern formed from three sinusoidal waves due to the interference between the interfaces of the fibre sensor. These interfering waves will contain different frequency components depending of the different sizes of the cavities that they form, the speed of the scan of the tunable laser source and the range of the scan in wavelength of the tunable laser source. The smallest cavity will produce the lowest frequency component and the biggest cavity will produce the highest frequency component. It is expected that there will be three main frequency components that the signal comprises of – one for the capillary, the other for the cavity that is formed between the capillary and the cleaved end of the fibre tip and another cavity that is formed due to the combination of the other two cavities. Although there should be three distinct frequencies in the spectra, it might be difficult to view as the optical source that scans through wavelength in time does so in a non-linear manner, making the results more unclear and adding different frequency components to the system, broadening the energy spread of the three main frequency components. The resultant wave holds the information of the system is to be processed to extract the information of the system.

FC/PC Connected Fibre Piece forming a Fabry-Perot Cavity

For this experiment, a piece of single mode telecommunication fibre is connected at the end of the second port of the circulator, being the start of the sensing arm. This piece of optical fibre forms a cavity, much like the air capillary in the previous experiment. Figure 38 shows an example of a FC-PC fibre connector and the appropriate adaptor used.

Figure 38: FC-PC fibre connector and adaptor

The difference is that the cavity is now formed between the physical contact (PC) connectors – not using the angled physical contact (APC) connectors – since the PC connectors provide more reflected light. Figure 39 shows an example of a PC connection between fibres. This piece of fibre that is simply connected to the system, provides a low cost and easier fabrication method rather than the difficult splicing fabrication that has to be done for the air capillary to form the reference cavity.

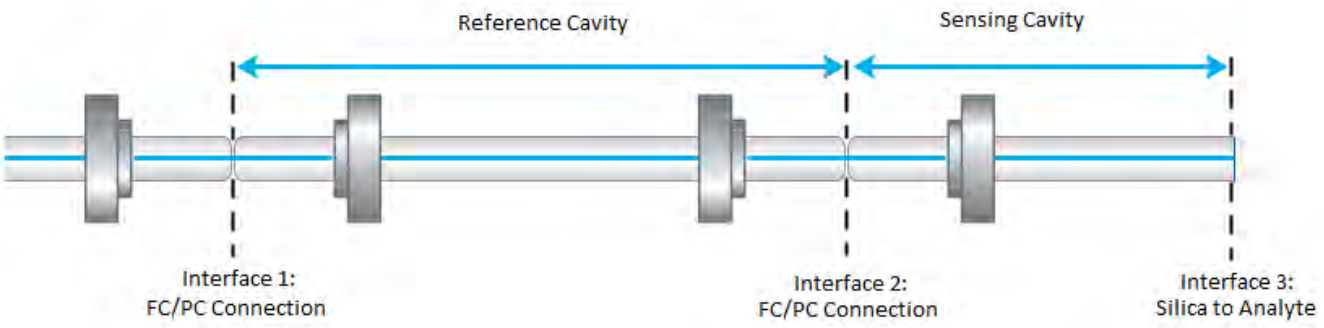

Figure 39: FC/PC fibre tip connection

Current Source

The laser source that is used in the experiment with the air capillary is a bulky laser. The Erbium doped fibre is small, but the Fabry-Perot filter with the voltage source is big and cannot be implemented in the prototype. Therefore, a different power source is needed for the prototype, which is more compact with good stability and power characteristics.

The current source that was designed and built needs to be tested before the connection to the DFB laser diode is made, since the laser diode is vital – without the laser the system will not work, therefore the tenability of the laser is critical in the performance of the fibre refractometer. Also, the laser is one of the expensive components in the system and care should be taken that the laser diode is not damaged or destroyed.

Although the simulation of the current source yielded good results, it is vital to build and test the circuit before it is implemented with the microcontroller or the laser diode, since the microcontroller will be controlling the input voltage to the current source. The microcontroller can be used to control the current source specifically, making the power source more intelligent than the Fabry-Perot filter implementation.

The current source is connected to a power supply that can provide the circuit with specific and accurate current and voltage. This is necessary, since the input voltage is directly proportional to the output current that will be supplied to the laser diode. Too much current and the laser diode can be damaged or destroyed, therefore, normal diodes or a low resistance resistor can be used for the testing of the output current with a multimeter in series with the diodes, to measure the exact output current that is provided to the diode.

The operating voltage for the laser diode is between 1.1 V and 1.5 V and the threshold current is typically 10 mA to maximum threshold current of 15 mA. The maximum current of the DFB laser diode is 100 mA. Thus the output of the designed current source must possess these characteristics. Figure 40 shows the experimental setup of the designed current source to drive the laser diode.

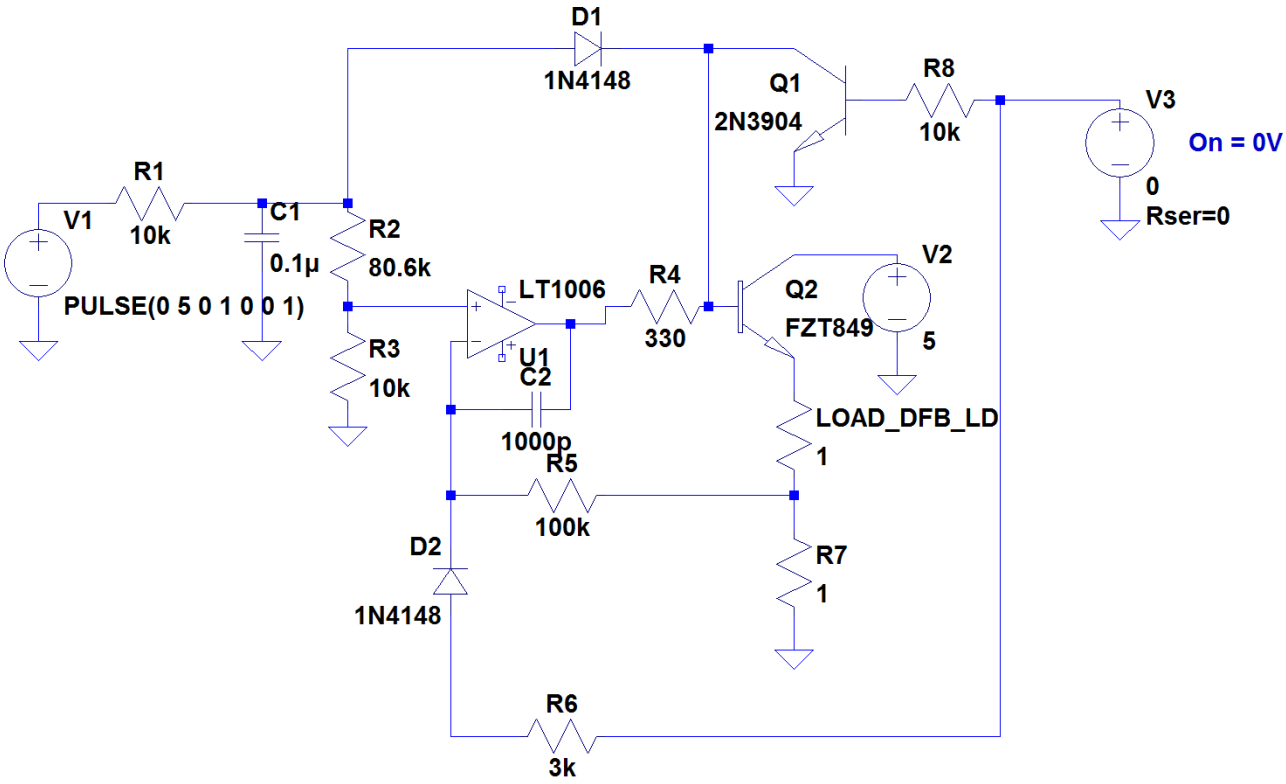

Figure 40: The setup of the designed current source

All the components with their respective values were used as shown in Figure 40. With the use of the LT1006 operational amplifier and the FZT849 transistor, the output current that can be achieved should be up to 500 mA [34] [30].

The current source must first be tested by a laboratory power supply that has stable output characteristics. This is done to see if the output of the laser is linear and does not fluctuate. After the current source is tested or characterized with the laboratory power supply, the more important test must be done with the microcontroller and the current source. This is divided in two parts – the first is to characterize the analogue output of the microcontroller itself, to know what the input to the current source will be. The analogue output of the microcontroller is used to modulate the current of the laser diode. The second will be to test the microcontroller with the current source

and view the results of the change in input voltage to the current source from the microcontroller. After this is successfully done, then the input to the laser can be strictly controlled.

Laser Characterization

The source of the prototype will be implemented using a DFB laser, as opposed to a EDF with a commercial Fabry-Perot filter that is voltage controlled, that have been used up to this point. A microcontroller is implemented to modulate the voltage supplied to the current source, via the analogue output of the microcontroller. This voltage is the input to the current source that then drives the laser according to this modulated voltage input from the microcontroller. For the DFB laser source to be properly controlled, it must be known what the output characteristics of the laser will be with the microcontroller that will be used for the voltage control of the input to the current source.

The output of the laser source is vital, as this controls the interrogation method and the accuracy of the system. The characteristics of the laser needs to be tested for when the laser will start lasing and where the most stable wavelength output will be in relation to the input of the current source.

For the implemented COFDR method, the laser will scan in a saw-tooth fashion through wavelength in time. Each cavity in the system will produce a reflection. This will cause an interferogram – a pattern generated from each reflection in the sensor. If these scans are ideal, meaning that they are perfectly linear, each cavity will produce a single frequency component. This can be seen by a single peak when a FFT is performed on this reflected interference pattern – also known as a beat signal. If the scan of the wavelength through time by the laser is not linear, the phase of the electromagnetic wave will change, causing more frequency components to exist in the interference signal. This means that the main frequency components will broaden, causing the magnitudes to decrease. This means that the accuracy of the system will decrease, because the exact frequency component cannot be determined. The more stable the output of the laser is and the better this can be controlled, the better the results will be in terms of accuracy and effort in signal processing, resulting in a possibility to not apply much linearization to the system.

The Final Experiment: The Integrated Prototype

For the final experiment, the prototype needs to be tested with all the different subsystems integrated, as if the prototype has been commercially produced and now being deployed to the field for application. The entire system must work as a whole – the microcontroller must control the voltage input which will control the current source, which will in turn control the laser and the output characteristics of the laser. The laser must then scan linearly through wavelength in time, which will enable the application of the chosen interrogation method – coherent optical frequency domain reflectometry. The sensor system consists of two pairs of physical contact connectors forming a Fabry-Perot cavity, with the end of the fibre sensor cleaved forming an inline sensor architecture. Figure 41 shows the final system, with all the subsystems fitting in place.

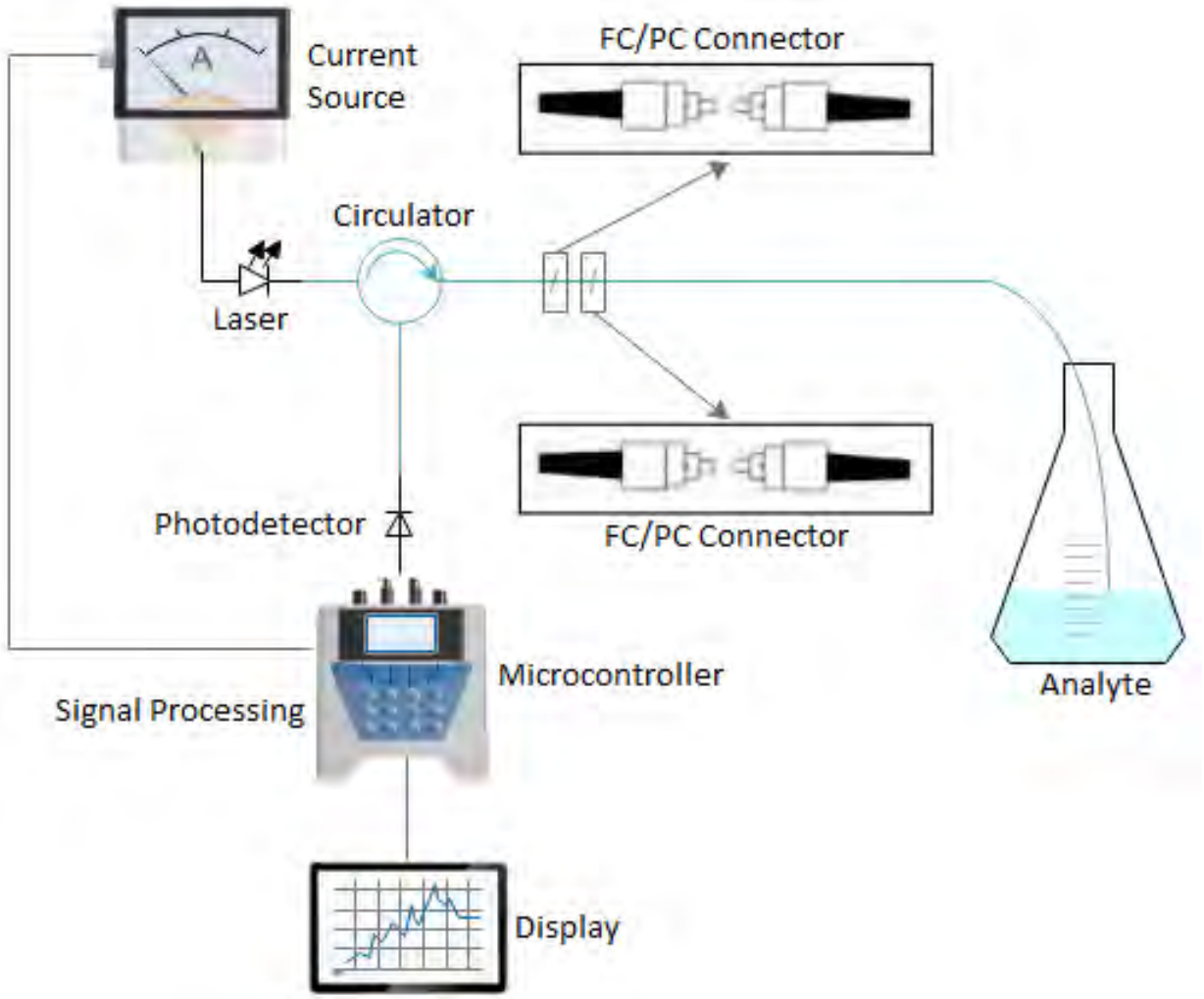

Figure 41: Subsystems working together, forming final system

The display of the system can show the user something like in the example of Figure 42.

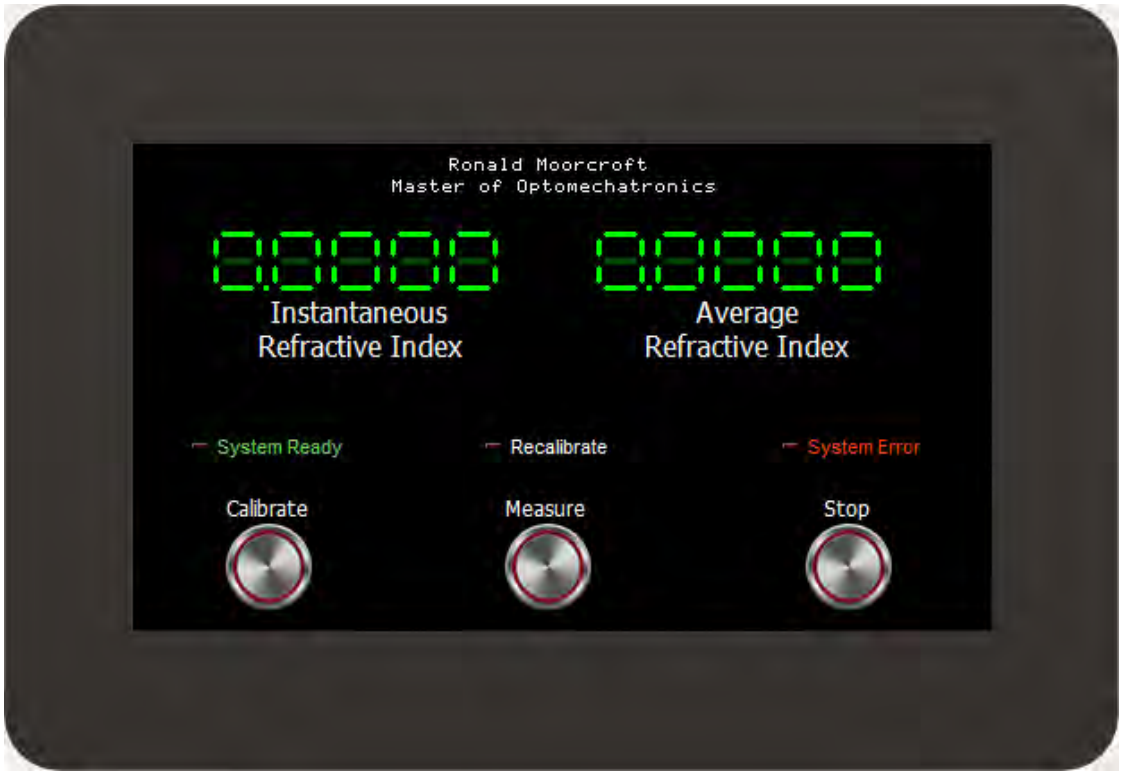

Figure 42: An example of what the display could show

Conclusion

The experiments that are presented here form part of the evolution and progression of the project.

The optical system is tested through a different range of optical setups and sensors. The initial experiments were done with the use of a Fabry-Perot interferometer utilizing an air capillary to form the reference cavity of the system. After this, FC/PC connectors were used to form the reference cavity.

A new compact, more intelligent power source is needed to control and drive the laser diode, since the fibre laser is too bulky, making it inappropriate for a prototype. The microcontroller is used for the control, and the current source is used to drive the DFB laser. The current source also needed to be tested to insure that sufficient current and voltage will be provided to the DFB laser diode. This entailed power characteristics that would not damage the laser diode. The laboratory power supply is first used as input to the current source, to determine if the architecture of the current

source is good enough to drive the laser diode and to be stable enough not to influence the output of the laser diode. After the laboratory power supply has been used, the microcontroller needs to be used for the effective control of the voltage input to the current source.

The source of the system will not be commercial and therefore the characteristics of the laser must be established with the custom built electronics. Thus the microcontroller and current source is used to control the laser source and therefore implement the COFDR method.

Finally, the system needs to be tested in its entirety, all the subsystems fitting in place and working together.

With all these experiments being performed successfully, the project can therefore be done successfully, since all the different aspects of the project will be tested with these experiments. The following chapter will provide the results of all these experiments.

Chapter 5: Results

Introduction

In the previous chapter of this dissertation, the different experiments are presented to test the different parts of the system, so that the entire system can be improved and integrated. In this section, the results of all the experiments that were conducted will be shown and discussed. Analyses of the results will be performed to show the ultimate results of the different systems and then the prototype as a whole. In order for analyses of the results, signal processing is used and the code can be found in the appendices.

Preliminary Results

The preliminary experiments were conducted to test each piece of the prototype and to see if the different ideas and subsystems would work. In this section, the results of those experiments are discussed, such as the optical parts that were focused on, i.e. the sensor.

The electronics of the system were also tested. The current source was tested to turn the laser on correctly, control the laser with good stability and to not destroy the laser by feeding it more than the maximum power specifications.

Once the current source was developed, it had to be tested with the laser to analyse the characteristics of the laser so that the laser could be used with the COFDR method.

The results will now be discussed.

Air Capillary forming a Fabry-Perot Cavity

The experiment using the capillary that is spliced between two pieces of SMF to form the Fabry-Perot cavity was conducted using the analytes distilled water and propanol, with air as reference. Using only one arm as the sensing probe is part of the requirements of the prototype that needs to be designed and constructed. The signal processing for this arrangement is somewhat more involved, since there are multiple frequencies that are generated in the sensing probe from the different cavities and the combination of the cavities.

Some results of the interference patterns measured by an oscilloscope using a photodetector will now be given:

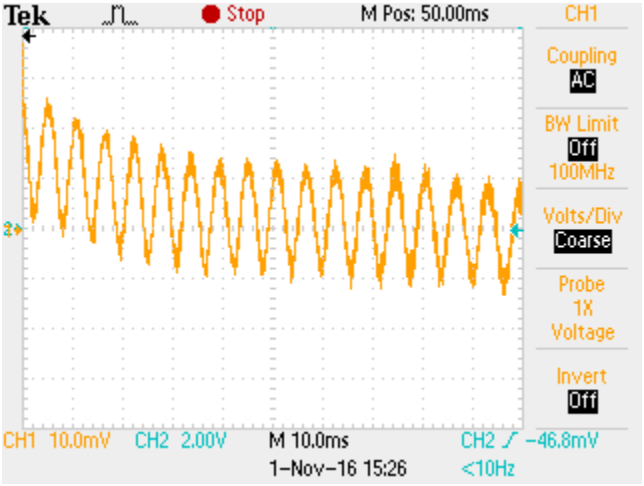

Figure 43: The beat signal generated by leaving the probe in air with 4cm length between the capillary and cleaved tip. There is a clear sinusoidal pattern seen due to the interference of the reflected waves.

Figure 43 shows the interference pattern from the sensing probe. There is a slight downward slope in the general wave that is due to the slope found in the emission spectrum of the Erbium doped fibre amplifier. The pattern of the sinusoidal wave is also not found to be symmetric compared to the theoretical model in shape. This is due to the non-linearity of the system. For the case of when the probe tip is left in air, the reflected power is equal to about 4%, due to the Fresnel reflection that takes place from the interface between the fibre core and air (taken when the value of the refractive index of the core of the fibre is 1.5 RIU). Looking at the reflectance from (6.1), it is expected that when the analyte changes to a substance with a refractive index closer to that of the core of the optical fibre, the intensity of the reflectance will decrease. Figure 44 shows one of the results of the probe dipped in propanol.

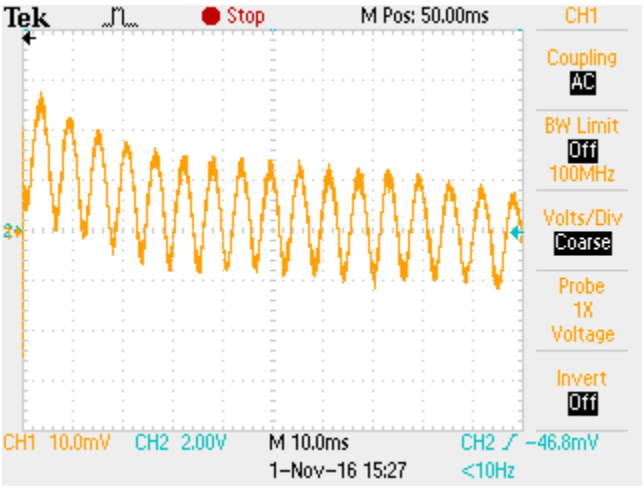

Figure 44: Probe in iso-propyl alcohol with 4cm distance between capillary and cleaved tip

Figure 44 and Figure 45 shows the recorded pattern from when the tip of the sensor was placed in propanol and distilled water, respectively. The longer cavity was used for these measurements and serve as a comparison between when the cavity was shortened (the tip was cleaved so that the distance between the capillary and cleaved tip was 0.5 cm instead of the initial 4 cm), which can be seen in Figure 46 and Figure 47.

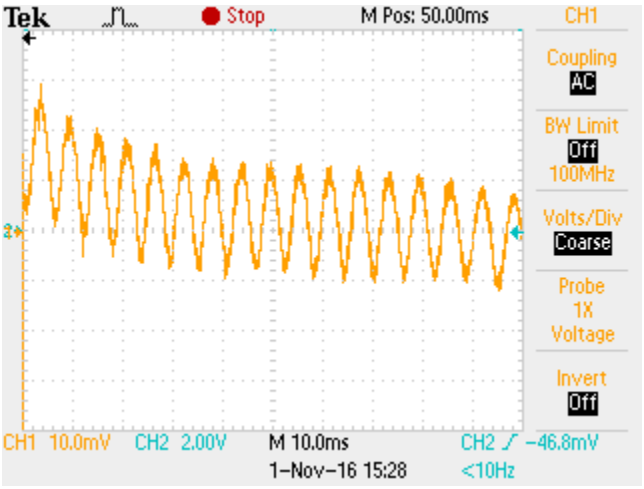

Figure 45: Probe in water with 4cm distance between capillary and cleaved tip

The result of making the cavity between the capillary and the tip of the fibre, smaller, is that the frequency that is generated by that cavity, will also be smaller, but the magnitude of the reflected power would remain the same, as the analyte which is in contact with the fibre's tip, remains the same substance.

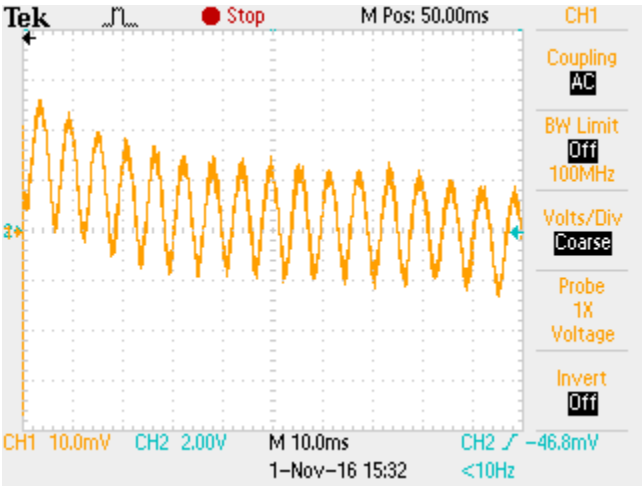

Figure 46: Probe in iso-propyl alcohol with 0.5cm distance between capillary and cleaved tip

Figure 46 and Figure 47 displays the pattern that was recorded from placing the tip of the probe in propanol and distilled water, respectively. These patterns are very similar to one another as the frequency and amplitude look the same.

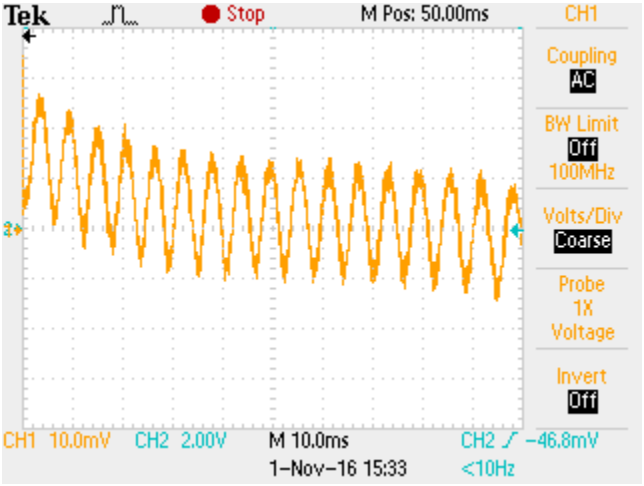

Figure 47: Probe in water with 0.5cm distance between capillary and cleaved tip

Figure 48 is the FFT that was performed by the oscilloscope on the beat signal produced from the tip being in air. Although the FFT that was used for further signal processing was derived with MATLAB that can be more accurately used to get the desired information from the system, these are included for the sake of comparison that the results of the FFT from MATLAB should correspond to it.

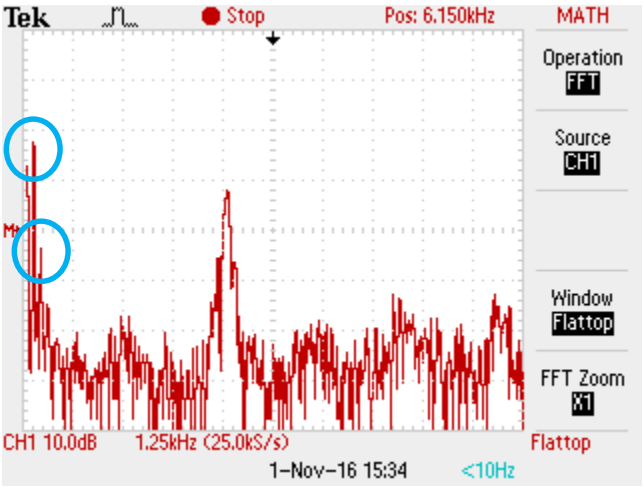

Figure 48: FFT of the probe in air with 0.5cm distance between capillary and cleaved tip, with the characteristic big peak at the start of the spectra and smaller peak that follows straight after.

Figure 48 shows the FFT peformed of the sensing probe when it is left in air. The characteristic of the FFT can be described as having a big peak at the start of the spectrum with a smaller peak that follows right after that big peak. Further in frequency spectrum there is another peak that is wide, therefore consisting of different frequency components, making further signal processing vital for the correct interpretation of the signal. For the identification of the individual frequencies that the signal consists of, the big peak at the start of the spectrum seems to be around (1.25 x 1/5) = 250 Hz. The division of the x-axis is 1.25 kHz. The smaller peak immediately after the bigger one seems to be double that – therefore 500 Hz. For the other peak down the spectrum, the main peak seems to be around (1.25 x 4) = 5 kHz. All of these results need to be similar when compared to the signal analysis done in MATLAB. Figure 49 shows the FFT from the oscilloscope for when the tip was placed in propanol.

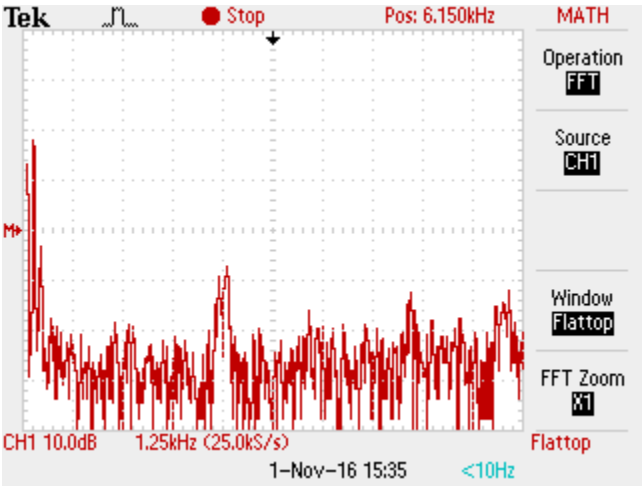

Figure 49: FFT of the probe in iso-propyl alcohol with 0.5cm distance between capillary and cleaved tip

For the FFT done on the signal that is seen in Figure 49, there are similarities like in Figure 48. The big peak at the start of the spectra is also seen with the same frequency. This big peak at the start of the frequency spectrum is the resonant cavity frequency generated by the capillary in the sensor. This can be seen due to the size of the cavity formed by the capillary and the magnitude of the peak, for all the cases of air, iso-propyl alcohol and distilled water. The size of the cavity formed by the capillary is the smallest in the sensor – thus generating the smallest frequency in the frequency spectrum. The magnitude of the peak is significant, because the percentage power that is reflected is due to the reflectance R (equation 2.30), and is given by:

$$R = \left|\frac{n_i - n_t}{n_i + n_t}\right|^2 \tag{2.30}$$

where n_i is the refractive index of the core of the optical fibre and n_t is the refractive index of the analyte. This means that when considering air, propanol and distilled water, the interface combination that occurs between the silica core and air and again between the air and silica core (thus describing the interfaces of the capillary), will produce a reflection of greater intensity than the sensing cavity.

The smaller peak that immediately follows is also present with the same frequency. There is also the wide peak with the higher frequency in the spectra that has a lower magnitude than the one in Figure 48, but here it can be seen that there are two main frequency components in that wide peak. The lower frequency of the two has a frequency just smaller than 5 kHz and the other peak has a

frequency just larger than 5 kHz. The two frequency peaks represent the two sensing cavities that are formed in the sensor – the one including the capillary, which is the peak with the greater frequency value, and the sensing cavity formed by excluding the capillary, which will be the frequency peak with the smaller frequency value. These peaks should be separated by the frequency value of the capillary and therefore can be seen that there could exist an instance of a single peak between these two, if the source does not provide a scan linear enough to distinguish the two peaks. This causes a need for a different source to arise, other than the EDF ring laser, since the peaks need to be clearly separated.

The figure that follows, Figure 50, is the FFT when the tip is placed in distilled water. The same frequency characteristics as the previous two FFT graphs are expected, since there is no change in the laser source nor the cavity lengths of the system.

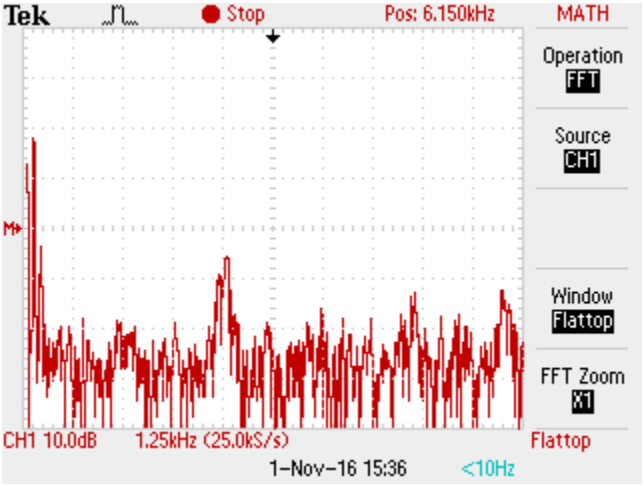

Figure 50: FFT of the probe in distilled water with 0.5cm distance between capillary and cleaved tip

The FFT that was performed for the signal when the tip was placed in water can be seen in Figure 50. The big peak with the smaller one is found at the start of the spectrum and the wide peak is also found at the same frequencies as in Figure 48 and Figure 49. In Figure 50 the wide peak also has a smaller magnitude than the one found in Figure 48 when the tip of the probe was left in air. The wide peak can also been seen two have two main frequency components – one before 5 kHz and one after 5 kHz, similar to Figure 49.

Figure 51 shows the FFT of when the probe is kept in air, plotted in MATLAB. Some points of interest are marked – the first one the left shows the frequency (as the X value) and the magnitude

(as the Y value) of the cavity with the smallest frequency. This graph is the same as Figure 48, with the difference of Figure 48 plotted with the oscilloscope and Figure 51 plotted in MATLAB, therefore the latter having more detail.

There were three cavities that existed in the sensing probe - the capillary, the last piece of SMF (from the end of the capillary to the end of the probe) and a combination of these two cavities. Each of these cavities produced three different beat signals. Figure 51 shows the FFT that was done on the global time domain spectra from these beat signals produced by the different cavities. There are three points of interest marked in Figure 51– the first is the frequency and magnitude of the smallest cavity in the system – the capillary (which was also used as the reference cavity). The frequency value of this cavity is 170 Hz with a magnitude of 0.008754.

The second point of interest is found at a frequency twice that of the reference cavity. This value is not due to a real cavity in the system, but due to the double reflection that occurs from the capillary.

The third point of interest shows the details of the biggest cavity in the system. This is the cavity that was formed from the combination of the capillary and the end piece of SMF. This cavity generated a frequency of 5080 Hz with a magnitude of 0.001822.

With the different magnitudes that were established, the constant K can be calculated with the known refractive index of the analyte, before the measurement of unknown refractive indices can take place. For this calibration, the results of Figure 51 was taken when the probe was kept in air.

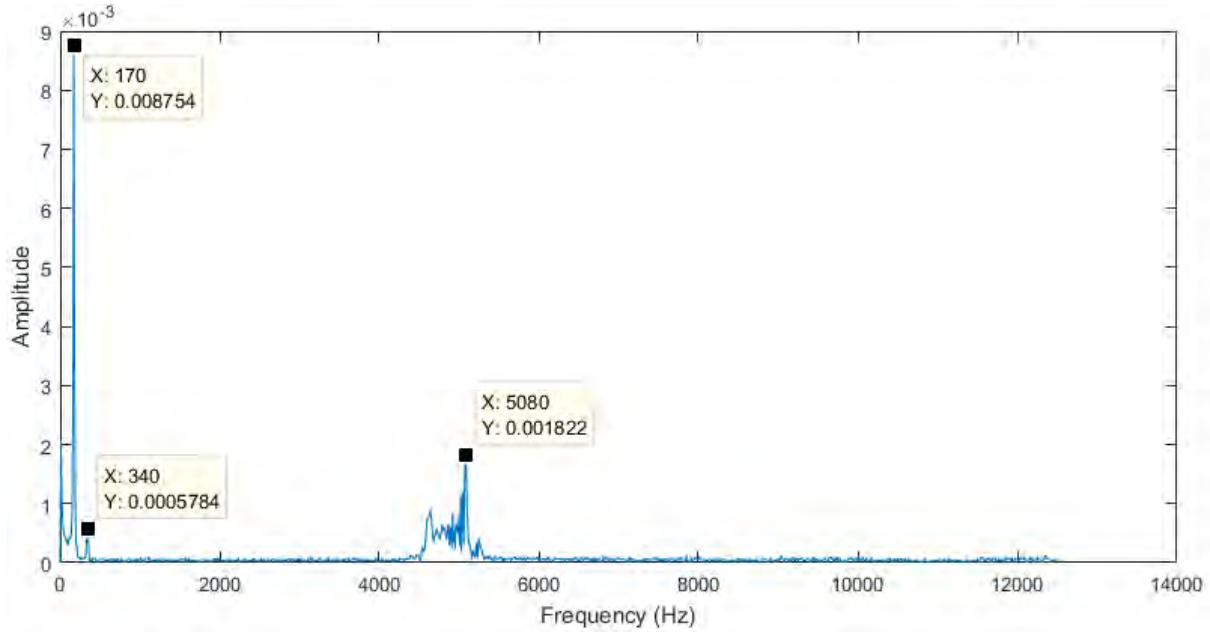

Figure 51: The FFT of the Fabry Perot interferometer for air as analyte

After the calibration was completed for the sensor, the probe was dipped into iso-propyl alcohol. The different cavities again produced different frequency components with the generation of the individual beat signals. The global time domain result of the beat signals was taken and a FFT was performed. The result of the FFT is shown in Figure 52. The first two peaks in the spectrum is the characteristic of the air capillary in the sensor. Further down the frequency spectrum there are other magnitudes generated related to the second and third cavities of the system.

Note for the second and third cavity of the system, how much frequencies are spread across the range of those two cavities, highlighting the fact that the laser source does not scan in an ideal linear fashion and does decrease the accuracy of the refractive index measurements.

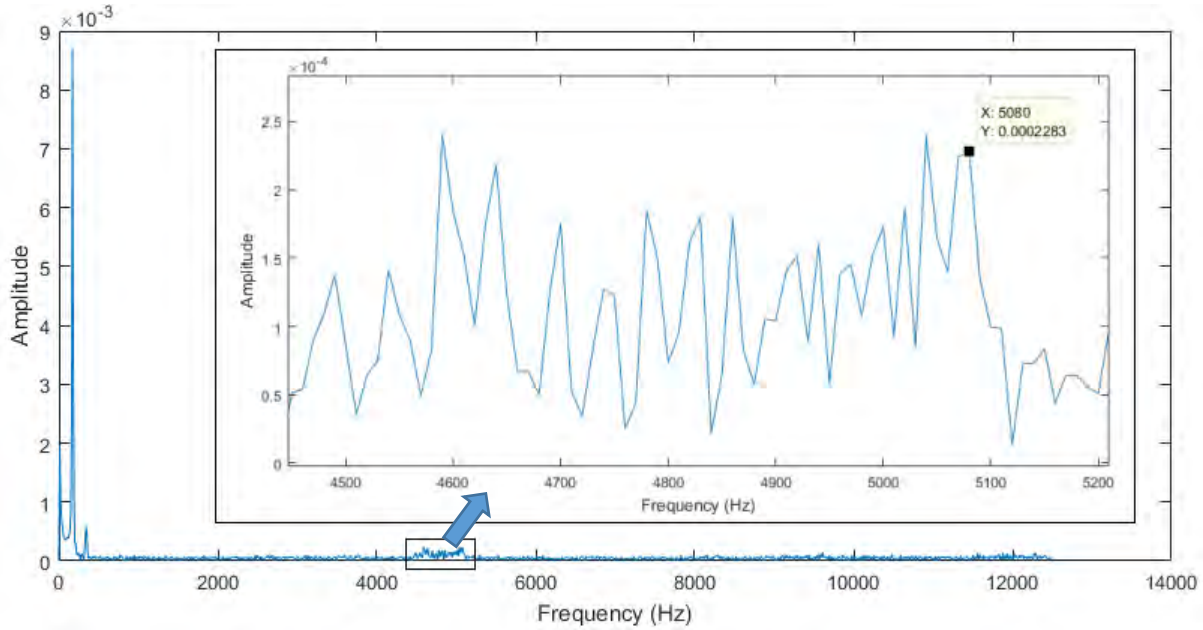

Figure 52: The FFT for the Fabry Perot interferometer for iso-propyl alcohol as analyte with inset of finer detail

The marker shows the details of the third cavity of the system – a frequency component of 5080 Hz is generated with a magnitude of 0.002283. This makes sense as the cavity did not change in size and therefore neither should the frequency component that is generated. The magnitude did however change and this makes sense, due to the change of the refractive index of the analyte. The refractive index of the iso-propyl alcohol was calculated to be 1.3729 in the 1550 nm wavelength spectrum. The theoretical result of the refractive index of propanol is between 1.3675 and 1.3738 [35] [36] [37] [38] [39] in the 1550 nm wavelength spectrum. This result gives no measurement error, as the result are exactly the same as the theoretical result values. The error could be due to the signal that has not been linearized yet and more measurements can be taken for a better average refractive index measurement of alcohol.

With the measurement of the refractive index of propanol completed, the probe was dipped in water. An FFT was done on the beat signals generated from the cavities in the sensor and the result is shown in Figure 53. The first two peaks are seen again and this is due to the reference cavity (air capillary). The peak at the 5080 Hz mark was produced by the biggest cavity in the sensor and the magnitude found at this mark is 0.004163. This magnitude is bigger than the magnitude of the cavity when the probe was placed in propanol, due to the refractive index being further away in value from the refractive index of silica, but is smaller than when the measurement was taken in

air, due to the refractive index of air having a bigger difference between the refractive index of silica. The result of the refractive index of distilled water was found to be 1.3282 at 1550 nm. The theoretical value of the refractive index of distilled water is 1.3154 to 1.3164 [35] [40] [39] at 1550 nm wavelength. The error in this result is 0.00896 %. The result can be improved by linearization and taking more samples of the measurements of the refractive index of water, providing a better average.

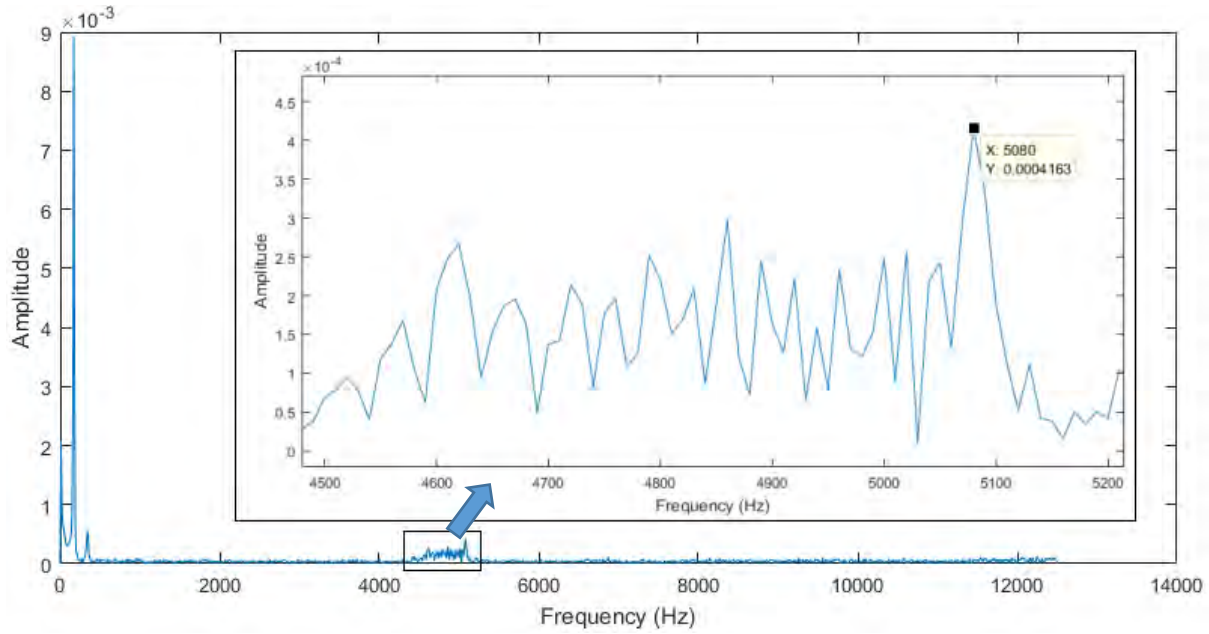

Figure 53: The FFT for the Fabry Perot interferometer for water as analyte with inset of more detail

With this system the refractive index could be measured with low error and the experimental setup does not have a high degree of complexity, making it very suitable for the objective to make a commercial refractometer. The sensor of the system provides an efficient and accurate solution for the refractometer.

An improvement to this system is to use a less complex tunable laser source, such as a DFB laser diode with the current being adjustable to provide a sweeping of the wavelength. This makes the tunable laser source more compact which will be advantageous since the commercial structure of the refractometer should be of a compact size and there are less components that can break or stop working.

Another improvement to this system is a different solution to the sensor probe. The working principle of the sensor probe provides a smart and effective way to measure the refractive index, but to splice the capillary to the two pieces of SMF requires the use of an expensive splicing machine that will increase the manufacturing price of the refractometer. Therefore a solution similar to that of using a capillary should be utilized which will cause a reference reflection to the system without the need of splicing a capillary in the sensor. A solution to this could simply be just to use a physical contact (PC) connector in the sensor, providing a reference reflection and simple integration in the system.

FC-PC Connected Fibre Piece forming a Fabry-Perot Cavity

One of the objectives for the project is the possible commercialization of the prototype and for that the fabrication of the prototype should not be expensive or very difficult to make. The sensor that was previously used, where the air capillary is spliced between two SMF's is not an expensive method, but the fabrication process can be difficult to make a sensor of such a type. For this experiment, a length of SMF is connected to the sensor with a FC-PC connector, which will act as the reference cavity of the sensor. This reference cavity, now replaces the air capillary in the previous experiment, removing the difficult fabrication process of the sensor and replaces it with a FC-PC connected piece of SMF.

Since the connector piece is not as small as the air capillary, the overall length of the sensor is larger than the entire sensor in the previous experiment, but the method of interrogation stays the same, as the reference peak with the smallest frequency will be the reference cavity with the smallest length.

The use of the COFDR method continues in this experiment. The laser source will scan as linear as possible through wavelength in time. With the reflection from the different interfaces in the sensor, interference patters will be formed – the beat signal of the system. The beat signal will consist of different frequencies, dependent of the number of cavities in the system. For this case, similar to the previous, there are three distinct frequencies that should be formed and then globally superimposed in the beat signal. Figure 54 shows the beat signals produced when the sensor probe is dipped into the different analytes that where tested.

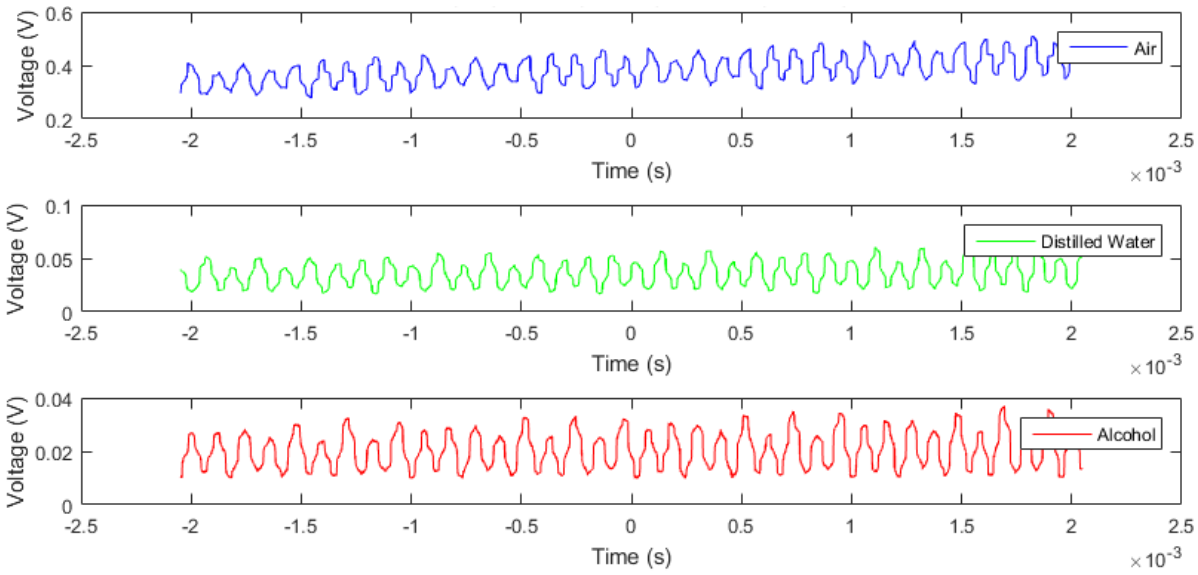

Figure 54: The beat signal that is generated for the different analytes in the system - the top in blue is from air, the middle in green is from distilled water and the bottom in red is formed when the sensor probe is dipped in iso-propyl alcohol

The beat signal for air as analyte is seen at the top in blue. This measurement is also used as the reference measurement of the system to determine the different properties of the system and can be adjusted and calibrated for the other analytes that follow. The middle graph in green shows the beat signal that is produced when the sensor is dipped in distilled water. The bottom graph in red shows the beat signal that is produced when iso-propyl alcohol or propanol is used as the analyte. When viewing the different voltage measurements from the oscilloscope, it is seen that the magnitudes become smaller, descending in magnitude from the top to the bottom. Figure 55 shows different graphs for the different analytes with FFTs performed on the beat signals.

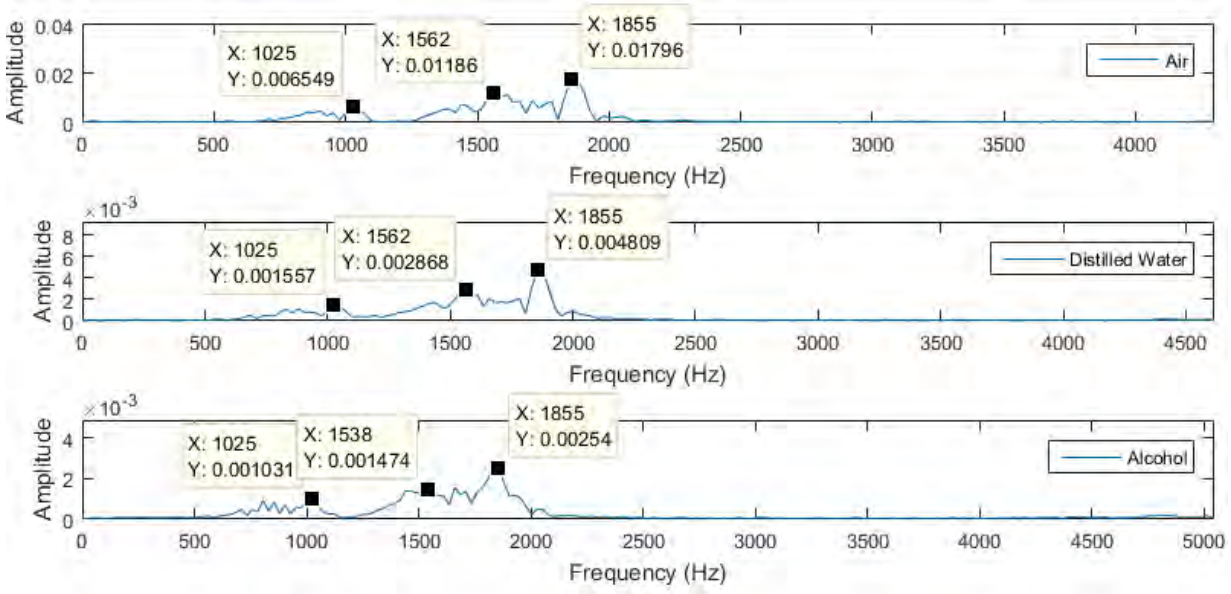

Figure 55: Graphs of the FFT performed on the different beat signals of top) air, middle) distilled water, and bottom) iso-propyl alcohol

Figure 55 contains important information about the system. It is noted that there are three main peaks in the range of frequencies – these show the different cavities that are found in the system. There are certain points of interest marked in the graphs – the first point to the left of all the graphs is the reference cavity, e.g. the cavity created by the connectors. This peak remains at the same frequency throughout the experiment, which it should. The second is one of the bigger cavity that starts after the "connector" fibre piece and the end of the fibre and the third peak is the combination of these two cavities. Notice that in all the points of interests, the peaks of the cavities stay at the same position – that is at the same discrete frequency value in the Fourier domain. This has to be so, since the scanning rate of the laser and the length of the cavities stay constant. There is an exception, in the second peak in the FFT of iso-propyl alcohol, there is a slight shift in the frequency value. This could be due to the non-linear scanning property of the laser source, where the energy is distributed through a range of frequencies around the main frequency peak.

From a set of 27 samples, the K value (representing a value unique to the setup of the current system) and refractive indices were calculated. With the ratio of the reference cavity and the combination of the reference and sensing cavity, the K value was calculated to be 14.274 is this system. The K value is calculated from the reference measurement set. The refractive index of water at 1550 nm was found to be 1.3268 (theoretically between 1.3154 and 1.3164 [39] [40]) and

the refractive index of propanol at 1550 nm was found to be 1.3545 (theoretically between 1.3675 and 1.3738 [38] [39]).

This experiment serves the proof of concept that the PC connectors can be used in the sensor of the system. This provides the prototype to be fabricated without a difficult procedure and without any expensive equipment.

Current Source

The current source was first tested with a power supply in the laboratory to have measurements that are accurate and stable. The current source was then tested with the microcontroller that was fitted in the prototype to control different input factors, such as the saw-tooth waveform, the minimum and maximum of the saw-tooth wave input and the frequency of this wave. To protect the DFB laser diode, the initial output characteristics of the source was tested with a 1 Ω resistor, just like in the simulation. The built current source is seen in Figure 56 and the results of this experiment is seen in Figure 57. The load denotes the power measurements taken across and through the resistor.

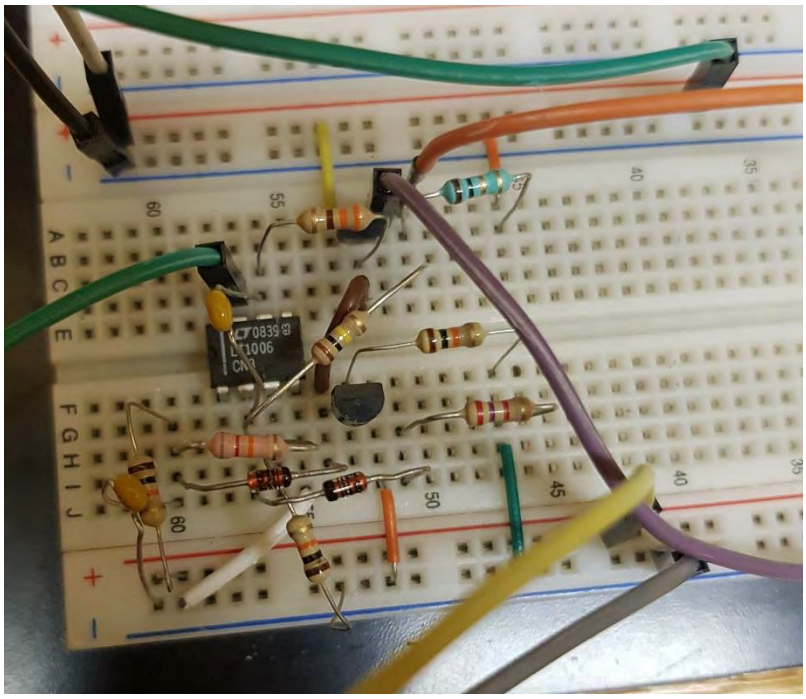

Figure 56: Picture of the built current source

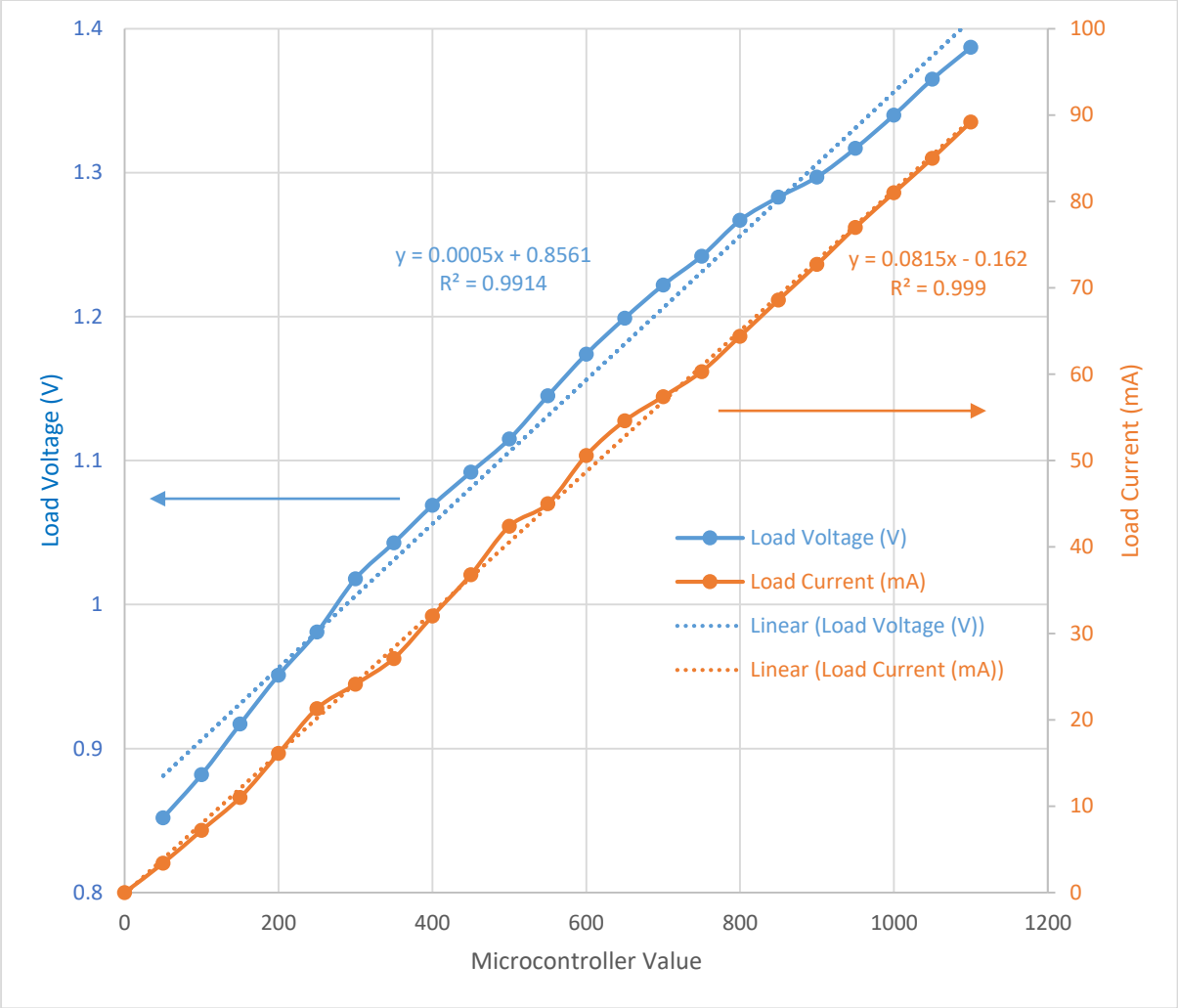

Figure 57: Results of the current source tested with the microcontroller

The implemented current source was first tested with a 1 Ω resistor to first observe what the output power characteristics of the current source would be and therefore prevent any damage that could occur to the laser diode. And rightfully so – the output characteristics that was provided by the current source clearly differed from the simulated circuit. Although all the same components were used in both the simulated circuit and the real implemented circuit, they both yielded different results. The input to the simulated circuit was a saw-tooth waveform with a minimum of 0 V to a maximum of 5 V, which then was change to a minimum of 1 V to prevent the lag of turning the transistor on, which provided a more ideal saw-tooth waveform for the input to the load/laser. In the case of the real circuit, 1 V was already over the limit that could be used for the laser diode.

The voltage over the load stayed within the recommended range of the laser diode. This insured that the diode had sufficient voltage to be turned on, but did not get damaged by too much potential difference. The current that was provided to the load was achieved without any difficulty. With the range that the current provided and with the low voltage required for the input to achieve this, there would not be a problem for the microcontroller to provide the current source with adequate voltage to obtain the needed current to drive the laser.

The graph in Figure 57 shows a plot of the results measured from the current source when using the microcontroller to generate a saw-tooth scan. The measured load voltage is shown in blue and the measured load current is shown in orange. Linear regression lines are added for the load voltage (dotted blue) and for the load current (dotted orange). Both the regression lines for the voltage and the current shows a correlation of over 99% with the measured results. This means that the results from the scans conform strongly to the increments, or in other words, the scans are very linear and linearly proportional to the values of the microcontroller.

The implementation of the current source is successful with supplying the laser diode with sufficient current and voltage to operate for the project, with an adequate scanning range that can be achieved through varying the input voltage and therefore the output current to the laser diode.

Laser Characterization

After the initial observations were made of the output power characteristics when using the resistor instead of the laser, the laser was installed and carefully tested with the current source. It is immediately noticed the results differ from the simulated circuit. Table IV provides the results of the laser characteristics with the testing of the laboratory power supply.

Table IV: Results of the current source and laser diode with power supply

V_{in} (mV)	V_{laser} (mV)	I_{laser} (mA)	Wavelength (nm)	Optical Power (dBm)
0	0	0	NA	-77,97
50	835	3,4	1546,42	-52,6

100	883	7,6	1546,16	-6,31
150	913	11,8	1546,22	-1,25
200	942	16,0	1546,06	1,05
250	970	20,1	1546,12	2,59
300	998	24,3	1546,22	3,66
350	1026	28,5	1546,28	4,54
400	1053	32,7	1546,36	4,78
450	1079	36,8	1546,42	5,81
500	1105	41,0	1546,52	6,05
550	1129	45,2	1546,62	6,55
600	1154	49,3	1546,72	7,14
650	1176	53,3	1546,84	7,37
700	1193	56,2	1546,94	7,47

The input voltage was only taken to a maximum of 0.7 V, as the optical power measured from the DFB laser diode was already pushing the limits of this 2 mW laser diode [32], although the voltage across the laser diode and the current through the laser diode were still well within the specifications of the DFB laser.

Taking a look at the table with the emission results of the laser, the jump in the optical power is between 3.4 mA and 7.6 mA. Therefore, the threshold current of the laser is in this range of current values, since this is where the laser starts to lase and the spontaneous emission is replaced by the majority of stimulated emission photons. Therefore, it is only above this point where the laser can be used for the COFDR method.

Before 16 mA is applied to the laser diode, there seem to be some irregular jumps in the wavelength emission spectrum and can cause a big non-linear effect on the frequency, making the results less accurate, thus after 16 mA the laser can be tuned to 56 mA, where the experiment was stopped due to the high optical power output of the laser diode.

The concept was proven that the DFB laser diode can be used for the COFDR method, but there is still quite a bit of non-linearity that will exist, causing a frequency spread in the beat signal.

After the DFB laser diode was tested with the current source and laboratory power supply, it was necessary to be tested with the microcontroller. Table V shows the details of the measurements taken from the experiment.

Table V: Results of the current source and laser diode with microcontroller

Microcontroller Value	**V_{in} (mV)**	**I_{laser} (mA)**	**Wavelength (nm)**	**$P_{optical}$ (dBm)**
500	56	4	1545,96	-46,81
1000	60	4,3	1545,88	-44,54
1100	61,6	4,4	1545,88	-45,29
1200	66,4	4,9	1545,96	-39,9
1300	71,2	5,3	1545,76	-32,24
1400	75,2	5,7	1545,72	-14,81
1500	80	6,1	1545,72	-10,6
2000	104,4	8,3	1545,72	-4,57
2500	129,6	10,5	1545,72	-2,17
3000	156	12,7	1545,76	-0,58
3500	182,4	14,9	1545,8	0,58

4000	207,2	17,2	1545,84	1,47
4500	232,8	19,4	1545,88	2,22
5000	257,6	21,6	1545,92	2,87
5500	282,4	23,8	1545,96	3,42
6000	308,8	26,1	1546	3,91
6500	333,6	28,3	1546,04	4,35
7000	360	30,5	1546,08	4,67
7500	384,8	32,7	1546,16	5,05
8000	409,6	34,9	1546,2	5,41
8500	435,2	37,2	1546,28	5,7
9000	460	39,4	1546,32	5,94
9500	487,2	41,5	1546,4	6,2
10000	512	43,8	1546,44	6,5
10500	536,8	46	1546,48	6,7
11000	562,4	48,2	1546,56	6,91

The microcontroller value column in the table is the value for the microcontroller in the code. This value is simply a value concerning this specific microcontroller used to control the voltage output of the analogue port of the microcontroller that was used. This needed to be tested for a few different values before the current source and laser could be connected, since that value does not directly correspond to an output voltage value. The V_{in} column is the value of the voltage that the microcontroller inputs to the current source. The I_{laser} column shows the values of the current through the DFB laser diode. The wavelength column is the specific wavelength that is produced

by the laser, measured by an optical spectrum analyser (OSA). The final column, $P_{optical}$, shows the measured optical power by the OSA. The wavelength and optical power is compared graphically with the current in Figure 58.

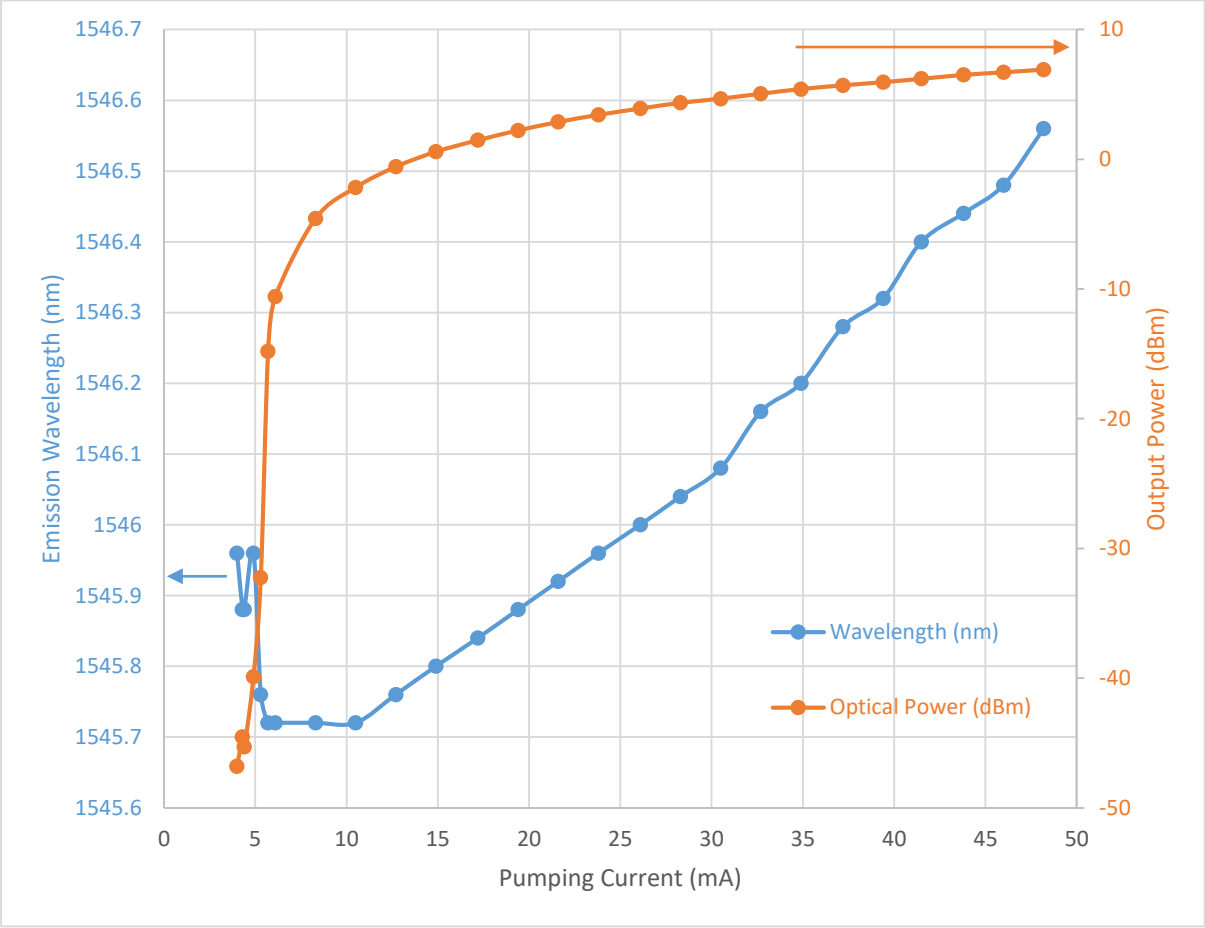

Figure 58: Graph of the wavelength and optical power of the laser versus the current through the laser

Figure 58 shows the wavelength in blue and the optical power in orange. From this graph it can be seen that the wavelength jumps and does not follow a linear form before stimulated emission is achieved. The big jump in the optical power shows the starting point where the majority of the emission is now stimulated and the lesser part of the optical power comes from the spontaneous stimulation of photons. The microcontroller has a linear effect on the current source and therefore on the DFB laser. The closer the microcontroller can control the current source to ideal linear behaviour, the more accurate the results will be without the need for a sophisticated algorithm for linearization. For each change in the microcontroller value (the integer value in code controlling the output voltage of the port) of a 100, there is a change of about 0.44 mA in the current though

the laser diode. There is somewhat of a delay in the current provided till the value of 1500 of the microcontroller, therefore values lower than this should be avoided, but looking at the values of the wavelengths emitted by the laser diode, it is better to start at a microcontroller value of 3000, providing 12.7 mA to the laser diode. This is the mark for this setup where the laser is producing stimulated emission and changes in wavelength "linearly" with 0.018181818 nm for every 1 mA.

When the optical characteristics are viewed, it is seen that the DFB laser started to lase when there was 7.6 mA flowing through the laser diode with 883 mV measured across the laser diode. Therefore, the threshold current is 7.6 mA. This is with an input voltage of 100 mV to the current source. The optical power generated from the laser diode jumped from -52.6 dBm to -6.31 dBm, thus from a point of spontaneous emission to stimulated emission. The peak wavelength that was generated at this point was 1546.16 nm. Figure 59 shows the details of the linear scan of the wavelength more closely.

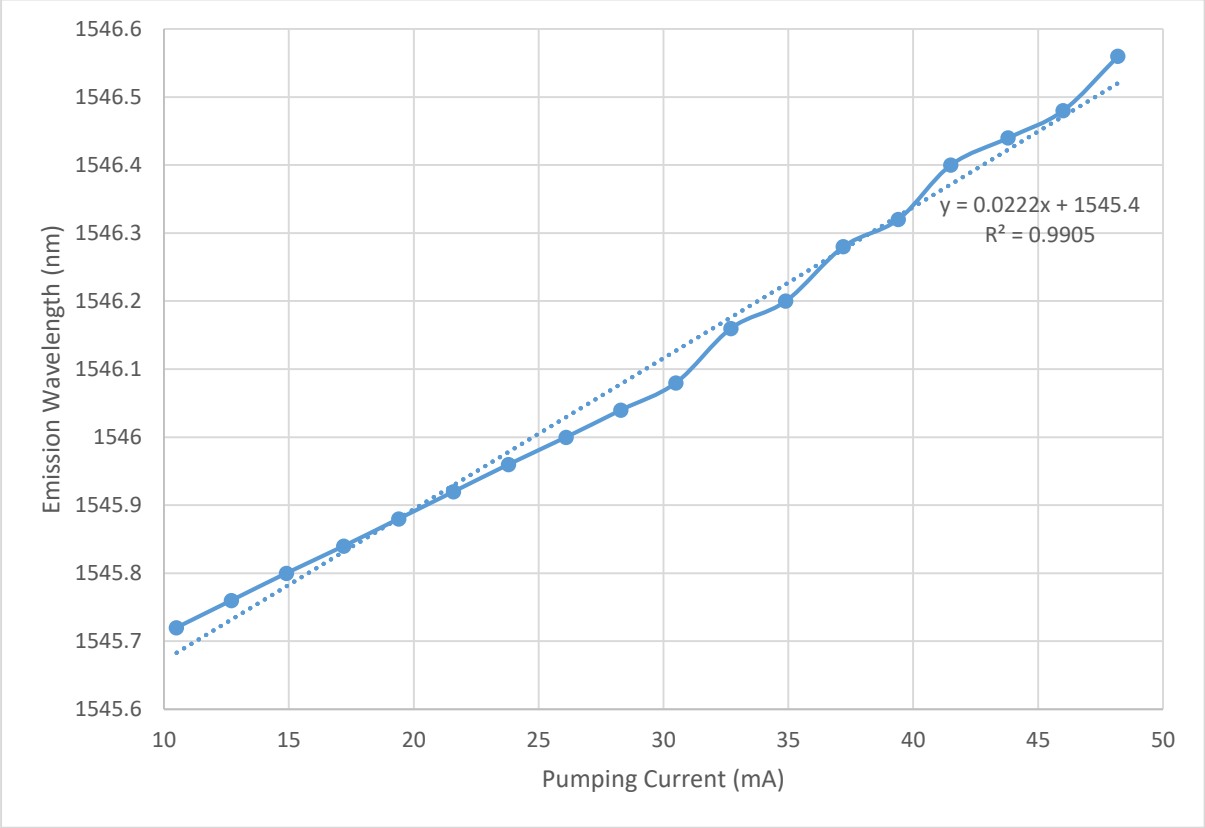

Figure 59: Graph of the linearity of the wavelength emitted by the laser versus laser current

Figure 59 shows the regression line lining up over 99% with the measurements of the wavelength. Although this linearity is a high percentage, there will still be some spread in the energy through a certain range of frequencies around the peak frequency when applying the COFDR method. The DFB laser provides a scanning range of 0.78 nm in wavelength, between 1546.16 nm where stimulated emission started to happen, and 1546.94 nm, where the testing range stopped for the laser to prevent any damage. The optical power at this point was 7.47 dBm, with a supplied voltage of 1193 mV across the laser and a current of 56.2 mA through the laser.

This experiment determined the output characteristics of the laser when using the microcontroller and current source. This enables the laser to be used at the optical emission points that would result in closer to ideal linear scans and improve results of the refractometer.

Final Results

The final results of this chapter comes from the final experiment, where the prototype was tested with all the different subsystems integrated, as if the prototype has been commercially produced and now deployed to the field for application. The entire system worked as a whole – the microcontroller controlled the voltage input which controlled the current source, which in turn controlled the output characteristics of the laser. The laser then scanned linearly through wavelength in time, which enabled the application of the chosen interrogation method – coherent optical domain reflectometry. The sensor system that was used was the physical contact connectors forming the Fabry-Perot cavity, with the end of the fibre sensor cleaved forming an inline sensor architecture.

The Integrated Prototype

In this section, the final results of the project will be discussed. These results are from the integrated system, with all the different subsystems integrated and functioning as one system. The integrated prototype is seen in Figure 60.

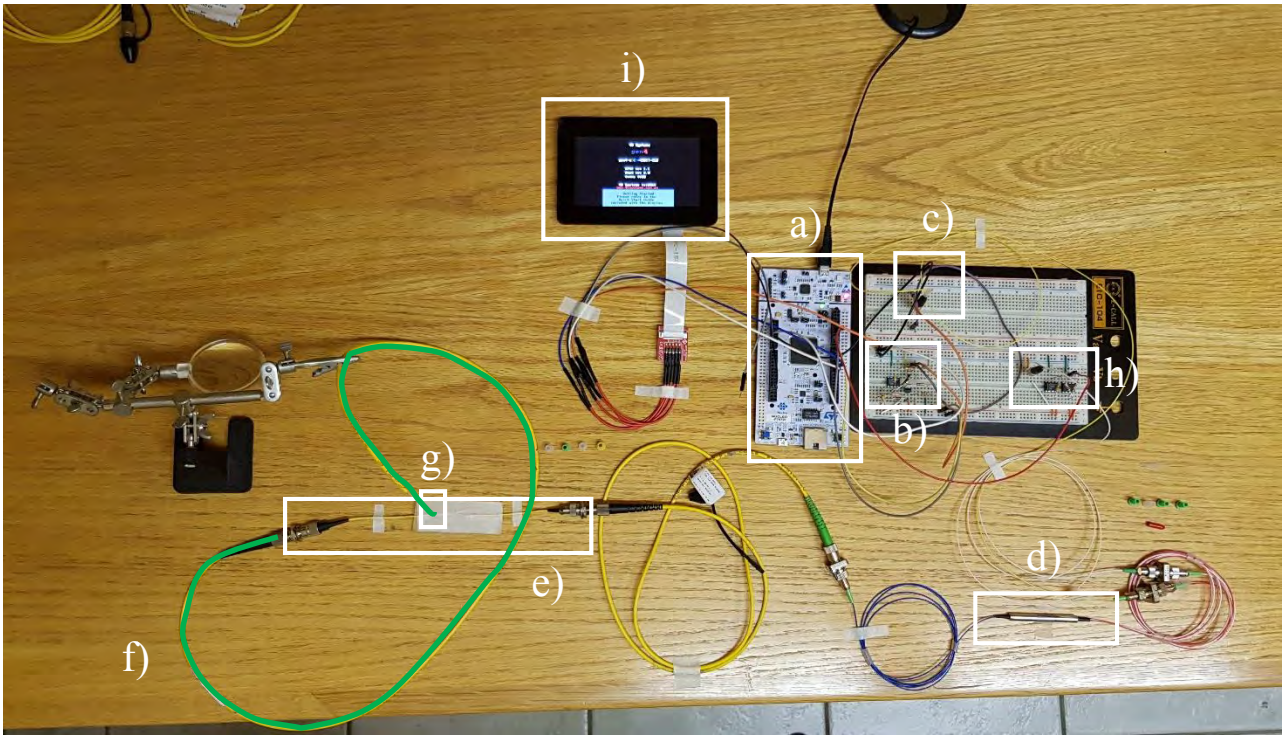

Figure 60: The prototype, laid out so all the different integrated subsystems can be seen: a) the microcontroller, b) current source, c) DFB laser diode, d) circulator, e) reference cavity, f) sensing cavity (in green), g) sensor tip, h) InGaAs photodiode and amplifier, i) display.

The microcontroller value, which is a set integer value in code used in this specific microcontroller to control the analogue output of the port used, was used to change the voltage input to the current source and was changed in increments of 1, assisting in the current through the DFB laser diode to be changed as linearly as possible. The modulation frequency of the saw-tooth waveform was also varied using the microcontroller, to test if a lower or higher modulation frequency will yield better results or have any impact on the system. As the microcontroller value grows, so does the wavelength and the power output of the laser diode. This causes the measured signal from the photodetector to look like a hill, with a steep drop when the value of the generated saw-tooth signal drops in value for the microcontroller to start scanning for the lowest range again. Some of the chemicals measured are seen in Figure 61 and Figure 62 shows examples of this saw-tooth wave when using air, distilled water and iso-propyl alcohol as analyte.

Figure 61: Some of the chemicals used for refractive index measurement, e.g. distilled water, iso-propyl alcohol, glycerin and acetone

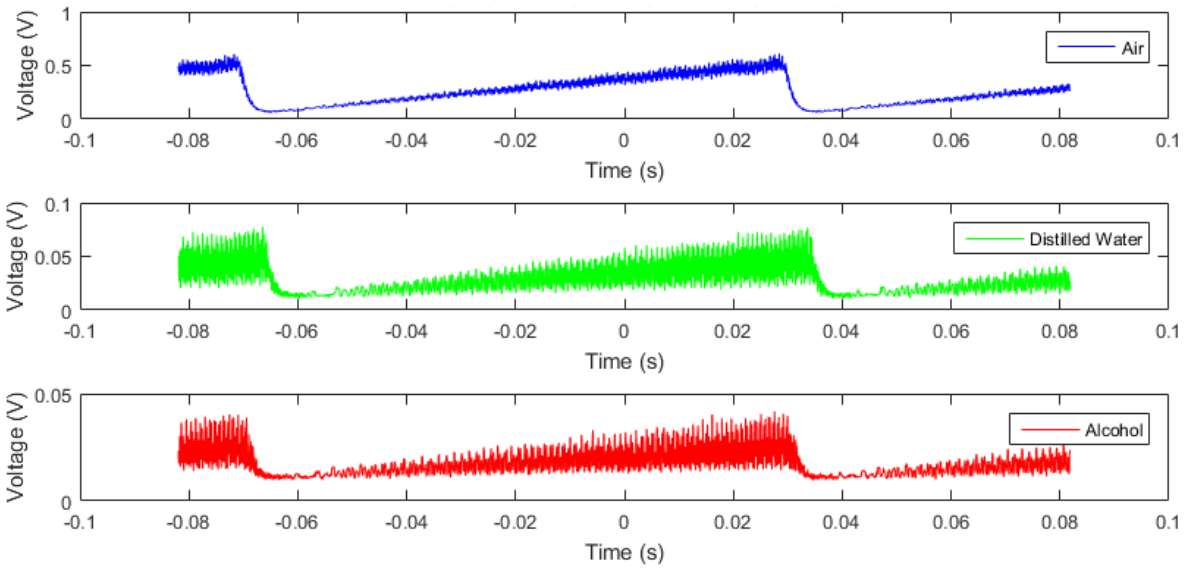

Figure 62: An example of the saw-tooth waves produced due to the saw-tooth voltage input to the current source

Figure 62 shows the saw-tooth wave produced from the laser. When this signal is taken to perform the FFT on, the results that are produced are not optimal – there is a lot of frequency spread in the

Fourier domain, causing results to be less accurate. Therefore, the time domain increments had to be experimented on. These time domain increments are the size of the time domain samples that were taken. The bigger the time domain increment that was taken, the more of the time domain spectra can be seen, but lesser detail of that spectra. With a smaller time domain increment, the smaller the time spaces between samples and the more detail can be seen of the spectra, but only a part of the spectra can be seen. Figure 63 shows the example of the FFTs performed of the waves with a big time increment – thus a bigger range of the time domain spectrum, but also a bigger time lapse between the samples, therefore giving less detail. Figure 64 below shows four different time increments of the same reference signal, with a modulation frequency of 1 Hz.

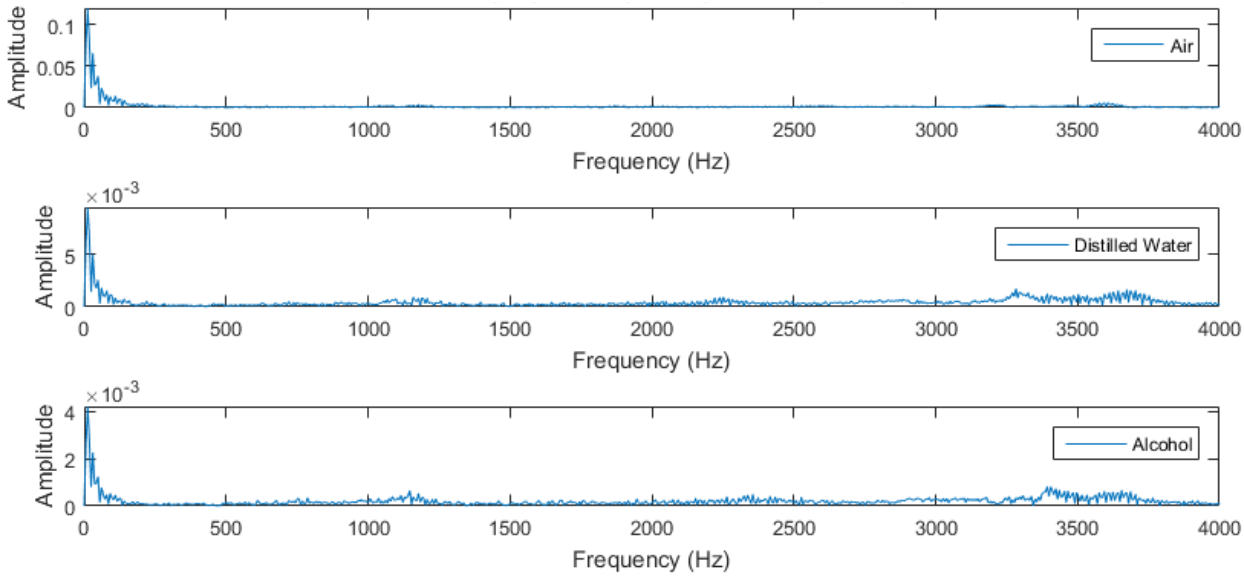

Figure 63: The FFTs for air, distilled water and iso-propyl alcohol when performed on the large time increment

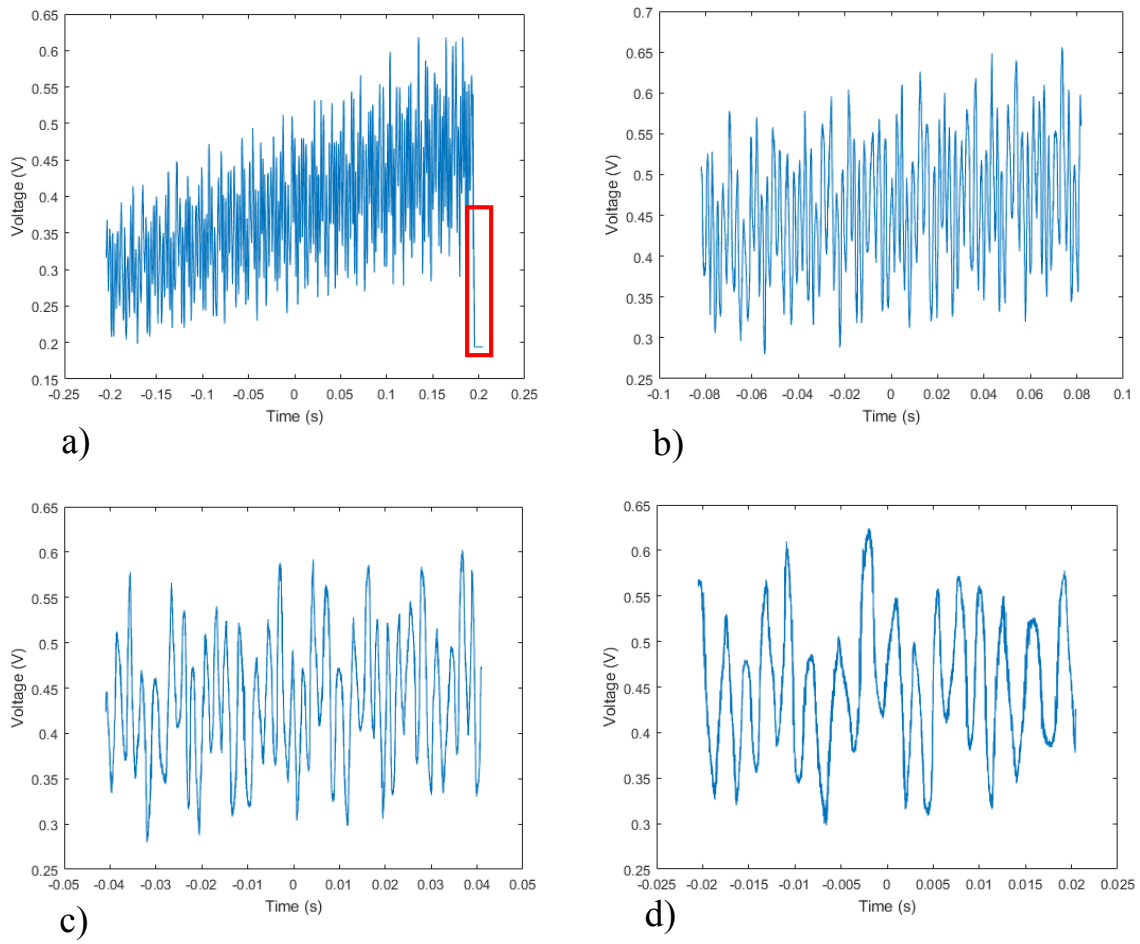

Figure 64: The different time increments for the reference signal using a modulation frequency of 1 Hz: a) the graph of the biggest time increment – more of the overall time domain spectra can be seen, but lesser detail, a sharp fall indicated with the red block, b) a decrease of the time increment between samples, c) bigger decrease in the time increment and d) the smallest time increment that was used – provides less of the overall time domain spectra, but the most detail

Figure 63 shows no real peaks in the system to find a reference measurement with the reference cavity and the sensing cavity. This is the spread in the frequency when there is not adequate detail in the time domain measurements and requires the adjustment of the time increments to provide better results.

The different time increments used for signal processing has an effect on the results of the system. The steep fall in the upper left graph (figure 64 a)) shows the end of the positive scanning cycle of the microcontroller and the start of the new cycle. From the characterisation of the laser, the wavelength produced from the end of the cycle is noted to be more linear than the start, so that area is focused on to get the results. To have the sharp fall included in the signal, there is a noticeable frequency spread in the FFT and must be pre-processed for the FFT. The fall of the

voltage is therefore cut from the signal to provide better results. The FFTs that are performed on the different time increments in the time domain also causes the results to fluctuate in accuracy. Figure 65 shows the differences in the FFTs when the time increment is adjusted in the measurements.

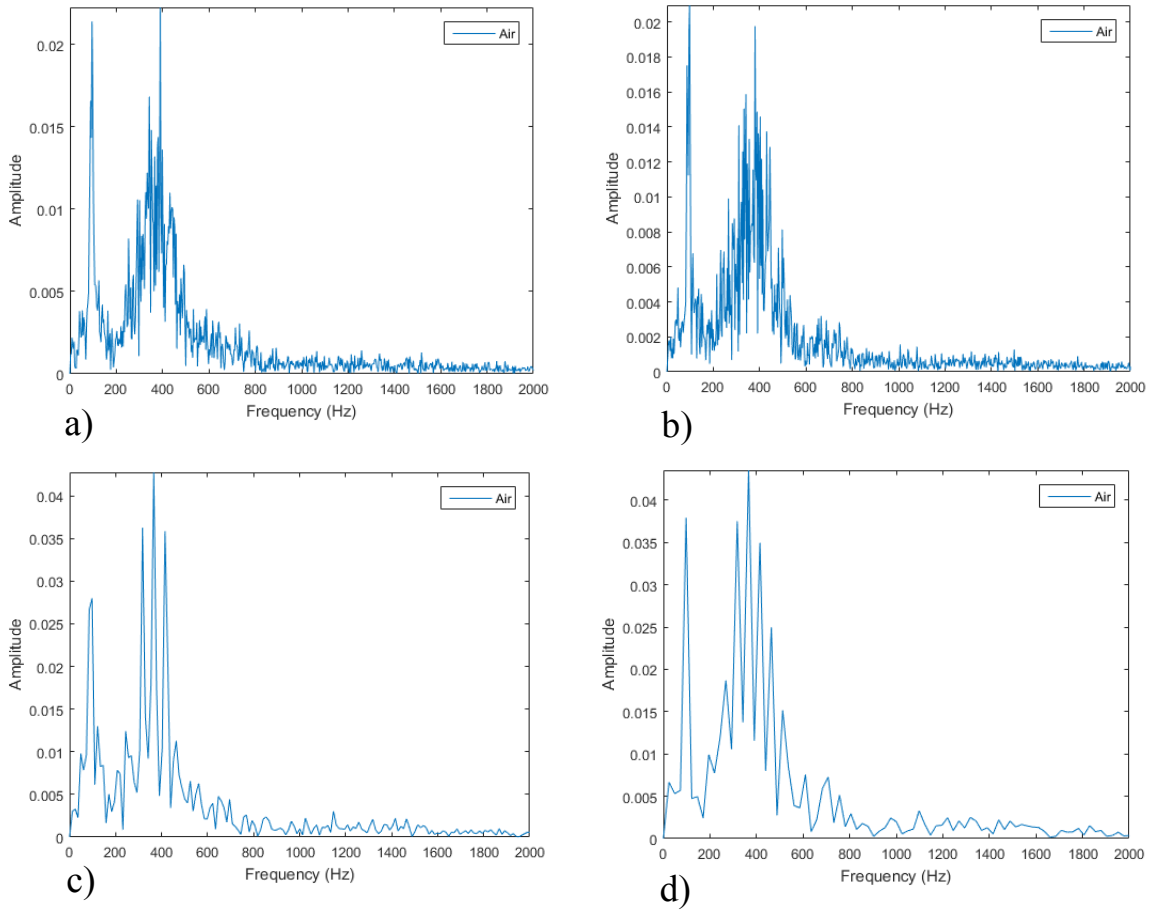

Figure 65: The FFTs of the different time increment measurements using a modulation frequency of 1 Hz, correlating to the time increments of the time domain: a) the biggest time domain increments, resulting in what appears to be a noisy FFT signal, b) the time increments is decreased between samples, c) time increments are further decreased and d) the smallest time spaces between samples, resulting in a cleaner FFT of the time domain signal.

Figure 64 and Figure 65 are the measurements and FFTs with the probe tip in air. These form part of the reference measurement. As the time increments decrease, clearer results are shown in the FFTs.

Next, the modulation frequency was changed to 10 Hz. This had an impact on the beat signal that was formed in the time domain and then consequently also impacted the shape of the FFTs that were performed on those beat signals.

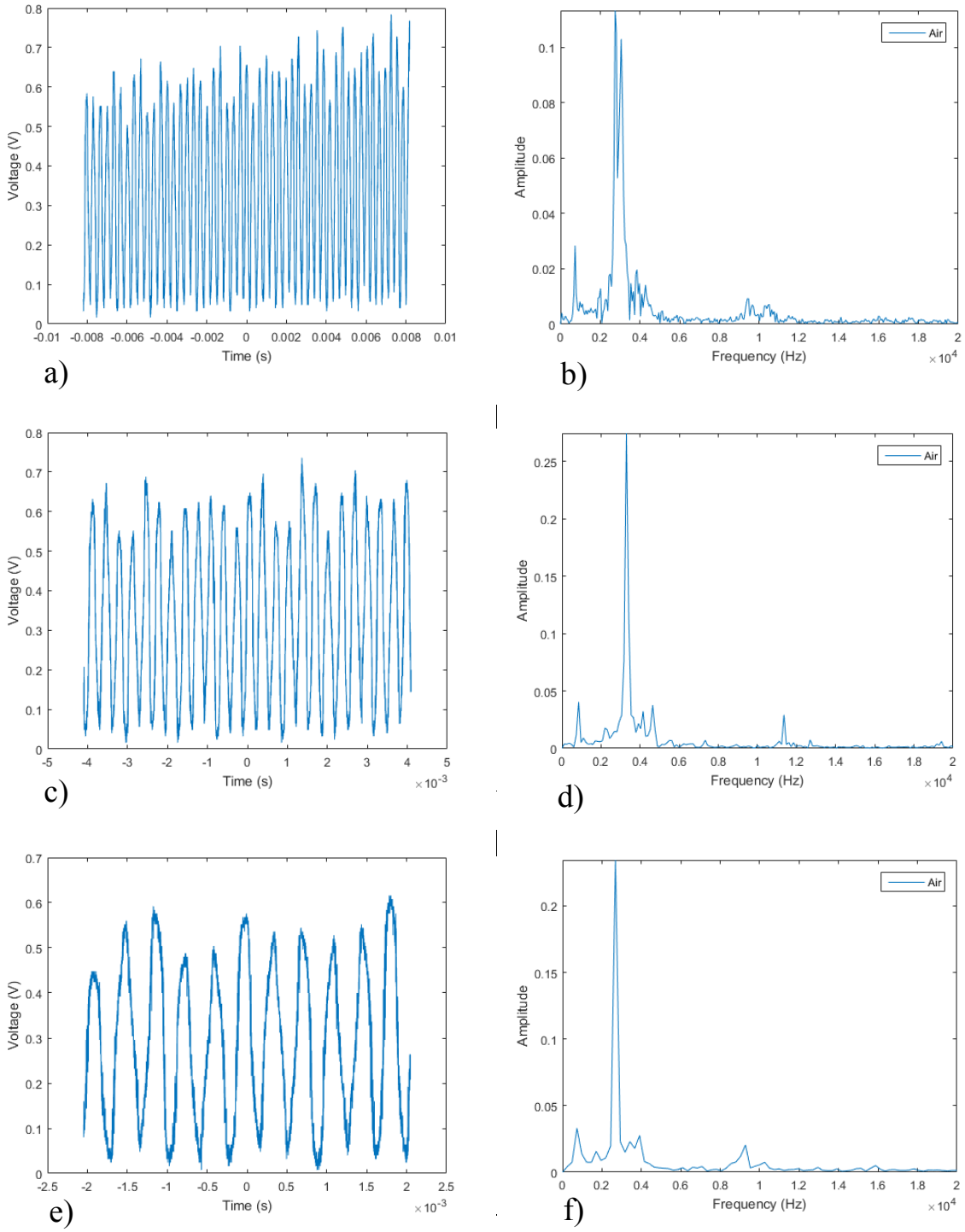

Figure 66: The beat signals and the FFTs performed on the different time increments of air using a modulation frequency of 10 Hz: a) the biggest time domain increments – note that more of the time domain spectra can be seen, but with lesser detail, b) the FFT of the time domain with the biggest time increments, c) decrease of time spaces between samples, d) FFT of the decrease time intervals, e) the smallest time increments between samples, showing more detail of the signal and f) the FFT of the time domain signal with the smallest time increments.

Increasing the modulation frequency of the microcontroller will increase the sweeping rate of the laser. This sweeping rate will in turn change the frequency of the resonant cavity in the sensor, changing the beat signal in other words. This change is linear, thus the frequency of the beat signal using 10 Hz instead of 1Hz modulation frequency with increase the beat signal to have a frequency that is 10 times higher.

Different analytes were measured with the prototype and some of these can be seen in Figure 67. These include distilled water, propanol, acetone, vodka and glycerine. The beat signals of these different substances, including air for the reference measurement, is shown below in Figure 68 and Figure 69.

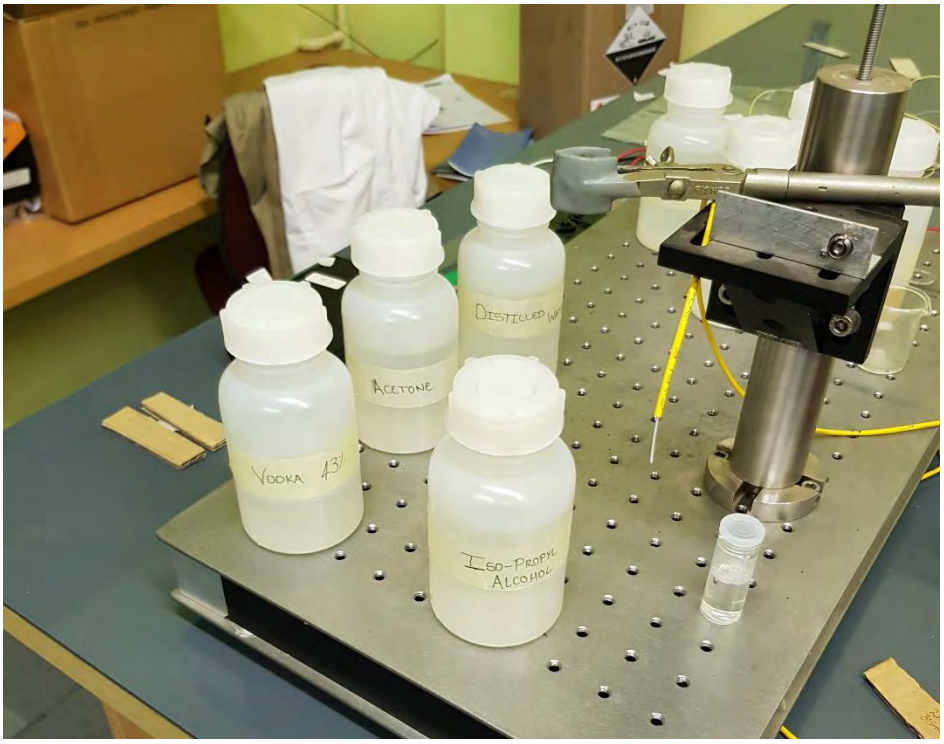

Figure 67: The dipping platform with the different chemicals that were measured (glycerin is in the small container)

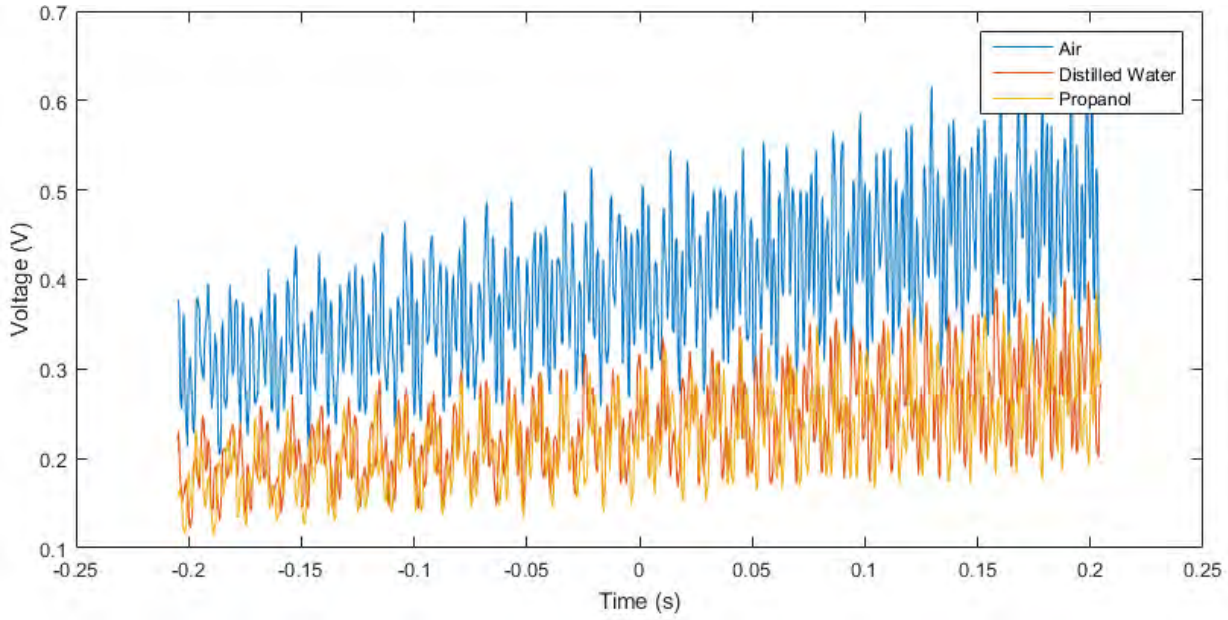

Figure 68: Beat signals of air, distilled water and propanol at 1 Hz modulation frequency

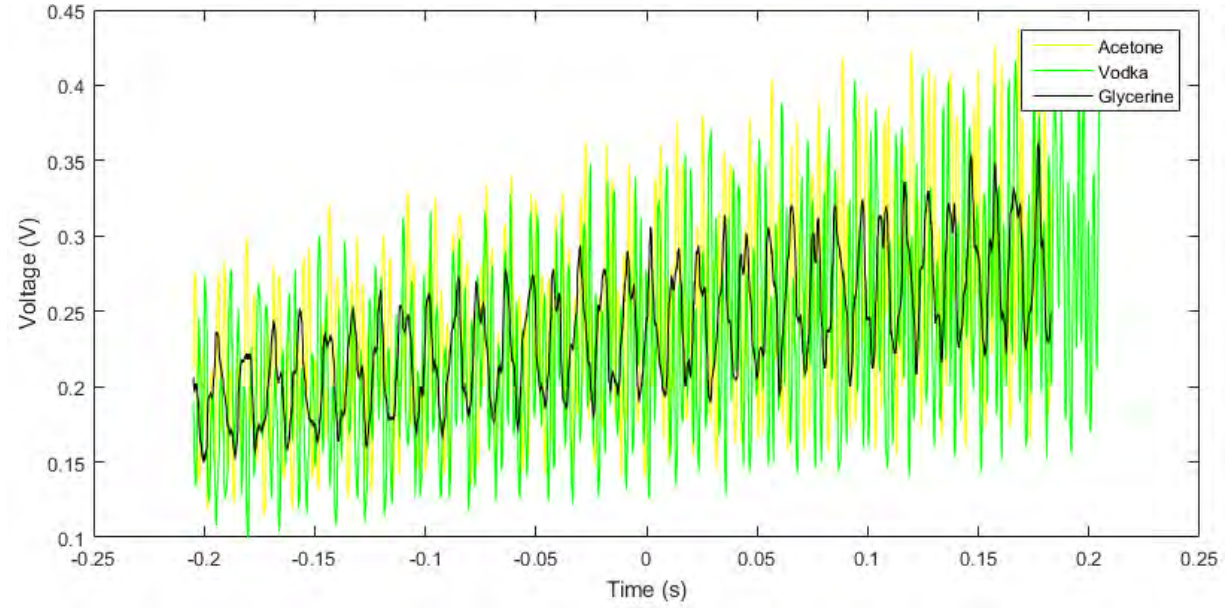

Figure 69: Beat signals of acetone, vodka and glycerine at 1 Hz modulation frequency

The beat signal were split into two different graphs to avoid cluttering. From Figure 68 the amplitude of distilled water and alcohol can be seen to be quite similar and in Figure 69 the amplitudes of acetone and vodka to be close to each other too, making it vital to apply FFTs on these results for further processing. Figure 68 and Figure 69 show the results of the beat signals at

1 Hz modulation frequency. Figure 70 and Figure 71 below are the results of the beat signals at 10 Hz modulation frequency.

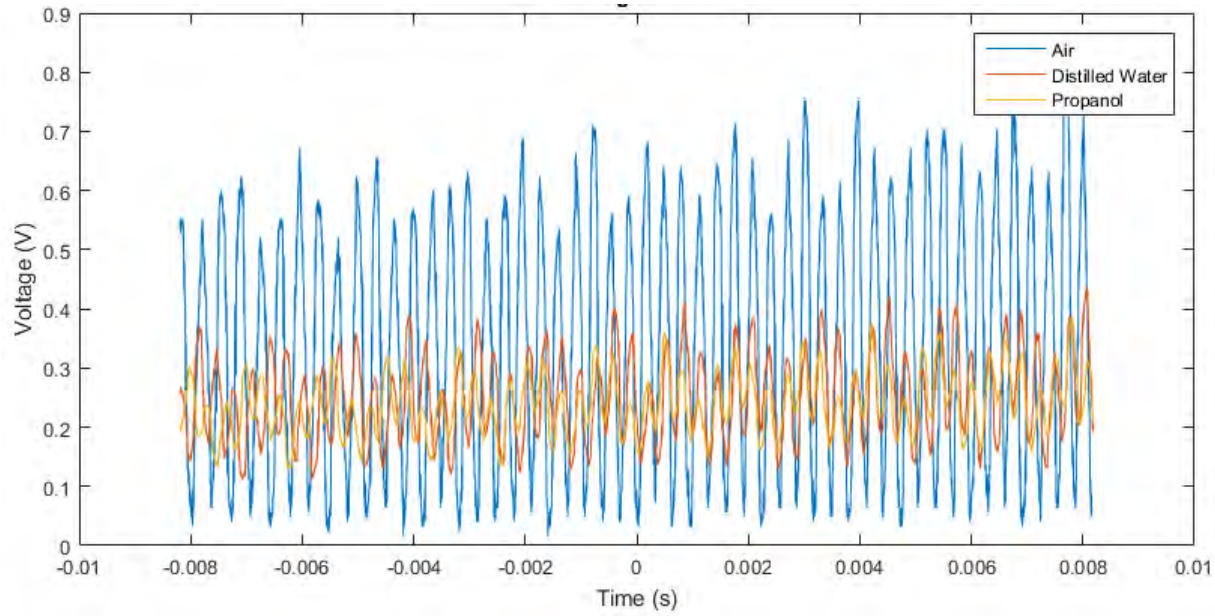

Figure 70: Beats signals of air, distilled water and propanol at 10 Hz modulation frequency

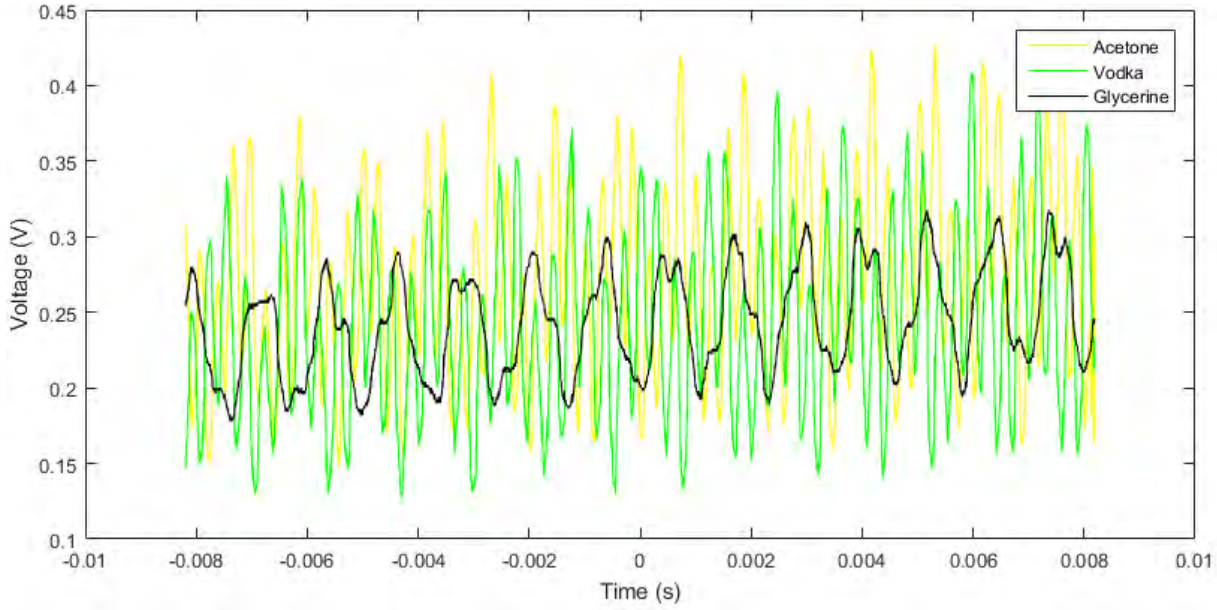

Figure 71: Beat signals of acetone, vodka and glycerine at 10 Hz modulation frequency

Similar results can be seen between distilled water and propanol in both the 1 and 10 Hz modulation frequency as well as for acetone and vodka. The FFTs for the 1 Hz modulated beat signals are shown in the figures to follow: Figure 72 shows the comparison of the FFTs of air,

distilled water and propanol and Figure 73 shows the comparisons between the FFTs of acetone, vodka and glycerine.

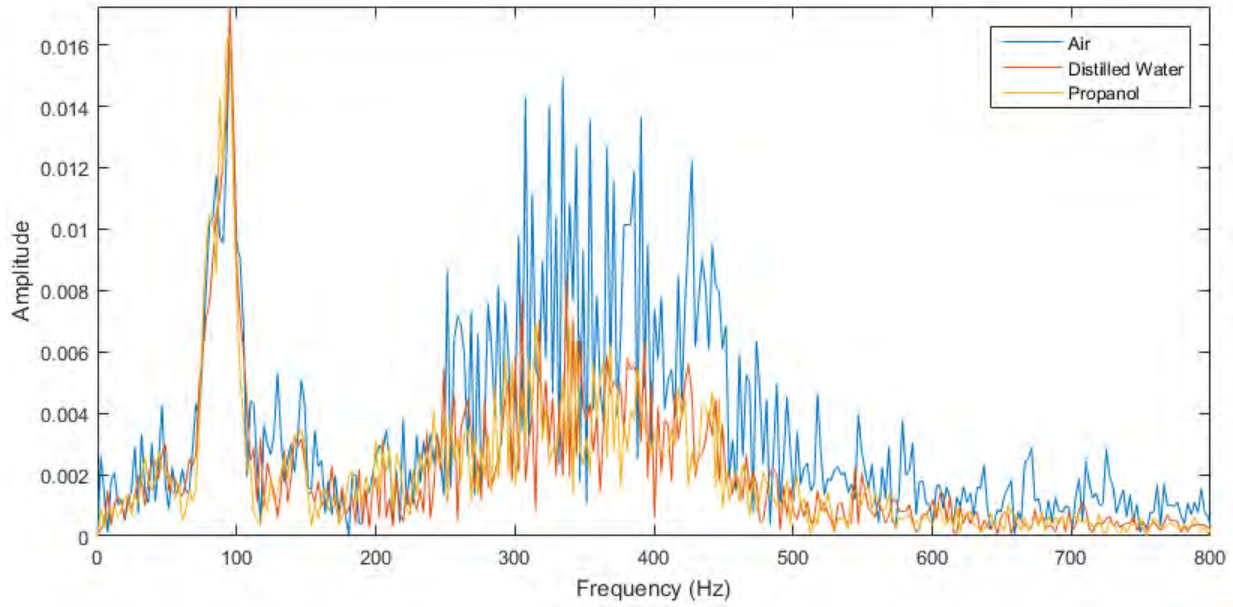

Figure 72: FFT of air, distilled water and propanol using 1 Hz modulation

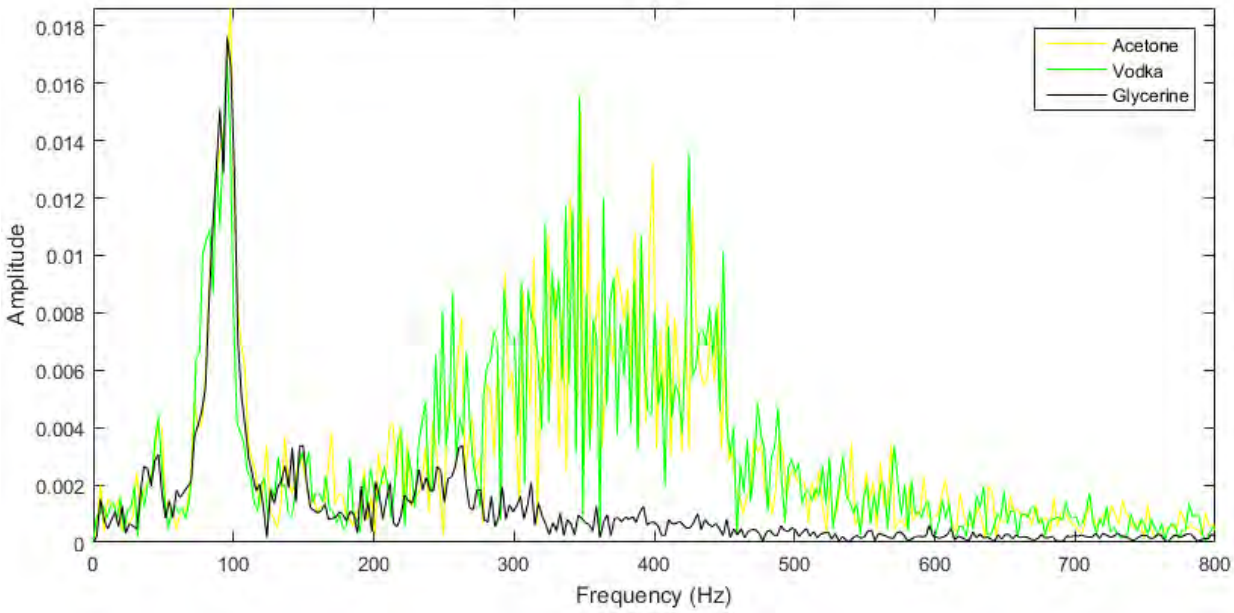

Figure 73: FFT of acetone, vodka and glycerine using 1 Hz modulation

The FFTs of the 10 Hz modulated signal are shown in Figure 74 and Figure 75, where Figure 74 contains the FFTs of air, distilled water and propanol and Figure 75 contains the FFTs of acetone, vodka and glycerine. The FFTs of the 10 Hz modulated signals have peaks similar in relation to the 1 Hz modulated signals, but are 10 times higher in frequency, since the sweeping rate is 10 times higher in frequency. This is a linear change in the modulation frequency that will have a linear change in the resonating cavity in the sensor, producing this frequency that is 10 times higher.

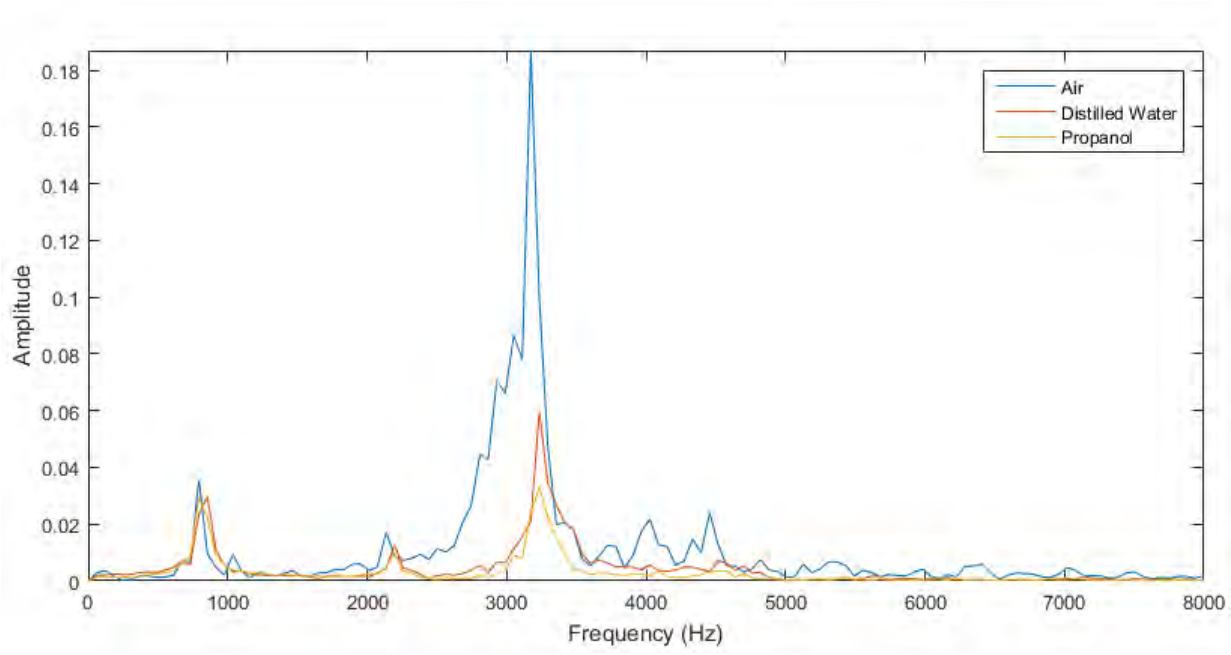

Figure 74: FFT of air, distilled water and propanol using 10 Hz modulation

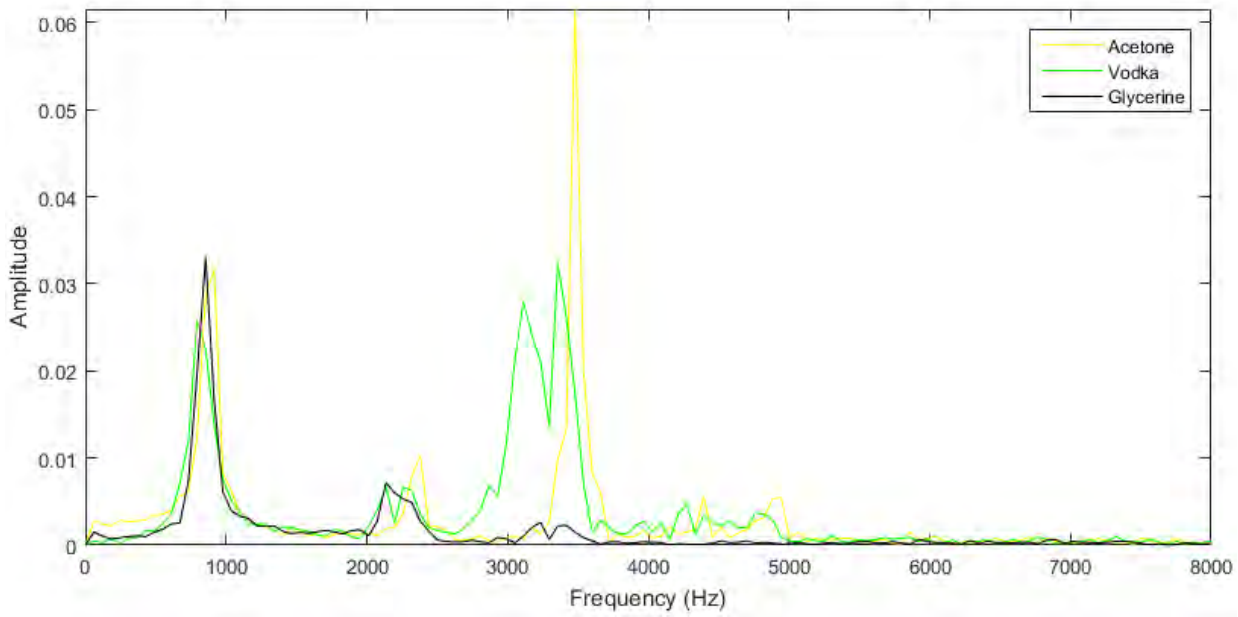

Figure 75: FFT of acetone, vodka and glycerine using 10 Hz modulation

These results are without any linearization processing and are taken just from the system that is connected as is. The results of the system will be tested and can then be improved by more signal processing methods. The total number of samples taken for the 1 Hz modulation and the 10 Hz modulation were 2570 measurements for each substance/analyte. The algorithm that was used to calculate the refractive indices for each analyte has been discussed in the previous experiments, but will be repeated here in a detailed overview.

There are 2 distinct cavities found in the sensor of the prototype, with a third formed by the summation of these two. Each cavity of the sensor will cause a beat signal to be generated. This beat signal is due to interference of the electromagnetic wave of the start and end of the cavity (for example in Figure 39). The frequency of this resonant cavity is dependent on the sweep rate (modulation frequency) of the source, the range of swept wavelengths of the source and the length of the cavity – therefore the difference in frequency between the cavities will be determined by the length of the cavities, as the source is the same for all the cavities. The smallest cavity will have the smallest frequency of all the beat signals and the largest cavity will have the highest frequency. Thus, in this system, the reference cavity is the smallest and will contain the smallest frequency component. The amplitude of the reference beat signal is dependent on the same interfaces and therefore can be used as the reference. The amplitudes of the other cavities are dependent on the

external refractive indices of whatever the probe is in contact with and either can be used to make the refractive index measurement. The ratio of either of the cavities with the reference cavity is thus used for the refractive index measurement. However, before this can be used, the system parameter has to be determined and is denoted by the letter K. The K value is calculated from the reference measurement using air. The average K value for the system using a modulation frequency of 1 Hz is 5.4248 and for the modulation frequency of 10 Hz is 35.1054.

Following are graphs of the results taken from thee different analytes – air, distilled water, propanol, acetone, glycerine and then vodka, which is calculated with the help of the compensation curve that was made from the compensation factors across the different refractive indices throughout the range measured. The first batch of results were taken when the modulation frequency of the source was set at 1 Hz, the second batch of results were taken with a modulation frequency of 10 Hz. The first batch of measurements included a sample size of 1640 measurements per analyte, the second batch of measurements are 930 in size per analyte. In all of the following figures, the measurement points are plotted as a scattered plot with a red line through the graph, indicating the theoretical value of the refractive index for each of the substances. The standard deviation is then calculated after the plots of the results are presented.

Figure 76 to Figure 82 are the plots of the results of air, distilled water, propanol, acetone, glycerine and vodka, respectively, at 1 Hz modulation frequency. The compensation curve was calculated and graphed from the results of the analytes that has a theoretical value backed up by numerous sources. The compensation curve was used to calculate the value of the refractive index of alcohol. The compensation curve for the 1 Hz modulation frequency is shown in Figure 81 and for the 10 Hz frequency in Figure 88.

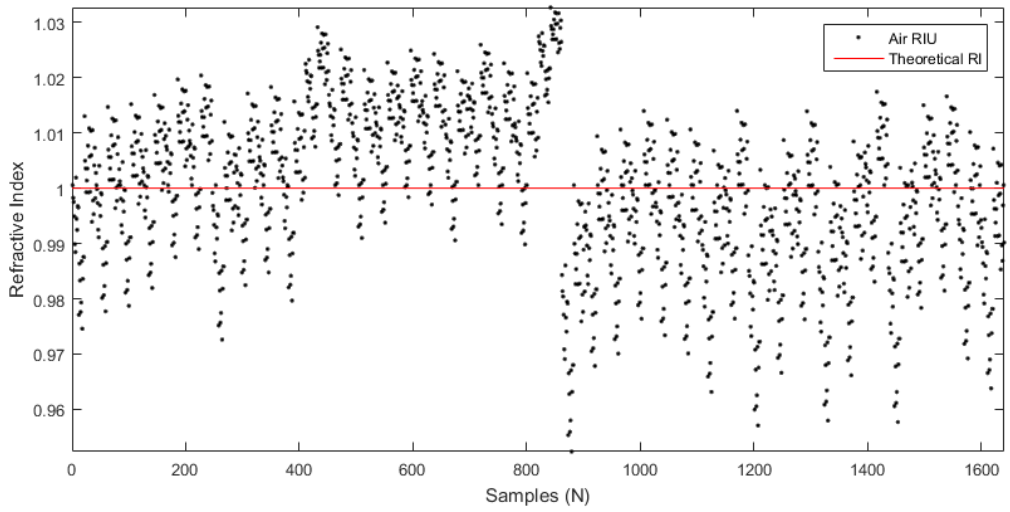

Figure 76: Results of air as analyte at 1 Hz modulation frequency

What is shown in Figure 76 is the results of air as analyte, with a modulation frequency of 1 Hz used for the saw-tooth wave sweeping. The theoretical value of air is indicated with the red line. Up to the middle of the graph, the majority of the results are above the red line, after this the results are below the theoretical line. Although not being aware of it, the tip of the fibre could have been damaged after approximately half of the results were measured, causing the intensity of the reflected wave to lose power and therefore having lower results.

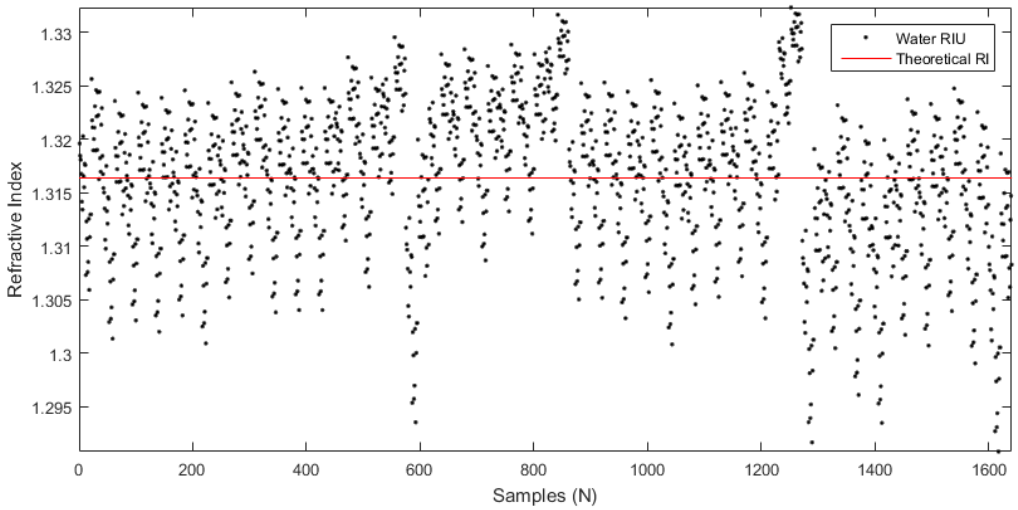

Figure 77: Results of distilled water as analyte at 1 Hz modulation frequency

Figure 77 displays the results of when distilled water was used as the analyte. The theoretical line is generally in the middle of the results throughout the plot, showing that the variance stays around the theoretical value of the refractive index of water.

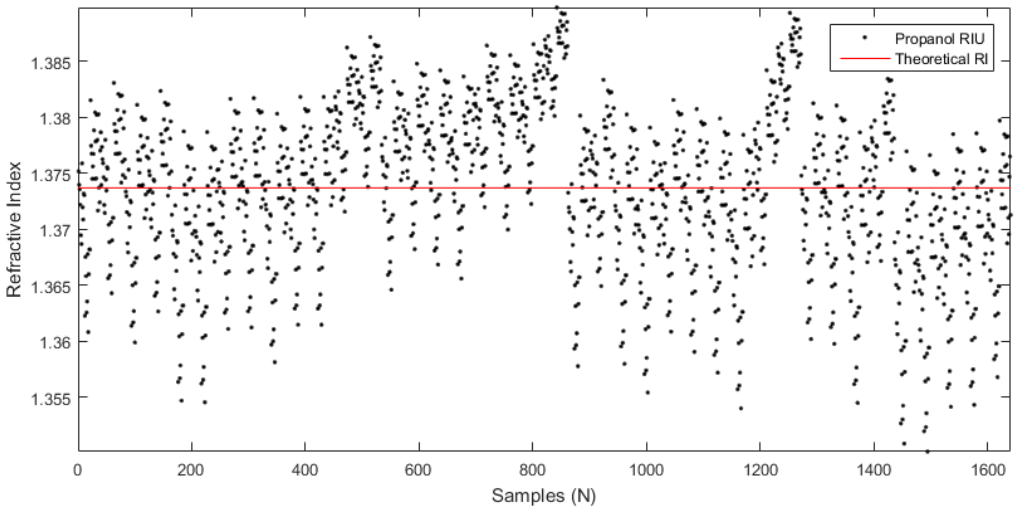

Figure 78: Results of propanol as analyte at 1 Hz modulation frequency

Figure 78 shows the results of propanol as analyte. The theoretical value remain in the middle of the measured results. The prototype displays good repeatability for these measurements. The results for acetone as analyte is similar, shown in Figure 79.

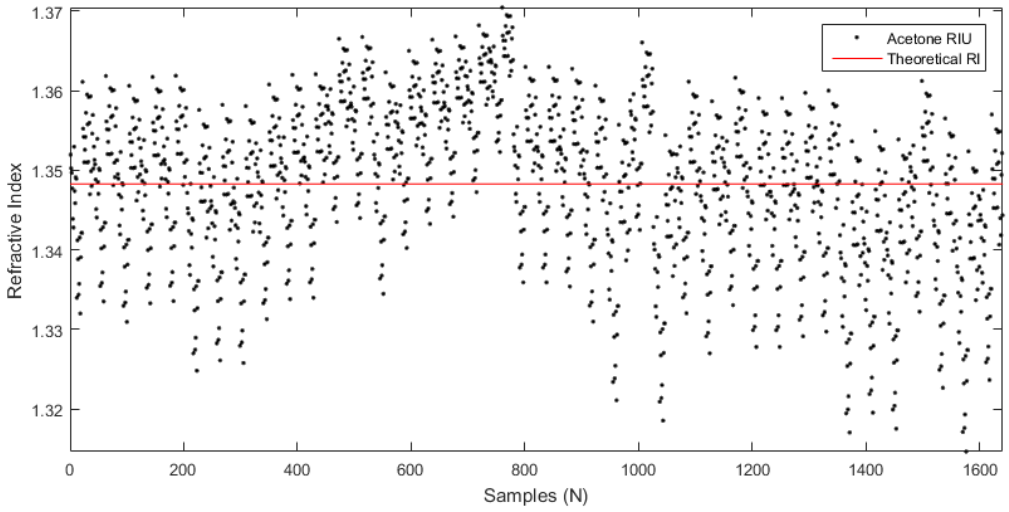

Figure 79: Results of acetone as analyte at 1 Hz modulation frequency

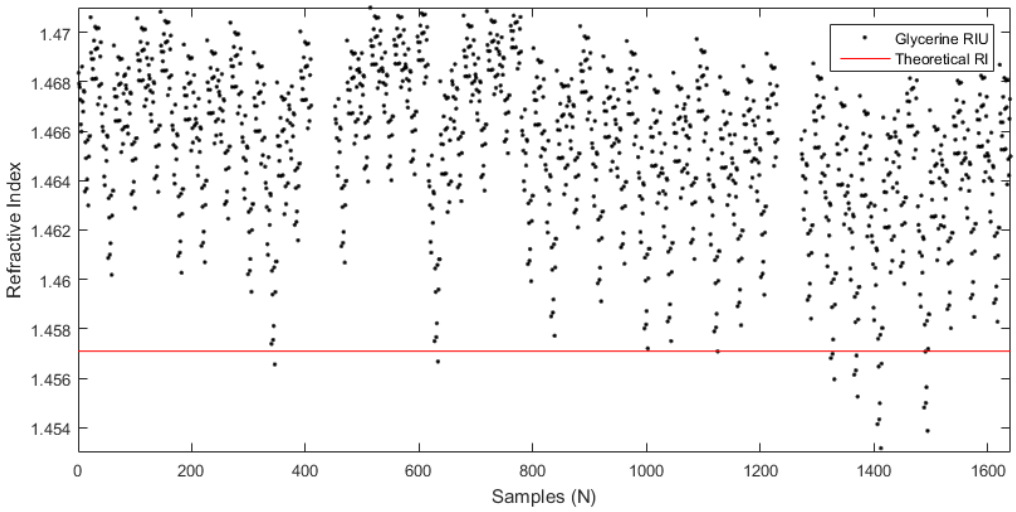

Figure 80: Results of glycerine as analyte at 1 Hz modulation frequency

Most of the results of glycerine as analyte are above the theoretical line, as shown in Figure 80. Glycerine could be slightly more difficult to measure, since the refractive index is similar to that of the core refractive index of the optical fibre.

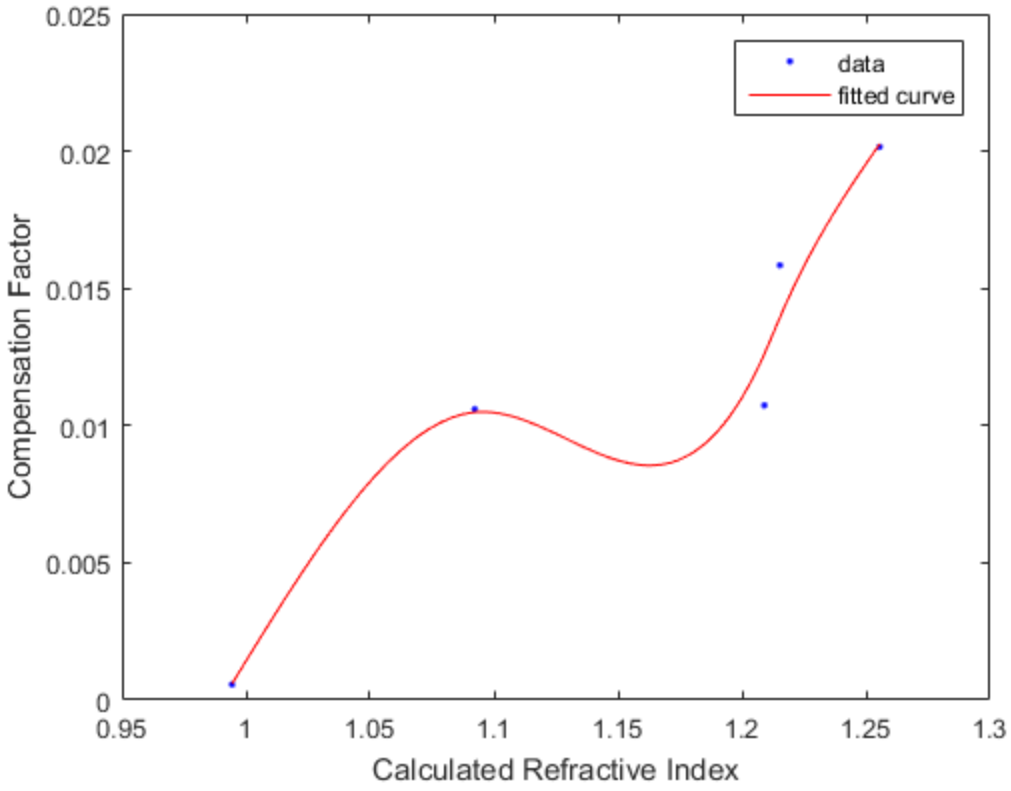

Figure 81: Compensation curve for the 1 Hz modulation frequency

The compensation curve for a modulation frequency of 1 Hz shows a polynomial fit to the graph. This was selected for the best fitting line, since it passes through most of the points, but it is noted that the compensation curve is better compared to the curve of the 10 Hz modulation frequency curve, which shows more of an exponential type of graph, but note, it is not exponential. The 1 Hz modulation frequency does produce different results than that of the 10 Hz modulation frequency, therefore yielding a different compensation graph as well. This could be due to the analyte of that particular refractive index reacting differently and therefore producing this jump in the compensation graph.

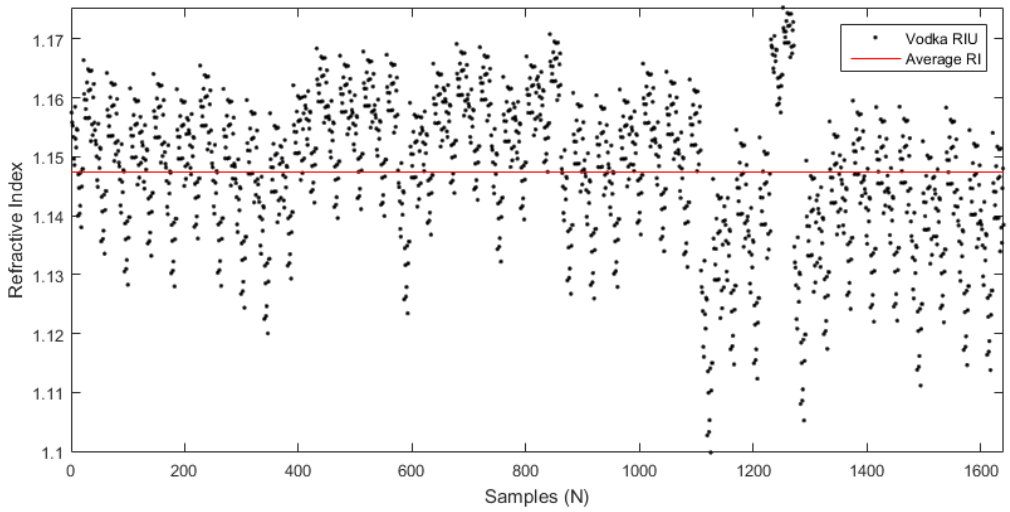

Figure 82: Results of vodka as analyte at 1 Hz modulation frequency

Figure 82 shows the different values of the measured refractive index of vodka. The compensation graph was implemented for these measurements, as there is no theoretical value for vodka that can be taken, since the refractive index of vodka can change from brand to brand and bottle to bottle, depending on the chemicals released in the fermentation process. The average of this result is 1.1474 refractive index units, but was expected to be between that of water and propanol, around the 1.35 RI mark. The modulation frequency can have a variance in this result, as well as the compensation curve, not being an exponential curve.

Figure 83 to Figure 89 are the plots of the results of air, distilled water, propanol, acetone, glycerine and vodka, respectively, at 10 Hz modulation frequency.

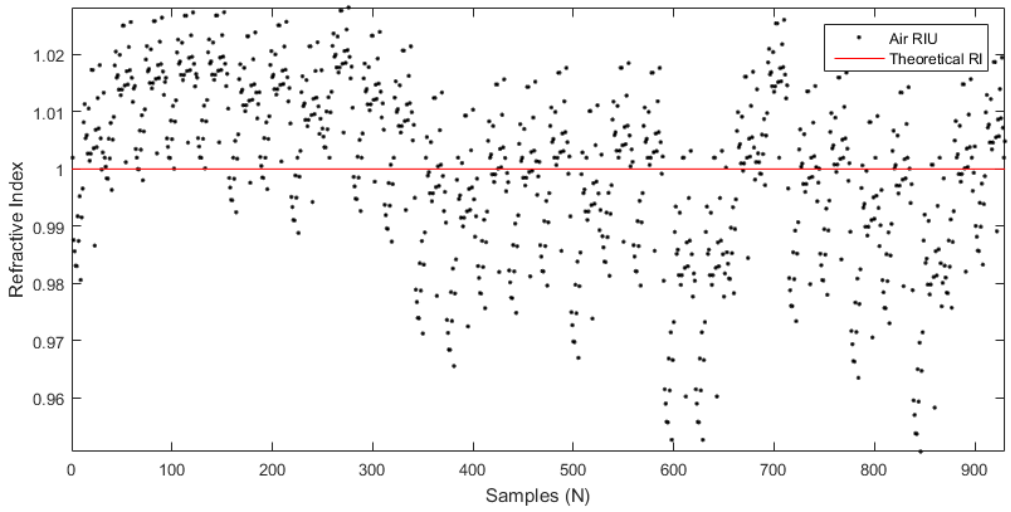

Figure 83: Results of air as analyte at 10 Hz modulation frequency

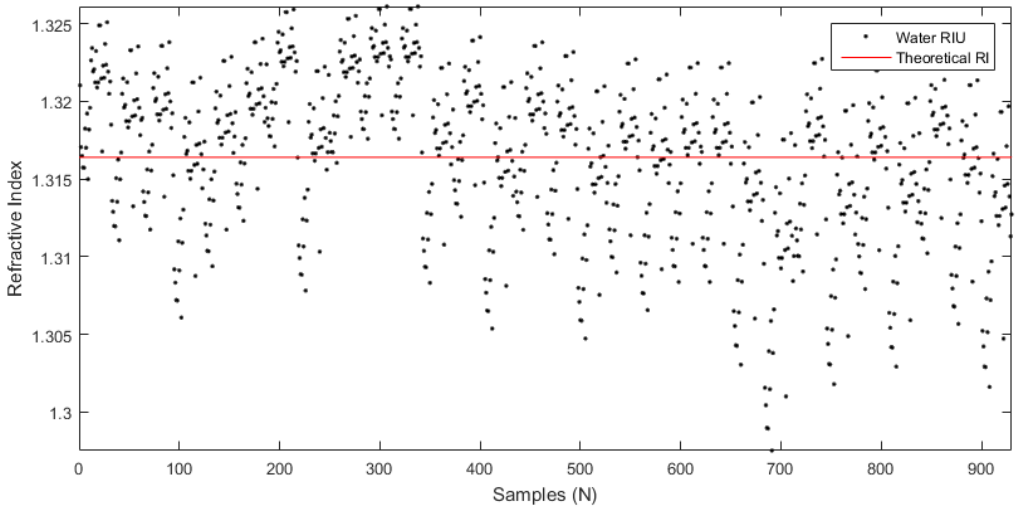

Figure 84: Results of distilled water as analyte at 10 Hz modulation frequency

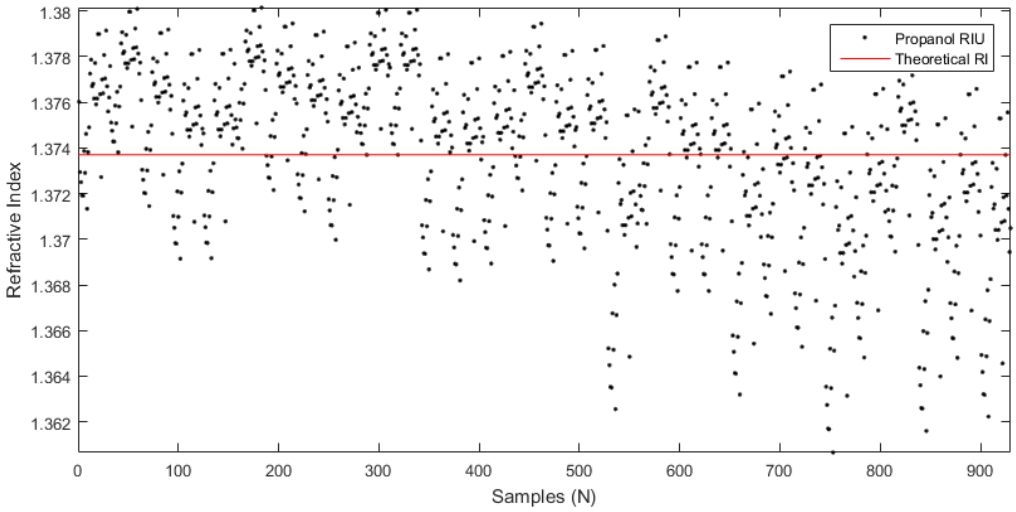

Figure 85: Results of propanol as analyte at 10 Hz modulation frequency

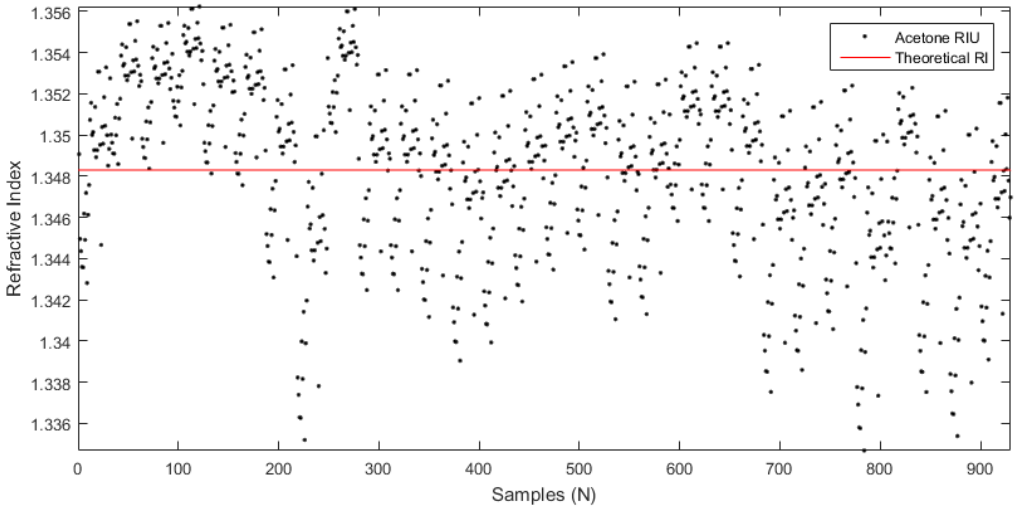

Figure 86: Results of acetone as analyte at 10 Hz modulation frequency

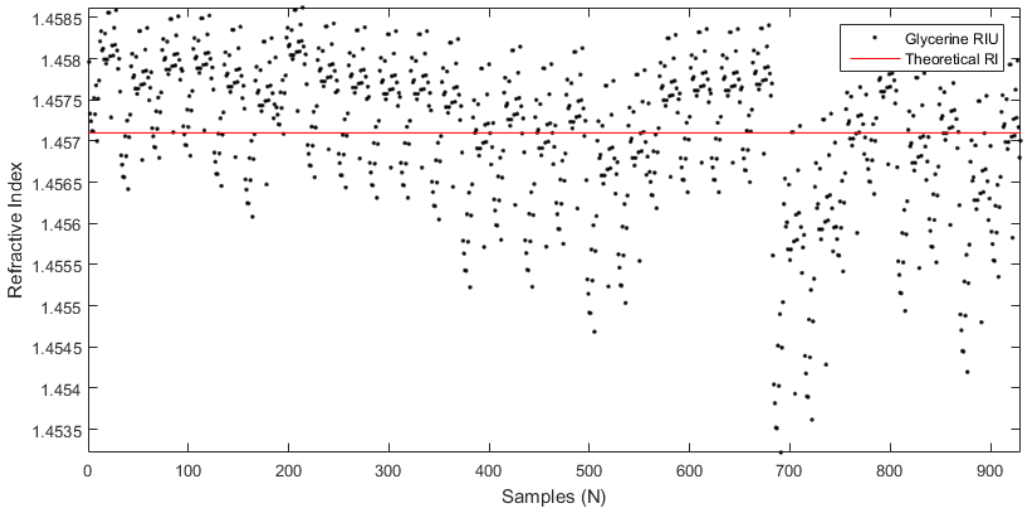

Figure 87: Results of glycerine as analyte at 10 Hz modulation frequency

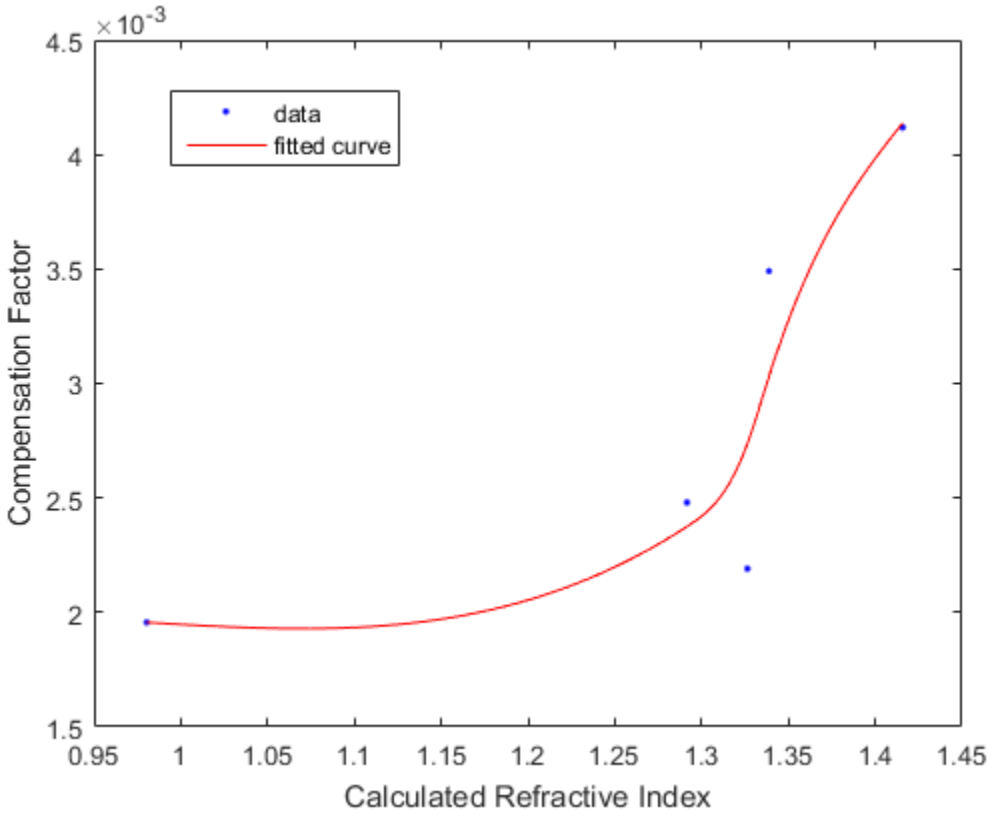

Figure 88: Compensation curve for the 10 Hz frequency

The compensation curve produced when using the 10 Hz modulation frequency seems to provide a better fit than that of the 1 Hz modulation frequency. The results of the refractive index of vodka

also provides better logical results, as the average refractive index is situated between that of water and propanol.

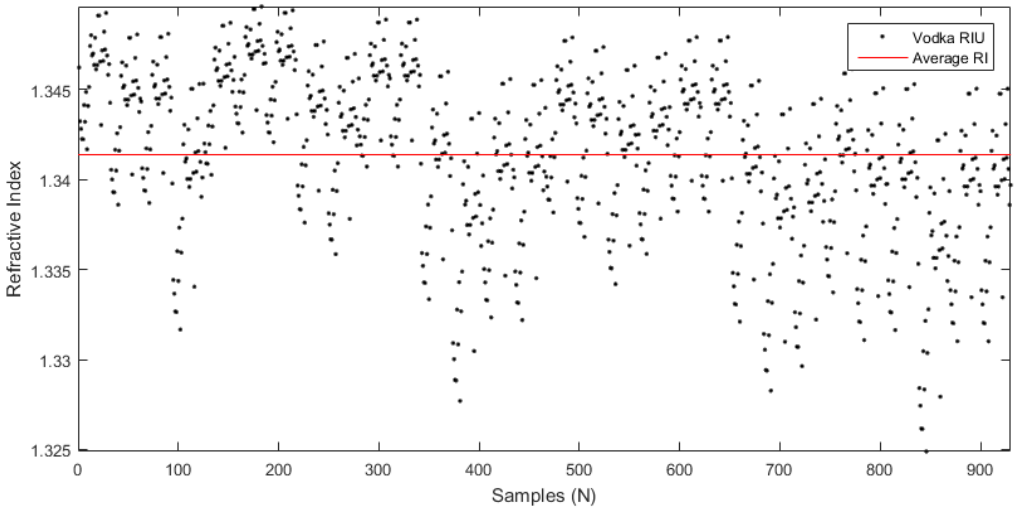

Figure 89: Results of vodka as analyte at 10 Hz modulation frequency

Figure 89 shows the results of Vodka using a 10 Hz modulation frequency. The average is calculated to be 1.3414. This is a better presumed result, since the refractive index lies between that of distilled water and propanol. The standard deviation of vodka can be seen in Table VI, also showing the standard deviation of the other substances.

Table VI: Standard deviation of the different substances

Analyte	**Standard Deviation at 1 Hz**	**Standard Deviation at 10 Hz**
Acetone	0.009763069003096	0.004221363411419
Air	0.014062148966424	0.015231348223477
Glycerine	0.036673932910357	0.000919321727133
Propanol	0.007120025926352	0.003748746563909
Distilled Water	0.006952462359593	0.005168367849060

Vodka	0.012226087618792	0.004588736872472

In general, the results for the 10 Hz modulation frequency is more stable than the ones for the 1 Hz frequency. This could be due to less noise in the system caused by a more detailed scan of the wavelength.

Conclusion

In this chapter the various results of the experiments are shown. All these experiments form part of the evolution of the final design of the project. With the successful implementation of these experiments, the prototype has been tested through all the individual parts that need to function together.

The optical sensing started with the air capillary in the sensor, where the refractive indices of propanol and distilled water were measured with air as the reference. The Fabry-Perot interferometer with the air capillary yielded good results with propanol and distilled water as analytes.

The Fabry-Perot interferometer formed by the piece of standard telecommunication grade optical fibre with FC-PC connectors was also tested. This was to prove that the measurements can be made with a simple fabricated sensor.

When the Erbium fibre laser was used as the scanning optical source, it did provide acceptable results, but the need arose for a custom current source, as this EDF laser was bulky and some scans caused indistinguishable peaks in the FFT that was performed on the beat signals, meaning that the scans of the tunable laser source did not provide the level of linearity needed. With this came the need for a DFB laser and a source to drive the laser diode.

The current source was tested and the results were given. The microcontroller provided the linear saw-tooth scan through voltage as the input to the current source. This was used by the current source to provide the necessary current to drive the laser diode. The microcontroller scans through voltage starting at 56 mV and ending with 562.4 mV. This in turn yields a current starting at 4 mA

and ending at 48.2 mA provided by the current source. The DFB laser has a wavelength scan of just under 1 nm, giving a range that is usable for the COFDR interrogation method.

In the following chapter, the refractometer prototype will be discussed with regards to the advantages and uniqueness that the system possesses.

Chapter 6: Discussion

Introduction

In the previous chapters, experiments were set for the successful testing and implementation of the prototype, with the results that were analysed and discussed. In this chapter, the importance of the prototype will be elaborated upon, showing the advantages over existing systems and further potential of the prototype.

Power Source Advantages

The power source that was built consisted of a microcontroller and a current source. The microcontroller was used to modulate the voltage input to the current source, through the output of the analogue pins of the microcontroller.

One of the advantages of using the microcontroller include having control of the modulation rate. Different modulation rates yield different results, as seen in chapter 5 providing the results – using the 10 Hz modulation rate overall had better results than the 1 Hz modulation rate. The microcontroller also calibrates the system that can be automated to perform after several scans, a set time or when there has been damage to the sensor tip.

Another advantage of using the microcontroller was that the offset voltage could be controlled, which has the effect of controlling the starting current that was provided to the DBF laser diode. This means that the laser diode could be used only in the region of stable stimulated emission, giving a linear scan through wavelength in time – a good enough scan that without any linearization, provided accurate refractive index measurements.

The current source was compact, having the advantage of being easily implemented in the prototype. The current source also provided stable current to the laser diode, not fluctuating, which would have caused the change of phase in the linear sweeping of wavelength that results in the broadening and decrease of the frequency components, if it did fluctuate. This then would have led to inaccurate results.

The current source was also designed that the maximum voltage allowed across the diode does not get exceeded, keeping the laser diode safe within the power characteristics.

Although the power source works well, it has a great potential of further development and can be implemented to "learn" what modulation rate would provide the most stable results. This would improve the repeatability of the system. The future implementation provides for an automatic adaption to see what rate yields the best results, which allows for a smarter device.

The designed power source is compact, has the ability to control the laser with good stability and has future potential to "learn".

Optical System Advantages

The optical system consisted of a DFB laser diode, a circulator, the sensor and a photodiode. The optical system had to be fabricated in such a way that would not be difficult or expensive. The optical system also needed to be compact.

The laser diode used was tested with the power source and provided a near linear change in the emitted wavelength as the current through the diode changed linearly. This means that the change in phase was kept small enough, which provided prominent peaks in magnitude of the discrete frequency points after a FFT was performed on the beat signal. These distinct peaks were then used for the calculation of the refractive index of whatever substance was being measured.

The circulator with the photodiode were standard pieces of the optical system. No special fabrication or implementation was needed for these components, adding to the simplicity of construction of the prototype.

The sensor of the system, consisting of silica, possesses all the advantages of an optical fibre. These include being chemically passive, immune to electromagnetic interference, small in size, robust and light weight.

The sensor that was built consisted of two pairs of FC/PC connectors with a fibre end that was cleaved. This sensor is easy to fabricate – no expensive or special splicing or other fabrication equipment was needed to construct the sensor. This simplicity of design contributes to the production of the prototype – with no difficult procedures or time-intensive processes required for

the physical construction. The same simplicity of fabrication goes for the sensor of the prototype. The important part that makes the prototype get accurate results lies in the interrogation method and the signal processing code algorithms.

Another advantage of the optical sensor comes from the tip of the probe. If the tip of the probe does not provide clear results after time or if it gets damaged, it does not need to be totally discarded. The tip of the sensor can be cleaved if the sensor tip is damaged. Since this system is self-referred, it can be calibrated with the modification to the sensor tip and is once again ready for use. If there is any major damage to the sensor tip or fibre containing the sensor tip, then the solution for fixing this is not an expensive or difficult procedure. The piece from the second FC/PC connector can be replaced and the system can once again be used, keeping in mind that the system needs to be calibrated again (which is as simple as the press of a button). This is a cost effective attribute of the fibre sensor.

The sensor yielded good results – even though the setup of the sensor isn't complicated, the standard deviation was not big in the measurements. This means that the repeatability of the system is good – the results of the measured analyte will stay consistent.

Prototype Advantages

The advantages of the different components and subsystems add to the prototype, but the prototype as a refractometer, possesses other advantages. An important advantage is that the prototype is not bound to the laboratory, but is portable. For this prototype to be more user friendly and functional, it can be taken to a water source, brewery, chemical department or wherever the measurements need to be taken. With the integration of the subsystems, the prototype holds the advantages of functioning together as a compact and portable refractometer.

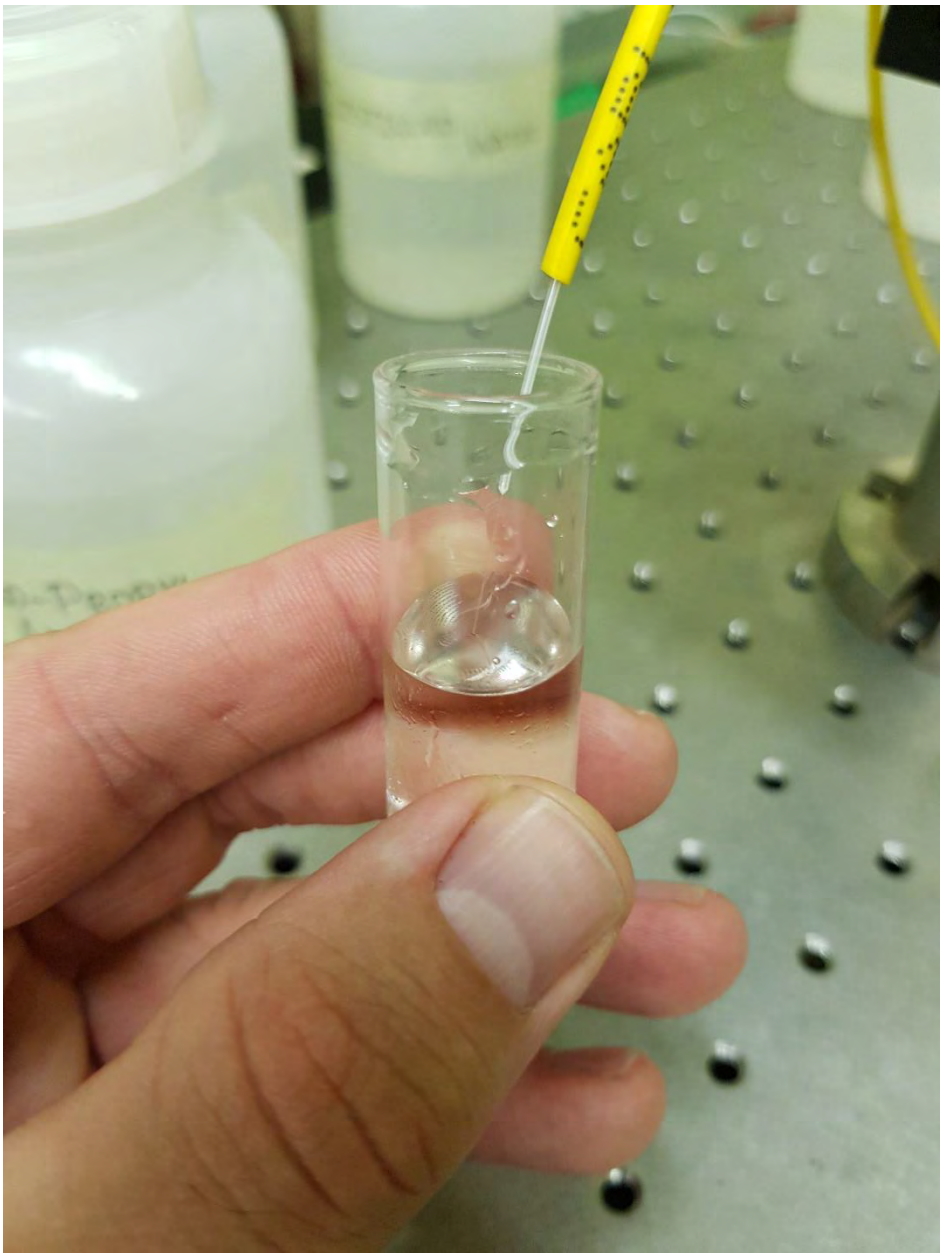

Figure 90: The small, lightweight and chemically passive sensor tip measuring the refractive index of a sample of glycerin. Even with the sample being held, being exposed to some vibration, the variance in measurements were small and accurate.

Adding to the portability and convenience of the system, the processing is done on-board, meaning that with the subsystems integrated in the prototype, there are no other computers or external processors needed for the analysis of the results – the measurement and identification of the analyte can all be done by the prototype.

This leads to an advantage making the refractometer consist of simplistic components and subsystems – the processing of the raw data is done by the algorithms implemented to make the subsystems function together. The microcontroller, current source, optical components, including the sensing head, can be swapped or replaced. This is due to the algorithms implemented to calibrate the system, measuring the beat signals, performing FFTs and calculating the refractive index. It is the applied algorithms that make the simplicity of the subsystems possible.

Conclusion

The novelty and advantages of the system is discussed in this chapter, starting with the electronic aspects and then moving to the optical aspects.

The power source provides good control, stability and is compact, with the ability to "learn" for future applications. The characteristics of the power source allow it to provide a linear emission of wavelength through the scan of the laser diode, which is very important to avoid frequency spread in the interference pattern of the sensor.

The optical system provides a simple design with many advantages other than only the advantages that are inherent to silica. The sensor is self-referred, making the system able to be calibrated if there is any change to the sensor tip. This gives a disposable advantage to the sensor tip, if the tip needs to be replaced then it can simply be cleaved shorter or if a bigger part of the sensor is damaged, then a new FC/PC connector can simply be connected.

In the next chapter, this project will be concluded.

Chapter 7: Conclusion

Introduction

The prototype has gone through various stages of development in this project. It started with an introduction, stating why the project is important, what was going to be done and how it was going to be done. Objectives were defined for the project to be a success. Literature studies and other projects were researched to know what the best techniques would be to implement in the project and the expertise of experienced researchers in the field were contacted to know what the best implementation of the system would be.

After a thorough understanding of what and how the project should be done, experiments were laid out to test the system – whether it be in parts for the subsystems or as a whole for the prototype. The experiments were done and the results were recorded and discussed. The prototype's uniqueness was shown, having advantages in many aspects, and the effectiveness of the prototype was discussed.

In this chapter, the overview of the prototype will be given, as the objectives will be arranged with what was achieved.

Achieved Objectives

The main objective of the project was to build a refractometer with custom electronics to control the optical source of the system which implements the coherent optical frequency domain reflectometry technique.

This main objective can be broken down into smaller objectives to test the subsystems, to make sure that all aspects of the prototype work individually and as a whole. The objectives that were listed in chapter 1 include:

Creation of a fully operational refractometer as a prototype.

The refractometer was designed and tested in many different forms – using an air capillary to have a self-referred element that can be used to calibrate the system, as well as an implemented reference cavity with a FC/PC connection.

Using an in-line interferometer. This requires implementation of simple reflectors that should be realized in the sensing probe to promote easy fabrication.

Both the interferometer implementations, when using the air capillary and the FC/PC connection, yield results with low error and small standard deviations. Both these implementations are in-line, with the latter providing the advantage of being an easy fabrication option for the prototype.

A laser diode requires a linear sweeping through wavelength in time and the electronics that are needed for this should be custom built, as there are none that can be used commercially for this specific arrangement.

The electronics of the system consist of two subsystems – the microcontroller and the current source. The microcontroller provides a voltage input to the current source. The current source then takes this voltage as input and drives the DFB laser diode with a current. The voltage input to the current source is modulated, in a saw-tooth pattern. When the voltage is changed linearly, so does the current. This saw-tooth modulation by the microcontroller is done at a certain frequency, which can be set by the microcontroller.

Together the electronics control the laser with great stability and enables it to do a linear sweep through wavelength in time. Although this linear sweep is not 100 % linear, it does produce a sufficient linear scan (99.05% linearity compared to the linear regression line) that results in prominent peaks in magnitude in discrete frequency components when a FFT is done on the beat signals. The current source provides 99.9% linear current values to the DFB laser diode.

Integration of the electronic and optical components and subsystems as a single unit.

All the subsystems had to work together for the prototype to function. The integration of all the subsystems, being it electronic or optical, is crucial for the implementation of the prototype. After the integration of these subsystems, the prototype was tested and worked well – results seen in the last experiment conducted in chapter 5 (The Integrated Prototype). A summary of the results with respect to the standard deviation at 10 Hz:

- acetone with 0.004221363411419 RIU,
- air with 0.015231348223477 RIU,
- glycerine with 0.000919321727133 RIU,
- propanol with 0.003748746563909 RIU,
- distilled water with 0.005168367849060 RIU and

- vodka with 0.004588736872472 RIU of standard deviation.

Characterization of the system for refractive index measurements.

The characterization was done for the system after all the subsystems were integrated to form the prototype. This is a necessary part of the measurement of the prototype, as there is systematic error. The characterization of the system produces a compensation curve for the measurement of the refractive index at different values. Each analyte will have a different refractive index and will not be compensated for in the same manner as another substance. Therefore the reason for producing the compensation curve – each analyte will experience a different compensation factor.

The importance of the system, when keeping the compensation curve in mind, is that the system needs to have a small variance for the measurements, even when the compensation curve is used. Although each analyte is compensated for differently, the same compensation curve is used for all the analytes. This means that the prototype must provide a great deal of repeatability, providing the same results for the same substance, producing minimal fluctuations for the measurements. These fluctuations are measured to be to the second decimal for air and up to the fourth decimal for glycerine.

The system should be user friendly.

With the touch of a button, the system can be calibrated and the measurement of the refractive index of a substance can be measured.

Also, the advantage of portability gives the user more freedom to access different sites for substance measurement. The refractometer can simply be taken to the location where the measurement needs to be made, not being inconvenienced by a set location, for example in the laboratory only, where samples of the analytes need to be taken for testing. This adds to the functionality and user friendliness of the system.

The final prototype can then be tested in various applications, such as with laboratory chemicals.

The final prototype was tested in air, distilled water, propanol, acetone, glycerine and vodka. The prototype measured a distinct difference in refractive index from all the analytes, with a variance of 10^{-3} for acetone, propanol, distilled water and vodka and a variance of 10^{-4} for glycerine. Therefore, a measurement can be made for an analyte, showing a distinct result and therefore, the analyte can be identified.

As the prototype can be transported due to the compactness and portability of the system, the measurements of different substances are made easier.

Future Potential

This project has major potential for further development. The microcontroller can be used for further testing and smart adjustment to get results with the least standard deviation. A database can be used for the identification of the analyte. The power from the tip can be monitored to advise the user to have it cleaved or replaced. The results of this project doesn't conclude all the capabilities.

Conclusion

This project has been shown to have potential for production. The prototype incorporates a power source that is able to do what is needed for the implementation of the COFDR method with further advantages of being compact and intelligent. The sensor system is easy to fabricate, inherits disposable properties and produces accurate results, which can be used for the measurement of the refractive index of a substance leading to the identification of that substance. All these show a working and unique prototype.

References

[1] H. Meng, W. Shen, G. Zhang, X. Wu, W. Wang, C. Tan and X. Huang, "Michelson interferometer-based fiber-optic sensing of liquid refractive index," *Sensors and Actuators B: Chemical,* vol. 160, pp. 720 - 723, 2011.

[2] O. Frazão, J. M. Baptista, J. L. Santos, J. Kobelke and K. Schuster, "Refractive index tip sensor based on Fabry-Pérot cavities by a suspended core fibre," *Journal of the European Optical Society - Rapid Publications,* vol. 4, pp. 09041 1 - 09041 4, 2009.

[3] Z. Li, Y. Wang, C. Liao, S. Liu, J. Zhou, X. Zhong, Y. Liu, K. Yang, Q. Wang and G. Yin, "Temperature-insensitive refractive index sensor based on in-fiber Michelson interferometer," *Sensors and Actuators B: Chemical,* vol. 199, pp. 31-35, 2014.

[4] M. Pospíšilová, G. Kuncová and J. Trögl, "Fiber-Optic Chemical Sensors and Fiber-Optic Bio-Sensors," *Sensors,* vol. 15, pp. 25208 - 25259, 2015.

[5] E. Hecht, Optics: Fourth Edition, San Fancisco: Pearson Education, Inc., 2002.

[6] K. Yuksel, M. Wuilpart and P. Megret, "Optical-frequency domain reflectometry: roadmap for high-resolution distributed measurements," in *IEEE/LEOS Benelux*, Brussels, 2007.

[7] K. Yuksel, M. Wuilpart, V. Moeyaert and P. Mégret, "Optical Frequency Domain Reflectometry: A Review," in *ICTON*, 2009.

[8] Exfo, "Optical Time-Domain Reflectometer," Exfo, 2017. [Online]. Available: http://www.exfo.com/glossary/optical-time-domain-reflectometer-otdr. [Accessed 09 February 2017].

[9] Optical Wavelength Laboratories, "OTDR Dead Zones and Dead Zone Boxes WHITE PAPER," 30 January 2013. [Online]. Available: http://owl-inc.com/literature/sub/pdf/wp/wp-dzb-021513.pdf. [Accessed 09 February 2017].

[10] F. L. Pedrotti and L. S. Pedrotti, Introduction to Optics: Second Edition, Englewood Cliffs: Prentice-Hall, Inc, 1993.

[11] W. V. Sorin, D. K. Donald, S. A. Newton and M. Nazarathy, "Coherent FMCW reflectometry using a temperature tuned Nd:YAG ring laser," *IEEE Photonics Technology Letters,* vol. 2, no. 12, pp. 902-904, 1990.

[12] S. Venkatesh, W. V. Sorin, D. K. Donald and B. L. Heffner, “Coherent FMCW Reflectometry Using A Piezoelectrically Tuned Nd:YAG Ring Laser,” in *Optical Fiber Sensors Conference (8th)*, New York, 1991.

[13] K. Shimizu, T. Horiguchi and Y. Koyamada, “Measurement of Rayleigh backscattering in single-mode fibers based on coherent OFDR employing a DFB laser diode,” *IEEE Photonics Technology Letters,* vol. 3, no. 11, pp. 1039-1041, 1991.

[14] K.-Y. Huang and G. M. Carter, “Coherent optical frequency domain reflectometry (OFDR) using a fiber grating external cavity laser,” *IEEE Photonics Technology Letters,* vol. 6, no. 12, pp. 1466 - 1468, 1994.

[15] R. Passy, N. Gisin, J. P. v. d. Weid and H. H. Gilgen, “Experimental and Theoretical Investigations of Coherent OFDR with Semiconductor Laser Sources,” *Journal of Lightwave Technology,* vol. 12, no. 9, pp. 1622-1630, 1994.

[16] K. Tsuji, K. Shimizu, T. Horiguchi and Y. Koyamada, “Coherent Optical Frequency Domain Reflectometry Using Phase-Decorrelated Reflected and Reference Lightwaves,” *Journal of Lightwave Technology,* vol. 15, no. 7, pp. 1102-1109, 1997.

[17] P. Oberson, B. Huttner, O. Guinnard, L. Guinnard, G. Ribordy and N. Gisin, “Optical Frequency Domain Reflectometry with a Narrow Linewidth Fiber Laser,” *IEEE Photonics Technology Letters,* vol. 12, no. 7, pp. 867-869, 2000.

[18] J. Geng, C. Spiegelberg and S. Jiang, “Narrow Linewidth Fiber Laser for 100-km Optical Frequency Domain Reflectometry,” *IEEE Photonics Technology Letters,* vol. 17, no. 9, pp. 1827-1829, 2005.

[19] M. S. Oh, H. S. Park and B. Y. Kim, “Optical Frequency-Domain Reflectometry Based on Wavelength-Swept Mode-Locked Fiber Laser,” *IEEE Photonics Technology Letters,* vol. 15, no. 2, pp. 266-268, 2003.

[20] C. Ndiaye, T. Hara and H. Ito, “Profilometry using a frequency-shifted feedback laser,” in *Conference on Lasers and Electro-Optics (CLEO)*, 2005.

[21] K. Yuksel, P. Megret and M. Wuilpart, “A quasi-distributed temperature sensor interrogated by optical frequency-domain reflectometer,” *Measurement Science and Technology,* vol. 22, no. 11, 2011.

[22] J. Zheng, Optical Frequency-Modulated Continuous-Wave (FMCW) Interferometry, New York: Springer Science + Business Media, Inc, 2005.

[23] A. J. Kumar, N. M. Gowri, R. V. Raju, G. Nirmala, B. S. Bellubbi and T. R. Krishna, “Study of fiber optic sugar sensor,” *Pramana,* vol. 67, no. 2, pp. 383 - 387, 2006.

[24] F. Abrishamian and K. Morishita, “A study on refractive index changes induced by heating the long-period fiber gratings in different temperatures,” in *Optical Fiber Communication Conference and Exposition (OFC/NFOEC), 2011 and the National Fiber Optic Engineers Conference*, Los Angeles, 2011.

[25] H. Meng, W. Shen, G. Zhang, X. Wu, W. Wang, C. Tan and X. Huang, “Michelson interferometer-based fiber-optic sensing of liquid refractive index,” *Sensors and Actuators B: Chemical,* vol. 160, pp. 720-723, 2011.

[26] K. Schroeder, W. Ecke, R. Mueller, R. Willsch and A. Andreev, “A fibre Bragg grating refractometer,” *Measurement Science and Technology,* vol. 12, pp. 757-764, 2001.

[27] M. Sheeba, M. Rajesh, C. P. G. Vallabhan, V. P. N. Nampoori and P. Radhakrishnan, “Fibre optic sensor for the detection of adulterant traces in coconut oil,” *Measurement Science and Technology,* vol. 16, no. 11, pp. 2247 - 2250, 2005.

[28] M. G. Shlyagin, R. M. Manuel and Ó. Esteban, “Optical-fiber self-referred refractometer based on Fresnel reflection at the fiber tip,” *Sensors and Actuators B,* vol. 178, pp. 263-269, 2013.

[29] S. Chin, “Practical Applications of Current Limiting Diodes,” *ECN,* pp. 49-54, 15 May 2000.

[30] J. Williams, “Current Sources for Fiber Optic Lasers,” Linear Technology Corporation, Milpitas, 2002.

[31] Texas Instruments, “LM134/LM234/LM334 3-Terminal Adjustable Current Sources,” Texas Instruments Incorporated, Texas, 2013.

[32] oeMarket, “1310nm or 1550nm DFB Laser - Coaxial Pigtail,” oeMarket.com, 2016. [Online]. Available: http://www.oemarket.com/catalog/product_info.php/1310nm-1550nm-dfb-laser-coaxial-pigtail-p-122. [Accessed 20 September 2016].

[33] The MathWorks, Inc., “Curve Fitting and Distribution Fitting,” The MathWorks, Inc., 2017. [Online]. Available: https://www.mathworks.com/help/stats/examples/curve-fitting-and-distribution-fitting.html?prodcode=ML. [Accessed 09 March 2017].

[34] Linear Technology Corporation, “LT1006: Precision, Single Supply Op Amp,” Linear Technology Corporation, Milpitas.

[35] The Engineering Toolbox, “Refractive Index for some common Liquids, Solids and Gases,” The Engineering Toolbox, [Online]. Available:

http://www.engineeringtoolbox.com/refractive-index-d_1264.html. [Accessed 19 March 2017].

[36] J. Rheims, J. Köser and T. Wriedt, “Refractive-index measurements in the near-IR using an Abbe refractometer,” *Measurement Science and Technology,* vol. 8, no. 6, pp. 601 - 605, 1997.

[37] PanaChem, “Isopropyl Alcohol 99 (IPA),” [Online]. Available: http://www.panachem.com/msds/iso_propyl_alcohol_IPA.pdf. [Accessed 21 July 2017].

[38] M. Polyanskiy, “Refractive Index of C3H7OH (Propanol),” refractiveindex.info, 2016. [Online]. Available: https://refractiveindex.info/?shelf=organic&book=propanol&page=Kozma. [Accessed 21 July 2017].

[39] J. E. Saunders, C. Sanders, H. Chen and H.-P. Loock, “Refractive indices of common solvents and solutions at 1550 nm,” *Applied Optics,* vol. 55, no. 4, pp. 947 - 953, 2016.

[40] M. Polyanskiy, “Optical constants of H2O, D2O (Water, heavy water, ice),” RefractiveIndex.INFO, 2016. [Online]. Available: https://refractiveindex.info/?shelf=main&book=H2O&page=Hale. [Accessed 19 March 2017].

[41] T. Pfeiffer, H. Schmuck and H. Bulow, “Output Power Characteristics of Erbium-Doped Fiber Ring Lasers,” *IEEE Photonics Technology Letters,* vol. 4, no. 8, pp. 847-849, 1992.

Appendix: Code of FC-PC Connector Fabry Perot Refractometer

```
%% Signal Processing for the FP Interferometer, ref cav 22 cm > sens 28 cav
%% Plot the F10 results
figure('Name','Time Domain: Air, Distilled Water and Iso-propyl Alcohol for
f10'); subplot(3,1,1);
plot(airX_f10, airY_f10, 'Color', 'b');
title('Air (top), water (middle), alcohol (bottom) f10'); xlabel('Time
(s)'); ylabel('Voltage (V)');
legend ('Air');
% axis([0 inf -0.02 0.03])
subplot(3,1,2);
plot(waterX_f10, waterY_f10, 'Color', 'g');
xlabel('Time (s)'); ylabel('Voltage (V)');
legend ('Distilled Water');
% axis([0 inf -0.02 0.03])
subplot(3,1,3);
plot(alcoholX_f10, alcoholY_f10, 'Color', 'r');
xlabel('Time (s)'); ylabel('Voltage (V)');
legend ('Alcohol');
% axis([0 inf -0.02 0.03])
%% Plot the F10 zoomed1 results
figure('Name','Time Domain: Air, Distilled Water and Iso-propyl Alcohol for
f10'); subplot(3,1,1);
plot(airXZ1_f10, airYZ1_f10, 'Color', 'b');
title('Air (top), water (middle), alcohol (bottom)'); xlabel('Time (s)');
ylabel('Voltage (V)');
legend ('Air');
% axis([0 inf -0.02 0.03])
subplot(3,1,2);
plot(waterXZ1_f10, waterYZ1_f10, 'Color', 'g');
xlabel('Time (s)'); ylabel('Voltage (V)');
legend ('Distilled Water');
% axis([0 inf -0.02 0.03])
subplot(3,1,3);
plot(alcoholXZ1_f10, alcoholYZ1_f10, 'Color', 'r');
xlabel('Time (s)'); ylabel('Voltage (V)');
legend ('Alcohol');
% axis([0 inf -0.02 0.03])
%% Plot the F10 zoomed2 results
figure('Name','Time Domain: Air, Distilled Water and Iso-propyl Alcohol for
f10'); subplot(3,1,1);
plot(airXZ2_f10, airYZ2_f10, 'Color', 'b');
title('Air (top), water (middle), alcohol (bottom)'); xlabel('Time (s)');
ylabel('Voltage (V)');
legend ('Air');
% axis([0 inf -0.02 0.03])
subplot(3,1,2);
plot(waterXZ2_f10, waterYZ2_f10, 'Color', 'g');
xlabel('Time (s)'); ylabel('Voltage (V)');
legend ('Distilled Water');
% axis([0 inf -0.02 0.03])
subplot(3,1,3);
plot(alcoholXZ2_f10, alcoholYZ2_f10, 'Color', 'r');
xlabel('Time (s)'); ylabel('Voltage (V)');
legend ('Alcohol');
% axis([0 inf -0.02 0.03])


%% Plot the F50 results
```

```
figure('Name','Time Domain: Air, Distilled Water and Iso-propyl Alcohol for
f50'); subplot(3,1,1);
plot(airX_f50, airY_f50, 'Color', 'b');
title('Air (top), water (middle), alcohol (bottom)'); xlabel('Time (s)');
ylabel('Voltage (V)');
legend ('Air');
% axis([0 inf -0.02 0.03])
subplot(3,1,2);
plot(waterX_f50, waterY_f50, 'Color', 'g');
xlabel('Time (s)'); ylabel('Voltage (V)');
legend ('Distilled Water');
% axis([0 inf -0.02 0.03])
subplot(3,1,3);
plot(alcoholX_f50, alcoholY_f50, 'Color', 'r');
xlabel('Time (s)'); ylabel('Voltage (V)');
legend ('Alcohol');
% axis([0 inf -0.02 0.03])
%% Plot the F50 zoomed1 results
figure('Name','Time Domain: Air, Distilled Water and Iso-propyl Alcohol for
f50'); subplot(3,1,1);
plot(airXZ1_f50, airYZ1_f50, 'Color', 'b');
title('Air (top), water (middle), alcohol (bottom)'); xlabel('Time (s)');
ylabel('Voltage (V)');
legend ('Air');
% axis([0 inf -0.02 0.03])
subplot(3,1,2);
plot(waterXZ1_f50, waterYZ1_f50, 'Color', 'g');
xlabel('Time (s)'); ylabel('Voltage (V)');
legend ('Distilled Water');
% axis([0 inf -0.02 0.03])
subplot(3,1,3);
plot(alcoholXZ1_f50, alcoholYZ1_f50, 'Color', 'r');
xlabel('Time (s)'); ylabel('Voltage (V)');
legend ('Alcohol');
% axis([0 inf -0.02 0.03])
%% Plot the F50 zoomed2 results
figure('Name','Time Domain: Air, Distilled Water and Iso-propyl Alcohol for
f50'); subplot(3,1,1);
plot(airXZ2_f50, airYZ2_f50, 'Color', 'b');
title('Air (top), water (middle), alcohol (bottom)'); xlabel('Time (s)');
ylabel('Voltage (V)');
legend ('Air');
% axis([0 inf -0.02 0.03])
subplot(3,1,2);
plot(waterXZ2_f50, waterYZ2_f50, 'Color', 'g');
xlabel('Time (s)'); ylabel('Voltage (V)');
legend ('Distilled Water');
% axis([0 inf -0.02 0.03])
subplot(3,1,3);
plot(alcoholXZ2_f50, alcoholYZ2_f50, 'Color', 'r');
xlabel('Time (s)'); ylabel('Voltage (V)');
legend ('Alcohol');
% axis([0 inf -0.02 0.03])


%% Plot the F222 results
figure('Name','Time Domain: Air, Distilled Water and Iso-propyl Alcohol for
f222'); subplot(3,1,1);
plot(airX_f222, airY_f222, 'Color', 'b');
title('Air (top), water (middle), alcohol (bottom)'); xlabel('Time (s)');
ylabel('Voltage (V)');
```

```
legend ('Air');
% axis([0 inf -0.02 0.03])
subplot(3,1,2);
plot(waterX_f222, waterY_f222, 'Color', 'g');
xlabel('Time (s)'); ylabel('Voltage (V)');
legend ('Distilled Water');
% axis([0 inf -0.02 0.03])
subplot(3,1,3);
plot(alcoholX_f222, alcoholY_f222, 'Color', 'r');
xlabel('Time (s)'); ylabel('Voltage (V)');
legend ('Alcohol');
% axis([0 inf -0.02 0.03])
%% Plot the F222 zoomed1 results
figure('Name','Time Domain: Air, Distilled Water and Iso-propyl Alcohol for
f222'); subplot(3,1,1);
plot(airXZ1_f222, airYZ1_f222, 'Color', 'b');
title('Air (top), water (middle), alcohol (bottom)'); xlabel('Time (s)');
ylabel('Voltage (V)');
legend ('Air');
% axis([0 inf -0.02 0.03])
subplot(3,1,2);
plot(waterXZ1_f222, waterYZ1_f222, 'Color', 'g');
xlabel('Time (s)'); ylabel('Voltage (V)');
legend ('Distilled Water');
% axis([0 inf -0.02 0.03])
subplot(3,1,3);
plot(alcoholXZ1_f222, alcoholYZ1_f222, 'Color', 'r');
xlabel('Time (s)'); ylabel('Voltage (V)');
legend ('Alcohol');
% axis([0 inf -0.02 0.03])
%% Plot the F222 zoomed2 results
figure('Name','Time Domain: Air, Distilled Water and Iso-propyl Alcohol for
f222'); subplot(3,1,1);
plot(airXZ2_f222, airYZ2_f222, 'Color', 'b');
title('Air (top), water (middle), alcohol (bottom)'); xlabel('Time (s)');
ylabel('Voltage (V)');
legend ('Air');
% axis([0 inf -0.02 0.03])
subplot(3,1,2);
plot(waterXZ2_f222, waterYZ2_f222, 'Color', 'g');
xlabel('Time (s)'); ylabel('Voltage (V)');
legend ('Distilled Water');
% axis([0 inf -0.02 0.03])
subplot(3,1,3);
plot(alcoholXZ2_f222, alcoholYZ2_f222, 'Color', 'r');
xlabel('Time (s)'); ylabel('Voltage (V)');
legend ('Alcohol');
% axis([0 inf -0.02 0.03])
 %% FFT of Air f10
Y = detrend(airY_f10);
fftY = fft(Y);
p2 = abs(fftY/length(fftY));
p1 = p2(1:length(fftY)/2+1);
p1(2:end-1) = 2*p1(2:end-1);
Sampling = 1/(airX_f10(2)-airX_f10(1));
f = fSampling*(0:(length(fftY)/2))/length(fftY);
figure ('Name','Frequency Domain: Air'); subplot(3,1,1);
plot(f,p1);
title('FFT: Air'); xlabel('Frequency (Hz)'); ylabel('Amplitude');
legend ('Air');
% phase = unwrap(angle(p1));
```

```
% figure
% plot(f, phase)
% title('Phase'); xlabel('Frequency (Hz)'); ylabel('Phase (\pi)');

% fftAirX_f10 = f;
% fftAirY_f10 = p1;

% FFT of Air Z1
Y = detrend(airYZ1_f10);
fftY = fft(Y);

p2 = abs(fftY/length(fftY));
p1 = p2(1:length(fftY)/2+1);
p1(2:end-1) = 2*p1(2:end-1);

fSampling = 1/(airXZ1_f10(2)-airXZ1_f10(1));
f = fSampling*(0:(length(fftY)/2))/length(fftY);

subplot(3,1,2);
plot(f,p1);
xlabel('Frequency (Hz)'); ylabel('Amplitude');
legend ('Air Z1');

% phase = unwrap(angle(p1));
% figure
% plot(f, phase)
% title('Phase'); xlabel('Frequency (Hz)'); ylabel('Phase (\pi)');

% fftWaterX_f10 = f;
% fftWaterY_f10 = p1;

% FFT of Air Z2
Y = detrend(airYZ2_f10);
fftY = fft(Y);

p2 = abs(fftY/length(fftY));
p1 = p2(1:length(fftY)/2+1);
p1(2:end-1) = 2*p1(2:end-1);

fSampling = 1/(airXZ2_f10(2)-airXZ2_f10(1));
f = fSampling*(0:(length(fftY)/2))/length(fftY);

subplot(3,1,3);
plot(f,p1);
xlabel('Frequency (Hz)'); ylabel('Amplitude');
legend ('Air Z2');

% phase = unwrap(angle(p1));
% figure
% plot(f, phase)
% title('Phase'); xlabel('Frequency (Hz)'); ylabel('Phase (\pi)');

% fftAlcoholX_f10 = f;
% fftAlcoholY_f10 = p1;
%% FFT of Water f10
Y = detrend(waterY_f10);
fftY = fft(Y);
```

```
p2 = abs(fftY/length(fftY));
p1 = p2(1:length(fftY)/2+1);
p1(2:end-1) = 2*p1(2:end-1);

fSampling = 1/(waterX_f10(2)-waterX_f10(1));
f = fSampling*(0:(length(fftY)/2))/length(fftY);

figure ('Name','Frequency Domain: Distilled Water'); subplot(3,1,1);
plot(f,p1);
title('FFT: Water'); xlabel('Frequency (Hz)'); ylabel('Amplitude');
legend ('Water');

% phase = unwrap(angle(p1));
% figure
% plot(f, phase)
% title('Phase'); xlabel('Frequency (Hz)'); ylabel('Phase (\pi)');

% fftAirX_f10 = f;
% fftAirY_f10 = p1;

% FFT of Water Z1
Y = detrend(waterYZ1_f10);
fftY = fft(Y);

p2 = abs(fftY/length(fftY));
p1 = p2(1:length(fftY)/2+1);
p1(2:end-1) = 2*p1(2:end-1);

fSampling = 1/(waterXZ1_f10(2)-waterXZ1_f10(1));
f = fSampling*(0:(length(fftY)/2))/length(fftY);

subplot(3,1,2);
plot(f,p1);
xlabel('Frequency (Hz)'); ylabel('Amplitude');
legend ('Water Z1');

% FFT of Water Z2
Y = detrend(waterYZ2_f10);
fftY = fft(Y);

p2 = abs(fftY/length(fftY));
p1 = p2(1:length(fftY)/2+1);
p1(2:end-1) = 2*p1(2:end-1);

fSampling = 1/(waterXZ2_f10(2)-waterXZ2_f10(1));
f = fSampling*(0:(length(fftY)/2))/length(fftY);

subplot(3,1,3);
plot(f,p1);
xlabel('Frequency (Hz)'); ylabel('Amplitude');
legend ('Water Z2');
%% FFT of Alcohol f10
Y = detrend(alcoholY_f10);
fftY = fft(Y);

p2 = abs(fftY/length(fftY));
p1 = p2(1:length(fftY)/2+1);
p1(2:end-1) = 2*p1(2:end-1);
```

```
fSampling = 1/(alcoholX_f10(2)-alcoholX_f10(1));
f = fSampling*(0:(length(fftY)/2))/length(fftY);

figure ('Name','Frequency Domain: Iso-propyl Alcohol'); subplot(3,1,1);
plot(f,p1);
title('FFT:  Alcohol '); xlabel('Frequency (Hz)'); ylabel('Amplitude');
legend ('Alcohol');


% FFT of Alcohol Z1
Y = detrend(alcoholYZ1_f10);
fftY = fft(Y);

p2 = abs(fftY/length(fftY));
p1 = p2(1:length(fftY)/2+1);
p1(2:end-1) = 2*p1(2:end-1);

fSampling = 1/(alcoholXZ1_f10(2)-alcoholXZ1_f10(1));
f = fSampling*(0:(length(fftY)/2))/length(fftY);

subplot(3,1,2);
plot(f,p1);
xlabel('Frequency (Hz)'); ylabel('Amplitude');
legend ('Alcohol Z1');

% FFT of Alcohol Z2
Y = detrend(alcoholYZ2_f10);
fftY = fft(Y);

p2 = abs(fftY/length(fftY));
p1 = p2(1:length(fftY)/2+1);
p1(2:end-1) = 2*p1(2:end-1);

fSampling = 1/(alcoholXZ2_f10(2)-alcoholXZ2_f10(1));
f = fSampling*(0:(length(fftY)/2))/length(fftY);

subplot(3,1,3);
plot(f,p1);
xlabel('Frequency (Hz)'); ylabel('Amplitude');
legend ('Alcohol Z2');

% phase = unwrap(angle(p1));
% figure
% plot(f, phase)
% title('Phase'); xlabel('Frequency (Hz)'); ylabel('Phase (\pi)');

% fftAlcoholX_f10 = f;
% fftAlcoholY_f10 = p1;

%% FFT of Air, Water and Alcohol f10
Y = detrend(airYZ2_f10);
fftY = fft(Y);

p2 = abs(fftY/length(fftY));
p1 = p2(1:length(fftY)/2+1);
p1(2:end-1) = 2*p1(2:end-1);
```

```
fSampling = 1/(airXZ2_f10(2)-airXZ2_f10(1));
f = fSampling*(0:(length(fftY)/2))/length(fftY);

figure ('Name','Frequency Domain: Air, Distilled Water and Iso-propyl
Alcohol'); subplot(3,1,1);
plot(f,p1);
title('FFT: Air (top), Water (middle), Alcohol (bottom)');
xlabel('Frequency (Hz)'); ylabel('Amplitude');
legend ('Air');

% phase = unwrap(angle(p1));
% figure
% plot(f, phase)
% title('Phase'); xlabel('Frequency (Hz)'); ylabel('Phase (\pi)');

fftAirX_f10 = f;
fftAirY_f10 = p1;

% FFT of Water
Y = detrend(waterYZ2_f10);
fftY = fft(Y);

p2 = abs(fftY/length(fftY));
p1 = p2(1:length(fftY)/2+1);
p1(2:end-1) = 2*p1(2:end-1);

fSampling = 1/(waterXZ2_f10(2)-waterXZ2_f10(1));
f = fSampling*(0:(length(fftY)/2))/length(fftY);

subplot(3,1,2);
plot(f,p1);
xlabel('Frequency (Hz)'); ylabel('Amplitude');
legend ('Distilled Water');

% phase = unwrap(angle(p1));
% figure
% plot(f, phase)
% title('Phase'); xlabel('Frequency (Hz)'); ylabel('Phase (\pi)');

fftWaterX_f10 = f;
fftWaterY_f10 = p1;

% FFT of Alcohol
Y = detrend(alcoholYZ2_f10);
fftY = fft(Y);

p2 = abs(fftY/length(fftY));
p1 = p2(1:length(fftY)/2+1);
p1(2:end-1) = 2*p1(2:end-1);

fSampling = 1/(alcoholXZ2_f10(2)-alcoholXZ2_f10(1));
f = fSampling*(0:(length(fftY)/2))/length(fftY);

subplot(3,1,3);
plot(f,p1);
xlabel('Frequency (Hz)'); ylabel('Amplitude');
legend ('Alcohol');
```

```
% phase = unwrap(angle(p1));
% figure
% plot(f, phase)
% title('Phase'); xlabel('Frequency (Hz)'); ylabel('Phase (\pi)');

fftAlcoholX_f10 = f;
fftAlcoholY_f10 = p1;
%% FFT of Air f50
Y = detrend(airY_f50);
fftY = fft(Y);

p2 = abs(fftY/length(fftY));
p1 = p2(1:length(fftY)/2+1);
p1(2:end-1) = 2*p1(2:end-1);

fSampling = 1/(airX_f50(2)-airX_f50(1));
f = fSampling*(0:(length(fftY)/2))/length(fftY);

figure ('Name','Frequency Domain: Air'); subplot(3,1,1);
plot(f,p1);
title('FFT: Air'); xlabel('Frequency (Hz)'); ylabel('Amplitude');
legend ('Air f50');

% FFT of Air Z1
Y = detrend(airYZ1_f50);
fftY = fft(Y);

p2 = abs(fftY/length(fftY));
p1 = p2(1:length(fftY)/2+1);
p1(2:end-1) = 2*p1(2:end-1);

fSampling = 1/(airXZ1_f50(2)-airXZ1_f50(1));
f = fSampling*(0:(length(fftY)/2))/length(fftY);

subplot(3,1,2);
plot(f,p1);
xlabel('Frequency (Hz)'); ylabel('Amplitude');
legend ('Air Z1');

% FFT of Air Z2
Y = detrend(airYZ2_f50);
fftY = fft(Y);

p2 = abs(fftY/length(fftY));
p1 = p2(1:length(fftY)/2+1);
p1(2:end-1) = 2*p1(2:end-1);

fSampling = 1/(airXZ2_f50(2)-airXZ2_f50(1));
f = fSampling*(0:(length(fftY)/2))/length(fftY);

subplot(3,1,3);
plot(f,p1);
xlabel('Frequency (Hz)'); ylabel('Amplitude');
legend ('Air Z2');
%% FFT of Water f50
Y = detrend(waterY_f50);
fftY = fft(Y);

p2 = abs(fftY/length(fftY));
```

```
p1 = p2(1:length(fftY)/2+1);
p1(2:end-1) = 2*p1(2:end-1);

fSampling = 1/(waterX_f50(2)-waterX_f50(1));
f = fSampling*(0:(length(fftY)/2))/length(fftY);

figure ('Name','Frequency Domain: Distilled Water'); subplot(3,1,1);
plot(f,p1);
title('FFT: Water'); xlabel('Frequency (Hz)'); ylabel('Amplitude');
legend ('Water f50');

% phase = unwrap(angle(p1));
% figure
% plot(f, phase)
% title('Phase'); xlabel('Frequency (Hz)'); ylabel('Phase (\pi)');

% fftAirX_f10 = f;
% fftAirY_f10 = p1;

% FFT of Air Z1
Y = detrend(waterYZ1_f50);
fftY = fft(Y);

p2 = abs(fftY/length(fftY));
p1 = p2(1:length(fftY)/2+1);
p1(2:end-1) = 2*p1(2:end-1);

fSampling = 1/(waterXZ1_f50(2)-waterXZ1_f50(1));
f = fSampling*(0:(length(fftY)/2))/length(fftY);

subplot(3,1,2);
plot(f,p1);
xlabel('Frequency (Hz)'); ylabel('Amplitude');
legend ('Water Z1');

% phase = unwrap(angle(p1));
% figure
% plot(f, phase)
% title('Phase'); xlabel('Frequency (Hz)'); ylabel('Phase (\pi)');

% fftWaterX_f10 = f;
% fftWaterY_f10 = p1;

% FFT of Air Z2
Y = detrend(waterYZ2_f50);
fftY = fft(Y);

p2 = abs(fftY/length(fftY));
p1 = p2(1:length(fftY)/2+1);
p1(2:end-1) = 2*p1(2:end-1);

fSampling = 1/(waterXZ2_f50(2)-waterXZ2_f50(1));
f = fSampling*(0:(length(fftY)/2))/length(fftY);

subplot(3,1,3);
plot(f,p1);
xlabel('Frequency (Hz)'); ylabel('Amplitude');
legend ('Water Z2');
```

```
% phase = unwrap(angle(p1));
% figure
% plot(f, phase)
% title('Phase'); xlabel('Frequency (Hz)'); ylabel('Phase (\pi)');

% fftAlcoholX_f10 = f;
% fftAlcoholY_f10 = p1;
%% FFT of Alcohol f50
Y = detrend(alcoholY_f50);
fftY = fft(Y);

p2 = abs(fftY/length(fftY));
p1 = p2(1:length(fftY)/2+1);
p1(2:end-1) = 2*p1(2:end-1);

fSampling = 1/(alcoholX_f50(2)-alcoholX_f50(1));
f = fSampling*(0:(length(fftY)/2))/length(fftY);

figure ('Name','Frequency Domain: Iso-propyl Alcohol'); subplot(3,1,1);
plot(f,p1);
title('FFT:  Alcohol '); xlabel('Frequency (Hz)'); ylabel('Amplitude');
legend ('Alcohol f50');

% phase = unwrap(angle(p1));
% figure
% plot(f, phase)
% title('Phase'); xlabel('Frequency (Hz)'); ylabel('Phase (\pi)');

% fftAirX_f10 = f;
% fftAirY_f10 = p1;

% FFT of Air Z1
Y = detrend(alcoholYZ1_f50);
fftY = fft(Y);

p2 = abs(fftY/length(fftY));
p1 = p2(1:length(fftY)/2+1);
p1(2:end-1) = 2*p1(2:end-1);

fSampling = 1/(alcoholXZ1_f50(2)-alcoholXZ1_f50(1));
f = fSampling*(0:(length(fftY)/2))/length(fftY);

subplot(3,1,2);
plot(f,p1);
xlabel('Frequency (Hz)'); ylabel('Amplitude');
legend ('Alcohol Z1');

% phase = unwrap(angle(p1));
% figure
% plot(f, phase)
% title('Phase'); xlabel('Frequency (Hz)'); ylabel('Phase (\pi)');

% fftWaterX_f10 = f;
% fftWaterY_f10 = p1;

% FFT of Air Z2
Y = detrend(alcoholYZ2_f50);
```

```
fftY = fft(Y);

p2 = abs(fftY/length(fftY));
p1 = p2(1:length(fftY)/2+1);
p1(2:end-1) = 2*p1(2:end-1);

fSampling = 1/(alcoholXZ2_f50(2)-alcoholXZ2_f50(1));
f = fSampling*(0:(length(fftY)/2))/length(fftY);

subplot(3,1,3);
plot(f,p1);
xlabel('Frequency (Hz)'); ylabel('Amplitude');
legend ('Alcohol Z2');
%% FFT of Air, Water and Alcohol f50
Y = detrend(airYZ2_f50);
fftY = fft(Y);

p2 = abs(fftY/length(fftY));
p1 = p2(1:length(fftY)/2+1);
p1(2:end-1) = 2*p1(2:end-1);

fSampling = 1/(airXZ2_f50(2)-airXZ2_f50(1));
f = fSampling*(0:(length(fftY)/2))/length(fftY);

figure ('Name','Frequency Domain: Air, Distilled Water and Iso-propyl
Alcohol'); subplot(3,1,1);
plot(f,p1);
title('FFT 50: Air (top), Water (middle), Alcohol (bottom)');
xlabel('Frequency (Hz)'); ylabel('Amplitude');
legend ('Air');

% phase = unwrap(angle(p1));
% figure
% plot(f, phase)
% title('Phase'); xlabel('Frequency (Hz)'); ylabel('Phase (\pi)');

fftAirX_f50 = f;
fftAirY_f50 = p1;

% FFT of Water
Y = detrend(waterYZ2_f50);
fftY = fft(Y);

p2 = abs(fftY/length(fftY));
p1 = p2(1:length(fftY)/2+1);
p1(2:end-1) = 2*p1(2:end-1);

fSampling = 1/(waterXZ2_f50(2)-waterXZ2_f50(1));
f = fSampling*(0:(length(fftY)/2))/length(fftY);

subplot(3,1,2);
plot(f,p1);
xlabel('Frequency (Hz)'); ylabel('Amplitude');
legend ('Distilled Water');

% phase = unwrap(angle(p1));
% figure
% plot(f, phase)
% title('Phase'); xlabel('Frequency (Hz)'); ylabel('Phase (\pi)');
```

```
fftWaterX_f50 = f;
fftWaterY_f50 = p1;

% FFT of Alcohol
Y = detrend(alcoholYZ2_f50);
fftY = fft(Y);

p2 = abs(fftY/length(fftY));
p1 = p2(1:length(fftY)/2+1);
p1(2:end-1) = 2*p1(2:end-1);

fSampling = 1/(alcoholXZ2_f50(2)-alcoholXZ2_f50(1));
f = fSampling*(0:(length(fftY)/2))/length(fftY);

subplot(3,1,3);
plot(f,p1);
xlabel('Frequency (Hz)'); ylabel('Amplitude');
legend ('Alcohol');

% phase = unwrap(angle(p1));
% figure
% plot(f, phase)
% title('Phase'); xlabel('Frequency (Hz)'); ylabel('Phase (\pi)');

fftAlcoholX_f50 = f;
fftAlcoholY_f50 = p1;
%% FFT of Air f222
Y = detrend(airY_f222);
fftY = fft(Y);

p2 = abs(fftY/length(fftY));
p1 = p2(1:length(fftY)/2+1);
p1(2:end-1) = 2*p1(2:end-1);

fSampling = 1/(airX_f222(2)-airX_f222(1));
f = fSampling*(0:(length(fftY)/2))/length(fftY);

figure ('Name','Frequency Domain: Air'); subplot(3,1,1);
plot(f,p1);
title('FFT: Air'); xlabel('Frequency (Hz)'); ylabel('Amplitude');
legend ('Air f222');

% phase = unwrap(angle(p1));
% figure
% plot(f, phase)
% title('Phase'); xlabel('Frequency (Hz)'); ylabel('Phase (\pi)');

% fftAirX_f10 = f;
% fftAirY_f10 = p1;

% FFT of Air Z1
Y = detrend(airYZ1_f222);
fftY = fft(Y);

p2 = abs(fftY/length(fftY));
p1 = p2(1:length(fftY)/2+1);
p1(2:end-1) = 2*p1(2:end-1);
```

```
fSampling = 1/(airXZ1_f222(2)-airXZ1_f222(1));
f = fSampling*(0:(length(fftY)/2))/length(fftY);

subplot(3,1,2);
plot(f,p1);
xlabel('Frequency (Hz)'); ylabel('Amplitude');
legend ('Air Z1');

% phase = unwrap(angle(p1));
% figure
% plot(f, phase)
% title('Phase'); xlabel('Frequency (Hz)'); ylabel('Phase (\pi)');

% fftWaterX_f10 = f;
% fftWaterY_f10 = p1;

% FFT of Air Z2
Y = detrend(airYZ2_f222);
fftY = fft(Y);

p2 = abs(fftY/length(fftY));
p1 = p2(1:length(fftY)/2+1);
p1(2:end-1) = 2*p1(2:end-1);

fSampling = 1/(airXZ2_f222(2)-airXZ2_f222(1));
f = fSampling*(0:(length(fftY)/2))/length(fftY);

subplot(3,1,3);
plot(f,p1);
xlabel('Frequency (Hz)'); ylabel('Amplitude');
legend ('Air Z2');

% phase = unwrap(angle(p1));
% figure
% plot(f, phase)
% title('Phase'); xlabel('Frequency (Hz)'); ylabel('Phase (\pi)');

% fftAlcoholX_f10 = f;
% fftAlcoholY_f10 = p1;
%% FFT of Water f222
Y = detrend(waterY_f222);
fftY = fft(Y);

p2 = abs(fftY/length(fftY));
p1 = p2(1:length(fftY)/2+1);
p1(2:end-1) = 2*p1(2:end-1);

fSampling = 1/(waterX_f222(2)-waterX_f222(1));
f = fSampling*(0:(length(fftY)/2))/length(fftY);

figure ('Name','Frequency Domain: Distilled Water'); subplot(3,1,1);
plot(f,p1);
title('FFT: Water'); xlabel('Frequency (Hz)'); ylabel('Amplitude');
legend ('Water f222');

% phase = unwrap(angle(p1));
% figure
```

```
% plot(f, phase)
% title('Phase'); xlabel('Frequency (Hz)'); ylabel('Phase (\pi)');

% fftAirX_f10 = f;
% fftAirY_f10 = p1;

% FFT of Air Z1
Y = detrend(waterYZ1_f222);
fftY = fft(Y);

p2 = abs(fftY/length(fftY));
p1 = p2(1:length(fftY)/2+1);
p1(2:end-1) = 2*p1(2:end-1);

fSampling = 1/(waterXZ1_f222(2)-waterXZ1_f222(1));
f = fSampling*(0:(length(fftY)/2))/length(fftY);

subplot(3,1,2);
plot(f,p1);
xlabel('Frequency (Hz)'); ylabel('Amplitude');
legend ('Water Z1');

% phase = unwrap(angle(p1));
% figure
% plot(f, phase)
% title('Phase'); xlabel('Frequency (Hz)'); ylabel('Phase (\pi)');

% fftWaterX_f10 = f;
% fftWaterY_f10 = p1;

% FFT of Air Z2
Y = detrend(waterYZ2_f222);
fftY = fft(Y);

p2 = abs(fftY/length(fftY));
p1 = p2(1:length(fftY)/2+1);
p1(2:end-1) = 2*p1(2:end-1);

fSampling = 1/(waterXZ2_f222(2)-waterXZ2_f222(1));
f = fSampling*(0:(length(fftY)/2))/length(fftY);

subplot(3,1,3);
plot(f,p1);
xlabel('Frequency (Hz)'); ylabel('Amplitude');
legend ('Water Z2');

% phase = unwrap(angle(p1));
% figure
% plot(f, phase)
% title('Phase'); xlabel('Frequency (Hz)'); ylabel('Phase (\pi)');

% fftAlcoholX_f10 = f;
% fftAlcoholY_f10 = p1;
%% FFT of Alcohol f222
Y = detrend(alcoholY_f222);
fftY = fft(Y);

p2 = abs(fftY/length(fftY));
```

```
p1 = p2(1:length(fftY)/2+1);
p1(2:end-1) = 2*p1(2:end-1);

fSampling = 1/(alcoholX_f222(2)-alcoholX_f222(1));
f = fSampling*(0:(length(fftY)/2))/length(fftY);

figure ('Name','Frequency Domain: Iso-propyl Alcohol'); subplot(3,1,1);
plot(f,p1);
title('FFT:  Alcohol '); xlabel('Frequency (Hz)'); ylabel('Amplitude');
legend ('Alcohol f222');

% phase = unwrap(angle(p1));
% figure
% plot(f, phase)
% title('Phase'); xlabel('Frequency (Hz)'); ylabel('Phase (\pi)');

% fftAirX_f10 = f;
% fftAirY_f10 = p1;

% FFT of Air Z1
Y = detrend(alcoholYZ1_f222);
fftY = fft(Y);

p2 = abs(fftY/length(fftY));
p1 = p2(1:length(fftY)/2+1);
p1(2:end-1) = 2*p1(2:end-1);

fSampling = 1/(alcoholXZ1_f222(2)-alcoholXZ1_f222(1));
f = fSampling*(0:(length(fftY)/2))/length(fftY);

subplot(3,1,2);
plot(f,p1);
xlabel('Frequency (Hz)'); ylabel('Amplitude');
legend ('Alcohol Z1');

% phase = unwrap(angle(p1));
% figure
% plot(f, phase)
% title('Phase'); xlabel('Frequency (Hz)'); ylabel('Phase (\pi)');

% fftWaterX_f10 = f;
% fftWaterY_f10 = p1;

% FFT of Air Z2
Y = detrend(alcoholYZ2_f222);
fftY = fft(Y);

p2 = abs(fftY/length(fftY));
p1 = p2(1:length(fftY)/2+1);
p1(2:end-1) = 2*p1(2:end-1);

fSampling = 1/(alcoholXZ2_f222(2)-alcoholXZ2_f222(1));
f = fSampling*(0:(length(fftY)/2))/length(fftY);

subplot(3,1,3);
plot(f,p1);
xlabel('Frequency (Hz)'); ylabel('Amplitude');
legend ('Alcohol Z2');
```

```
%% FFT of Air, Water and Alcohol f222
Y = detrend(airYZ2_f222);
fftY = fft(Y);

p2 = abs(fftY/length(fftY));
p1 = p2(1:length(fftY)/2+1);
p1(2:end-1) = 2*p1(2:end-1);

fSampling = 1/(airXZ2_f222(2)-airXZ2_f222(1));
f = fSampling*(0:(length(fftY)/2))/length(fftY);

figure ('Name','Frequency Domain: Air, Distilled Water and Iso-propyl
Alcohol'); subplot(3,1,1);
plot(f,p1);
title('FFT: Air (top), Water (middle), Alcohol (bottom)');
xlabel('Frequency (Hz)'); ylabel('Amplitude');
legend ('Air');

% phase = unwrap(angle(p1));
% figure
% plot(f, phase)
% title('Phase'); xlabel('Frequency (Hz)'); ylabel('Phase (\pi)');

fftAirX_f222 = f;
fftAirY_f222 = p1;

% FFT of Water
Y = detrend(waterYZ2_f222);
fftY = fft(Y);

p2 = abs(fftY/length(fftY));
p1 = p2(1:length(fftY)/2+1);
p1(2:end-1) = 2*p1(2:end-1);

fSampling = 1/(waterXZ2_f222(2)-waterXZ2_f222(1));
f = fSampling*(0:(length(fftY)/2))/length(fftY);

subplot(3,1,2);
plot(f,p1);
xlabel('Frequency (Hz)'); ylabel('Amplitude');
legend ('Distilled Water');

% phase = unwrap(angle(p1));
% figure
% plot(f, phase)
% title('Phase'); xlabel('Frequency (Hz)'); ylabel('Phase (\pi)');

fftWaterX_f222 = f;
fftWaterY_f222 = p1;

% FFT of Alcohol
Y = detrend(alcoholYZ2_f222);
fftY = fft(Y);

p2 = abs(fftY/length(fftY));
p1 = p2(1:length(fftY)/2+1);
p1(2:end-1) = 2*p1(2:end-1);
```

```
fSampling = 1/(alcoholXZ2_f222(2)-alcoholXZ2_f222(1));
f = fSampling*(0:(length(fftY)/2))/length(fftY);

subplot(3,1,3);
plot(f,p1);
xlabel('Frequency (Hz)'); ylabel('Amplitude');
legend ('Alcohol');

% phase = unwrap(angle(p1));
% figure
% plot(f, phase)
% title('Phase'); xlabel('Frequency (Hz)'); ylabel('Phase (\pi)');

fftAlcoholX_f222 = f;
fftAlcoholY_f222 = p1;


%% Get the K Value f10
MinPeakProminence = 0.003;
MinPeakDistance = 200;
MinPeakHeight = 5*10^-4;

[peakValues,peakLocations] = findpeaks(fftAirY_f10,
fftAirX_f10,'MinPeakHeight', MinPeakProminence, 'MinPeakDistance',
MinPeakDistance, 'SortStr','descend');
figure
findpeaks(fftAirY_f10, fftAirX_f10,'MinPeakHeight', MinPeakProminence,
'MinPeakDistance', MinPeakDistance, 'SortStr','descend');
title('Peak Search of Air FFT to get K Value');
xlabel('Frequency (Hz)'); ylabel('FFT Magnitude');

peakValues
peakLocations

nEff = 1.44;
nAir = 1;
rAir = (nEff - nAir)/(nEff + nAir);
CavRef = abs(peakValues(3));
CavSense = abs(peakValues(1));
K = (CavSense/CavRef)/rAir;
%% Get Refractive Index of Water f10
MinPeakProminence = 0.001;
MinPeakDistance = 200;
MinPeakHeight = 2*10^-4;

[peakValues,peakLocations] = findpeaks(fftWaterY_f10,
fftWaterX_f10,'MinPeakProminence', MinPeakProminence, 'MinPeakDistance',
MinPeakDistance, 'SortStr','descend');
figure
findpeaks(fftWaterY_f10, fftWaterX_f10,'MinPeakProminence',
MinPeakProminence, 'MinPeakDistance', MinPeakDistance,
'SortStr','descend');
title('Peak Search of FFT to get the Refractive Index');
xlabel('Frequency (Hz)'); ylabel('FFT Magnitude');
% axis([0 inf 0 inf])
peakValues
peakLocations

CavRef = abs(peakValues(3));
```

```
CavSense = abs(peakValues(1));
r = (CavSense/CavRef)/K;
%rAirCheck = (abs(peakValues(3))/abs(peakValues(1)))/K;
n = (nEff - r*nEff)/(1+r);
ncomp = nCompIndex(n) + n;
%% Get Refractive Index of Alcohol f10
MinPeakProminence = 0.001;
MinPeakDistance = 200;
MinPeakHeight = 2*10^-4;

[peakValues,peakLocations] = findpeaks(fftAlcoholY_f10,
fftAlcoholX_f10,'MinPeakProminence', MinPeakProminence, 'MinPeakDistance',
MinPeakDistance, 'SortStr','descend');
figure
findpeaks(fftAlcoholY_f10, fftAlcoholX_f10,'MinPeakProminence',
MinPeakProminence, 'MinPeakDistance', MinPeakDistance,
'SortStr','descend');
title('Peak Search of FFT to get the Refractive Index');
xlabel('Frequency (Hz)'); ylabel('FFT Magnitude');
% axis([0 inf 0 inf])
peakValues
peakLocations

CavRef = abs(peakValues(2));
CavSense = abs(peakValues(1));
r = (CavSense/CavRef)/K;
%rAirCheck = (abs(peakValues(3))/abs(peakValues(2)))/K;
n = (nEff - r*nEff)/(1+r);
ncomp = nCompIndex(n) + n;
%% Get the K Value f50
MinPeakProminence = 0.01;
MinPeakDistance = 2000;
MinPeakHeight = 5*10^-4;

[peakValues,peakLocations] = findpeaks(fftAirY_f50,
fftAirX_f50,'MinPeakProminence', MinPeakProminence, 'MinPeakDistance',
MinPeakDistance, 'SortStr','descend');
figure
findpeaks(fftAirY_f50, fftAirX_f50,'MinPeakProminence', MinPeakProminence,
'MinPeakDistance', MinPeakDistance, 'SortStr','descend');
title('Peak Search of Air FFT to get K Value');
xlabel('Frequency (Hz)'); ylabel('FFT Magnitude');

peakValues
peakLocations

nEff = 1.44;
nAir = 1;
rAir = (nEff - nAir)/(nEff + nAir);
CavRef = abs(peakValues(2));
CavSense = abs(peakValues(1));
K = (CavSense/CavRef)/rAir;
%% Get Refractive Index of Water f50
MinPeakProminence = 0.002;
MinPeakDistance = 2000;
MinPeakHeight = 2*10^-4;

[peakValues,peakLocations] = findpeaks(fftWaterY_f50,
fftWaterX_f50,'MinPeakProminence', MinPeakProminence, 'MinPeakDistance',
MinPeakDistance, 'SortStr','descend');
```

```
figure
findpeaks(fftWaterY_f50, fftWaterX_f50,'MinPeakProminence',
MinPeakProminence, 'MinPeakDistance', MinPeakDistance,
'SortStr','descend');
title('Peak Search of FFT to get the Refractive Index');
xlabel('Frequency (Hz)'); ylabel('FFT Magnitude');
% axis([0 inf 0 inf])
peakValues
peakLocations

CavRef = abs(peakValues(2));
CavSense = abs(peakValues(1));
r = (CavSense/CavRef)/K;
%rAirCheck = (abs(peakValues(3))/abs(peakValues(1)))/K;
n = (nEff - r*nEff)/(1+r);
ncomp = nCompIndex(n) + n;

%% Get Refractive Index of Alcohol f50
MinPeakProminence = 0.001;
MinPeakDistance = 2000;
MinPeakHeight = 2*10^-4;

[peakValues,peakLocations] = findpeaks(fftAlcoholY_f50,
fftAlcoholX_f50,'MinPeakProminence', MinPeakProminence, 'MinPeakDistance',
MinPeakDistance, 'SortStr','descend');
figure
findpeaks(fftAlcoholY_f50, fftAlcoholX_f50,'MinPeakProminence',
MinPeakProminence, 'MinPeakDistance', MinPeakDistance,
'SortStr','descend');
title('Peak Search of FFT to get the Refractive Index');
xlabel('Frequency (Hz)'); ylabel('FFT Magnitude');
% axis([0 inf 0 inf])
peakValues
peakLocations

CavRef = abs(peakValues(2));
CavSense = abs(peakValues(1));
r = (CavSense/CavRef)/K;
%rAirCheck = (abs(peakValues(3))/abs(peakValues(2)))/K;
n = (nEff - r*nEff)/(1+r);
ncomp = nCompIndex(n) + n;
%% Get the K Value f222
MinPeakProminence = 0.009;
MinPeakDistance = 100;
MinPeakHeight = 0.009;

[peakValues,peakLocations] = findpeaks(fftAirY_f222,
fftAirX_f222,'MinPeakHeight', MinPeakHeight, 'MinPeakDistance',
MinPeakDistance, 'SortStr','descend');
figure
findpeaks(fftAirY_f222, fftAirX_f222,'MinPeakHeight', MinPeakHeight,
'MinPeakDistance', MinPeakDistance, 'SortStr','descend');
title('Peak Search of Air FFT to get K Value');
xlabel('Frequency (Hz)'); ylabel('FFT Magnitude');

peakValues
peakLocations

nEff = 1.44;
nAir = 1;
```

```
rAir = (nEff - nAir)/(nEff + nAir);
CavRef = abs(peakValues(4));
CavSense = abs(peakValues(1));
K = (CavSense/CavRef)/rAir;
%% Get Refractive Index of Water f222
MinPeakProminence = 0.0015;
MinPeakDistance = 100;
MinPeakHeight = 2*10^-4;

[peakValues,peakLocations] = findpeaks(fftWaterY_f222,
fftWaterX_f222,'MinPeakProminence', MinPeakProminence, 'MinPeakDistance',
MinPeakDistance, 'SortStr','descend');
figure
findpeaks(fftWaterY_f222, fftWaterX_f222,'MinPeakProminence',
MinPeakProminence, 'MinPeakDistance', MinPeakDistance,
'SortStr','descend');
title('Peak Search of FFT to get the Refractive Index');
xlabel('Frequency (Hz)'); ylabel('FFT Magnitude');
% axis([0 inf 0 inf])
peakValues
peakLocations

CavRef = abs(peakValues(3));
CavSense = abs(peakValues(1));
r = (CavSense/CavRef)/K;
%rAirCheck = (abs(peakValues(3))/abs(peakValues(1)))/K;
n = (nEff - r*nEff)/(1+r);
ncomp = nCompIndex(n) + n;
%% Get Refractive Index of Alcohol f222
MinPeakProminence = 0.001;
MinPeakDistance = 100;
MinPeakHeight = 0.0011;

[peakValues,peakLocations] = findpeaks(fftAlcoholY_f222,
fftAlcoholX_f222,'MinPeakHeight', MinPeakHeight, 'MinPeakDistance',
MinPeakDistance, 'SortStr','descend');
figure
findpeaks(fftAlcoholY_f222, fftAlcoholX_f222,'MinPeakHeight',
MinPeakHeight, 'MinPeakDistance', MinPeakDistance, 'SortStr','descend');
title('Peak Search of FFT to get the Refractive Index');
xlabel('Frequency (Hz)'); ylabel('FFT Magnitude');
% axis([0 inf 0 inf])
peakValues
peakLocations

CavRef = abs(peakValues(3));
CavSense = abs(peakValues(1));
r = (CavSense/CavRef)/K;
%rAirCheck = (abs(peakValues(3))/abs(peakValues(2)))/K;
n = (nEff - r*nEff)/(1+r);
ncomp = nCompIndex(n) + n;
%% Get the K Value f555
MinPeakProminence = 0.005;
MinPeakDistance = 100;
MinPeakHeight = 5*10^-4;

[peakValues,peakLocations] = findpeaks(fftAirY_f555,
fftAirX_f555,'MinPeakProminence', MinPeakProminence, 'MinPeakDistance',
MinPeakDistance, 'SortStr','descend');
figure
```

```
findpeaks(fftAirY_f555, fftAirX_f555,'MinPeakProminence',
MinPeakProminence, 'MinPeakDistance', MinPeakDistance,
'SortStr','descend');
title('Peak Search of Air FFT to get K Value');
xlabel('Frequency (Hz)'); ylabel('FFT Magnitude');

peakValues
peakLocations

% nEff = 1.44;
% nAir = 1;
% rAir = (nEff - nAir)/(nEff + nAir);
% CavRef = abs(peakValues(4));
% CavSense = abs(peakValues(3));
% K = (CavSense/CavRef)/rAir;
%% Get Refractive Index of Water f555
MinPeakProminence = 0.0015;
MinPeakDistance = 100;
MinPeakHeight = 2*10^-4;

[peakValues,peakLocations] = findpeaks(fftWaterY_f555,
fftWaterX_f555,'MinPeakProminence', MinPeakProminence, 'MinPeakDistance',
MinPeakDistance, 'SortStr','descend');
figure
findpeaks(fftWaterY_f555, fftWaterX_f555,'MinPeakProminence',
MinPeakProminence, 'MinPeakDistance', MinPeakDistance,
'SortStr','descend');
title('Peak Search of FFT to get the Refractive Index');
xlabel('Frequency (Hz)'); ylabel('FFT Magnitude');
% axis([0 inf 0 inf])
peakValues
peakLocations

CavRef = abs(peakValues(3));
CavSense = abs(peakValues(2));
r = (CavSense/CavRef)/K;
%rAirCheck = (abs(peakValues(3))/abs(peakValues(1)))/K;
n = (nEff - r*nEff)/(1+r);

%% Get Refractive Index of Alcohol f555
MinPeakProminence = 0.00069;
MinPeakDistance = 100;
MinPeakHeight = 2*10^-4;

[peakValues,peakLocations] = findpeaks(fftAlcoholY_f555,
fftAlcoholX_f555,'MinPeakProminence', MinPeakProminence, 'MinPeakDistance',
MinPeakDistance, 'SortStr','descend');
figure
findpeaks(fftAlcoholY_f555, fftAlcoholX_f555,'MinPeakProminence',
MinPeakProminence, 'MinPeakDistance', MinPeakDistance,
'SortStr','descend');
title('Peak Search of FFT to get the Refractive Index');
xlabel('Frequency (Hz)'); ylabel('FFT Magnitude');
% axis([0 inf 0 inf])
peakValues
peakLocations

CavRef = abs(peakValues(3));
CavSense = abs(peakValues(2));
r = (CavSense/CavRef)/K;
```

```
%rAirCheck = (abs(peakValues(3))/abs(peakValues(2)))/K;
n = (nEff - r*nEff)/(1+r);
i
```

[i] THE END